

NONLINEAR ANALYSES TO QUANTIFY MOVEMENT VARIABILITY IN HUMAN-HUMANOID INTERACTION

by

MIGUEL P XOCHICALE

A thesis submitted to
The University of Birmingham
for the degree of
DOCTOR OF PHILOSOPHY

School of Engineering
College of Engineering and Physical Sciences
The University of Birmingham
September 2018

Table of contents

1	Introduction	1
1.1	Background	1
1.2	Movement Variability (MV)	3
1.2.1	Modelling Human Movement Variability	4
1.2.2	Movement Variability in Human-Humanoid Interaction	9
1.3	Research questions	13
1.4	Outline of the thesis	14
1.5	Publications	15
2	Quantifying Movement Variability	19
2.1	Introduction	19
2.2	Fundamentals of time-series analysis	19
2.2.1	Linear and nonlinear systems	20
2.2.2	Stationary and nonstationary signals	20
2.2.3	Deterministic and stochastic systems	20
2.2.4	Deterministic chaotic time series	21
2.3	Quantifying Movement Variability with Nonlinear Dynamics	21
2.3.1	Introduction	21
2.3.2	What to measure in MV?	23
2.3.3	Which nonlinear tools are appropriate to measure MV?	24

Table of contents

2.4 Nonlinear analyses with real-world data	27
2.4.1 Nonsationarity	28
2.4.2 Data length	29
2.4.3 Sampling rate	29
2.4.4 Noise	30
3 Nonlinear Analyses	33
3.1 Introduction	33
3.2 State Space Reconstruction Theorem	34
3.3 Uniform Time-Delay Embedding (UTDE)	35
3.4 Estimation of Embedding Parameters	37
3.4.1 False Nearest Neighbours (FNN)	37
3.4.2 Average Mutual Informationi (AMI)	41
3.4.3 Overall minimum embedding parameters	43
3.5 Reconstructed State Space with UTDE	45
3.6 Recurrence Plots (RP)	45
3.6.1 Structures of Recurrence Plots	46
3.7 Recurrence Quantifications Analysis (RQA)	48
3.7.1 Measures of RP based on the recurrence density	49
3.7.2 Measures of RP based on diagonal lines	49
3.7.3 Measures of RP based on vertical lines	51
3.7.4 The weakness and strengths of RP and RQA.	52
4 Experiments	55
4.1 Aims	55
4.2 Participants	55
4.2.1 Human-Image Imitation Activities	56

Table of contents

4.2.2	Human-Humanoid Imitation Activities	56
4.3	Equipment	56
4.4	Ethics	56
4.5	Experiments	57
4.5.1	Human-Image Imitation Activities	57
4.5.2	Human-Humanoid Imitation Activities	58
4.6	Preparation of time series	60
4.6.1	Raw time-series	60
4.6.2	Postprocessing time-series	62
4.6.3	Normalization of time-series	62
4.6.4	Smoothing time-series	62
4.6.5	Window size of time-series	63
5	Quantifying Human Imitation Activities	65
5.1	Introduction	66
5.2	Time series	66
5.3	Minimum Embedding Parameters	66
5.4	Reconstructed state spaces with UTDE	66
5.5	Recurrences Plots	66
5.6	Recurrence Quantification Analysis	66
5.6.1	REC values	66
5.6.2	DET values	66
5.6.3	RATIO values	66
5.6.4	ENTR values	66
6	Quantifying Human-Humanoid Imitation Activities	67
6.1	Introduction	67

Table of contents

6.2	Time series	68
6.3	Minimum Embedding Parameters	68
6.4	Reconstructed state spaces with UTDE	72
6.5	Recurrences Plots	76
6.6	Recurrence Quantification Analysis	77
6.6.1	REC values	77
6.6.2	DET values	77
6.6.3	RATIO values	78
6.6.4	ENTR values	78
6.7	The weaknesses and strengths of RQA	78
7	Conclusions, contributions and future work	97
7.1	Conclusions	97
7.1.1	What are the effects of different parameters for Nonlinear Tools with different characteristics of time series?	97
7.1.2	How sensitive or robust are RQA metrics when quantifying MV?	98
7.1.3	Is it fine to smooth raw time series for the quantification of MV?	100
7.2	Contributions	100
7.3	Future work	101
7.3.1	Inertial sensors	101
7.3.2	Nonlinear analyses	101
7.3.3	Variability in perception of velocity	103
7.3.4	A more rich dataset of time series	104
Appendix A	Examples of Uniform Time-Delay Embedding	105
A.1	20 sample lenght vector.	105
A.2	Time series from an horizontal movement of a triaxial accelerometer.	107

Table of contents

Appendix B Equipment	111
B.1 NeMEMsi IMU sensors	111
B.2 Time-series preprocessing	114
B.2.1 Organising Data in Multidimensional Arrays	114
B.2.2 Data Synchronisation	114
B.2.3 Time Alignment	115
B.3 Humanoid robot	115
B.3.1 Hardware	115
B.3.2 Software	115
Appendix C Experiment Design	117
C.1 Experiment Check List	117
C.2 Ethics	117
C.3 Information Sheet	117
Appendix D Results for all data	119
D.1 Time Series	119
D.2 Embedding parameters	119
D.3 RSSs	119
D.4 RPs	119
D.5 RQAs	119
References	121

Chapter 1

Introduction

1.1 Background

Human movement is a complex system which involves not only multiple joints and limbs for a specific task in a determined environment but also external information processed through with all of our available senses and our prior experiences, which all play a crucial role in the way each person moves. Recent studies in human motion recognition have revealed the possibility to estimate features from lower dimension signals to distinguish differences between styles of movement, such as pedalling (Quintana-Duque, 2012, 2016), gait identification (Frank et al., 2010; Samà et al., 2013) or pattern recognition of physiological signals (speech and heart pathologies or epilepsy) (Gómez-García et al., 2014).

The lower dimension signals from biological signals are generally time series of one-dimension in \mathbb{R} which commonly have high nonlinearity, complexity, and non-stationarity (Caballero et al., 2014; Gómez-García et al., 2014; Huffaker et al., 2017). Traditional methods, in time-domain or frequency-domain, tend to fail when detecting tiny modulations in frequency or phase (Marwan, 2011). This can mean that subtle signatures of each individual's movement could be missed. However, methods of

Introduction

nonlinear time series analysis can quantify such human movement variability (Frank et al., 2010; Gómez-García et al., 2014; Marwan, 2011; Packard et al., 1980; Quintana-Duque, 2012, 2016; Samà et al., 2013; Stergiou and Decker, 2011). With this in mind, Bradley and Kantz (2015) reviewed methods for nonlinear time series analysis, such as the reconstructed state space (RSS) (Takens, 1981), recurrence plots (RP) (Eckmann et al., 1987) and recurrence quantification analysis (RQA) (Zbilut and Webber, 1992), which are explained below. Such methodologies are implemented using embedding parameters (m and τ). However, the computation of embedding parameters is still an open problem since there is no general technique to compute the embedding parameters because time series are system-dependent, meaning that these may only work for one purpose, e.g., prediction, and may not work well for other purposes e.g., computing dynamical invariants (Bradley and Kantz, 2015).

In addition, the quality of the time series affects the reliability of the results for nonlinear tools. For instance, methodologies to compute embedding parameters e.g., autocorrelation, mutual information, and nearest neighbour, require data which are well sampled and with little noise (Garland et al., 2016) or need to have purely deterministic signals (Kantz and Schreiber, 2003). Similarly, methodologies such as RSS, RP and RQA can break down when datasets have different length, different values of accuracy and precision (Frank et al., 2010), or data is contaminated with different or unknown sources of noise (Garland et al., 2016). It is surprising that despite these problems arising from the previous constraints with regard to the quality of data and the estimation of embedding parameters, nonlinear dynamics have proven to be helpful to understand and characterise time series in the context of human movement (Bradley and Kantz, 2015; Frank et al., 2010; Gómez-García et al., 2014; Marwan, 2011; Quintana-Duque, 2012, 2016; Samà et al., 2013; Stergiou and Decker, 2011).

1.2 Movement Variability (MV)

Another point to consider when analysing time series analysis using nonlinear dynamics is the appropriate use of post-processing techniques such as interpolation, filtering or normalisation. However, there is little research on the effects of post-processing techniques in the result interpretation for RSSs, RPs and metrics of RQA.

1.2 Movement Variability (MV)

Variability is inherent within and between all biological systems (Newell and Corcos, 1993). For instance, variability has been studied in electroencephalographic signals in human brains (Klonowski, 2007), in physiological signals like the heart rate variability (Rajendra Acharya et al., 2006; Schumacher, 2004), respiratory patterns of rats (Dhingra et al., 2011), in speech variability where not only the linguistic aspect is investigated but factors like gender, age, social, state of health, emotional state are strongly related to uniqueness of the speaker (Benzeghiba et al., 2007) or even in odor responses based on cultural background and gender (Ferdenzi et al., 2013).

Variability has also been well studied in human body movement, where, for instance, Bernstein (1967) stated that no human movement is repeated exactly with the same trajectory. With that in mind, movement variability has been used as a model of fatigue to prevent chronic musculoskeletal disorders (Mathiassen, 2006; Srinivasan and Mathiassen, 2012). Movement variability has also been considered as an indicator of skilled performance in sport science where, for instance, Wagner et al. (2012) show how movement variability based on statistical analysis varies with skill for three levels of throwing techniques (low-skilled, skilled, and high-skilled). Therefore, Bartlett et al. (2007) concluded that movement variability is ubiquitous across sports (javelin throwing, basketball shooting or running). Another interesting example is that movement variability can be considered as a identifier for personal trait (Sandlund et al., 2017), where many factors of the human body can be considered for identification, such

Introduction

as: age (Krüger et al., 2013; MacDonald et al., 2006; Stergiou et al., 2016; Vaillancourt and Newell, 2003), gender (Svendsen and Madeleine, 2010), pain status (Madeleine et al., 2008; Sandlund et al., 2008), body composition (Chiari et al., 2002), work experience (Madeleine and Madsen, 2009), pace, movement direction or cognitive demands like perception, memory or capacity of introspection (Kanai and Rees, 2011; Srinivasan and Mathiassen, 2012). Additionally, Bartlett et al. (2007) highlighted that movement variability can be interpreted from different theoretical disciplines. For instance, a cognitive control theorist considers variability as undesirable noise and variability is reduced as skill increases, meaning that "becoming dexterous freezes unwanted degrees of freedom in the kinematic chain" (Bartlett et al., 2007, p. 238). In contrast, an ecological motor control specialist considers movement variability either as a functional role in human movement for "coordination change and flexibility to adapt" in different environments (Bartlett et al., 2007, p. 238) or as an exploration and exploitation of body parts in the "perceptual-motor workspace" (Herzfeld and Shadmehr, 2014; Wu et al., 2014).

With regard to the evaluation of healthiness, Stergiou and Decker (2011) highlighted that an optimal state of movement variability is associated with healthiness. Similarly, motor disabilities are associated with either wide range of behaviours such as random, unfocussed and unpredictable or narrow range of behaviours e.g, rigid, inflexible and predictable. For instance, postural sway variability was larger for patients with Parkinson disease or the likelihood of falling in elderly individuals were associated with too little or too much step width variability.

1.2.1 Modelling Human Movement Variability

The human body movement involves a complex system where many sensorimotor variables such as joints, muscles, nervous system, motor unit and cells are the sources for

1.2 Movement Variability (MV)

different types of variability (Newell and Corcos, 1993). Hence, variability encompasses different types, sources and views of variability. For instance, from a biomechanical view, motion variability can be modelled as system of differential equations for the neuro-musculoskeletal control system where motion variations can occur because of "perturbations of initial states of the skeletal", perturbations of "muscular or neural subsystems ", or "external torques and forces acting on the skeletal system" (Hatze, 1986, p. 13). According to Hatze (1986) motion variability can be caused by (a) direct consequences of adaptive learning process, and (b) random fluctuations which are the result of stochastic processes in the nervous system. Hence, Hatze (1986) proposed measures of dispersion (e.g. Fourier series and entropy measures) to quantify the deviation of motion from a certain reference. For which, Hatze (1986) pointed out that the combination of deviations from angular coordinates (radians) and linear coordinates (meters) for Fourier series were unacceptable as the units are different. Hence, Hatze (1986) proposed the use of entropy as a global quantifier for motion variability and concluded that any movement deviation on a body joint may be the result of deterministic and stochastic causes.

Another approach to model variability has been proposed by Müller and Sternad (2004), who decompose variability into exploration of task tolerance(T), noise reduction(N), and covariation(C). Müller and Sternad 2004, p. 229 considered that the quality of performance in goal-oriented tasks, e.g. hitting a target, is defined "by the accuracy and replicability of the results" (deviations from the target) "over repeated attempts of execution" (configuration of joint angles with its velocity, angles and position). For the experiment, Müller and Sternad (2004) considered an skittle task, where participants throwing a ball with a string that swings around a center post with the objective of knocking down the skittle at the opposite site. Hence, Müller and Sternad (2004) proposed D as the absolute average of distance to the targets in

Introduction

n trials and it is used as a measure of the collective performance that combines a function for movements results based on the execution vector with a function for the minimum distance from the target d . Therefore, the overall difference in performance D is decomposed into three unequal contributions of covariation C , noise reduction N and task tolerance T . Considering a 2-D task spaces that spanned the release angle α and absolute velocity v , the components of contributions of variability were calculated from five data sets (A , A_0 , A_{shift} , B and B_0): (i) the component of covariation where sets A and A_0 and B and B_0 have the same means and variances, (ii) the component of tolerance where sets A and A_{shift} differ only on their location in the task space, and (iii) the component of noise where sets A_{shift} and B_0 have the same means but different variances (see Fig.6 in Müller and Sternad (2004) for further details). With that in mind, Müller and Sternad (2004) conducted an experiment with forty-two participants for five different locations of the target skittle where for each target a participant performed 320 trials which is a total of 1600 trials and therefore presented statistical confirmation of the contributions of T , N and C using ANOVA. Hence, Müller and Sternad (2004) concluded that T and N contribute more to improvement of a performance of a task than C for initial practice, meaning that a new combination of angles and velocities explore a large region of solution space (hitting the target). However, for later practice, T diminished and N and C started to be more relevant. Also, Müller and Sternad (2004) showed in various experiments of throwing actions that variability in the movement results (deviations from the target) is generally smaller than variability in the execution (variables or release angles and velocities) for which it is concluded that covariation between execution variables is another component of variability. With that in mind, Müller and Sternad (2004) concluded that task space exploration is an essential contribution to the improvement of movement performances which is an explanation to the increase of noise in early practice phases.

1.2 Movement Variability (MV)

Seifert et al. (2011) investigated coordination profiles for recreational and competitive breaststroke swimmers and proposed an hourglass model of variability that illustrates the amount of variability as a function of expertise. Hence, Seifert et al. 2011, p. 551 stated recreational swimmers would show a considerable amount of intra-variability "as they seek an individually appropriate coordination pattern to accommodate the novel constraints of locomotion in water", whereas experts swimmers, after a considerable practice, will still explore new environments to optimise their technique that create another secondary blooming of variability which is the result of "the environment exploration to optimise their technique with their individual strengths (e.g. physical, anatomical, mental, etc.) and to gain an advantage over competitive swimmers". To test the hourglass model of variability, Seifert et al. (2011) considered the continuous relative phase (CRP) between the elbow phase angle and knee phase angle, therefore CRP is used as an indicator on how swimmers synchronise arm recovery (elbow extension) and leg recovery (knee flexion). Then, Seifert et al. (2011) analysed inter-individual variability of swimmers with the shape of the curves of CRP which provide an indication of the inter-limb coordination, applied statistical measures such as hierarchical clustering using eleven variables of CRP to classify the recreational swimmers into three cluster of coordination (intermediate, most-variable and in-phase) and used Fisher information to test which CRP variables were significantly differentiated the clusters. With that, Seifert et al. (2011) concluded that inter-individual coordination variability for recreational swimmers could be the result of (i) different state of process learning, (ii) environmental constraints (different perception of the aquatic resistance), or (iii) different perception of the task constraints (floating instead of swimming).

Recently, Preatoni (2007); Preatoni et al. (2010, 2013) reported that inter-trial variability is defined as combination of functional changes associated with the nonlinear

Introduction

properties of the neuro-musculo-skeletal system (V_{nl}) and random fluctuations in the neuro-motor-skeletal system (V_e). Additionally, Preatoni et al. 2013, p. 72 stated that the random fluctuations in movement variability can be composed by $V_e = V_{eb} + V_{ee} + V_{em}$, where V_{eb} is the "error in the sensory information and in the motor output commands", V_{ee} is the "changes in the environmental conditions" and V_{em} is the "changes in measuring and data processing procedures". Therefore, as similar as Hatze (1986), Preatoni et al. 2013, p. 77 pointed out that V_{nl} "may be interpreted as the flexibility of the system to explore different strategies to find the most effective strategy among the many available". Hence, Preatoni et al. 2010, p. 1328 concluded that the total variability represent the changes of contributions for V_e and V_{nl} and it is defined as $V_{tol} = V_e + V_{nl}$, where V_{tol} "may reveal the effects of adaptation, pathologies and skills learning". Also, Preatoni et al. (2013) noted that their work only investigate error from biological variability (e.g. V_{eb}) which does not consider non-biological noise resulting from measuring instruments or data post-processing techniques, such non-biological noise has high frequency components that are usually removed. Therefore, the work of Preatoni et al. (2010) and Preatoni et al. (2013) do not consider an overall index to quantify movement variability but the combination of both V_{eb} and V_{nl} . With that in mind, Preatoni (2007) analysed the influences of V_{eb} and V_{nl} for movement repeatability by comparing entropy measures (e.g. ApEn and SampEn) with values of their surrogate counterparts.

Generally, the previous approaches reported different models for movement variability which then are quantified with different tools. For instance, Hatze (1986) and Preatoni et al. (2010, 2013) use entropy measures as the authors consider that the origin of the signals in the human body is the result of deterministic and stochastic processes, whereas Müller and Sternad (2004) and Seifert et al. (2011) reported only statistics as a measure of magnitude that limited the evaluation of the whole trajectories as

1.2 Movement Variability (MV)

structures of movement variability in human body activities. Therefore, for this thesis, it is important to note that even with the proposed models for movement variability (Hatze, 1986; Müller and Sternad, 2004; Preatoni et al., 2010, 2013; Seifert et al., 2011) which have been quantified with either statistical or nonlinear tools, little has been investigated with regards to the reliability of the nonlinear tools when using real data that has the property of being noisy, deterministic, stochastic or nonstationary (Newell and Slifkin, 1998). A further reviewed of nonlinear tools is presented in Chapter 2.

1.2.2 Movement Variability in Human-Humanoid Interaction

Movement variability in the context of human-humanoid interaction has been investigated for exercising, rehabilitation and dancing purposes.

Görer et al. (2013) conducted an experiment of a robotic fitness coach where eight elderly participants performed five gestures: three for arm related exercises and two for leg strength exercises. Hence, Görer et al. (2013) with only graphical visualisation of joint angles trajectories, extracted from the pose estimation of a kinect sensor, stated that only one subject out of eight fail to imitate the gestures correctly. Additionally to the limitations of mapping human movements to a humanoid robot due to the differences in their degrees of freedom which were compensated with auditory feedback, Görer et al. (2013) surveyed participants using a 5-point Likert scale about the positive and negative effect, flow, immersion and challenge of the human-robot interaction activity, concluding that their system is easy to use based on the high scores for immersion and positive effect and low scores for challenge and negative effect.

Another example is the work of Guneysu et al. (2014) who conducted experiments with children for upper arm rehabilitation using a play-like child robot interaction. Hence, Guneysu et al. (2014), using a Kinect sensor to get data of joint angles of the participants' skeleton, performed an automatic evaluation of three upper body actions

Introduction

(shoulder abduction, shoulder vertical flexion and extension, and elbow flexion) of eight healthy children who mimicked an humanoid robot. To evaluate motion imitation, Guneysu et al. 2014, p. 202 considered similarity error using Dynamic Time Warping (DTW) that penalise large angle errors over ten percent in the area range of the motion type and applied recall measure as a representation of "how much of angular area of the baseline motion from the humanoid robot is also covered by the child's motion". Then, Guneysu et al. (2014) presented the evaluation of five physiotherapists using Intraclass correlation coefficient (ICC) which a metric for reliability of ratings for motion types, and reported that for the first motion, which consists of only one join, the metric and physiotherapist evaluations showed hight agreements, whereas for the second and third motions, which motions were harder and complicated consisting of more join values, the evaluation between the metrics and physiotherapist presented differences. Guneysu et al. 2014, p. 203 stated that during the evaluation of complicated and harder movements, children misperceived the actions for which "therapists compensated such misunderstanding by giving hight scores to the children while the proposed system only considered angles". With that, it is interesting to note that the proposed metrics of similarity error and recall measure with the ICC metric are not completely reliable since they did not model well complex movements. Recently, Guneysu et al. (2015) presented an improvement of their previous research where less complex movements from four physiotherapists performing five actions were analysed: opening a door with a key, touching the opposite shoulder with hand, taking an object from back to neck, taking an object from the back and reaching an object above the head. Then, Guneysu et al. 2015, p. 252 applied traditional statistics (e.g. sample mean and sample variance) to characterise the five actions. For instance, the initial positions of arms changed from person to person, specially for the key turning action which variation were affected

1.2 Movement Variability (MV)

by the sample mean, while performances of turning the amplitude of the arm were associated with the standard deviation of the data.

Movement variability in the context of human-humanoid interaction has also been investigated in robotic dance activities. For example, Tsuchida et al. (2013) explored four dance formations which were performed three times by nine participants who had three years of experience: dancing with a robot, dancing alone, dancing with a self-propelled robot and dancing with a projected video. To visualise dance movements, Tsuchida et al. (2013) presented two participant's movement positions with twelve trajectories each (four dance activities times three trials) of z and x directions obtained with a Kinect sensor. Although, dance experiment was rich in terms of movement variability for both participants and dance activities, only distance between each of the conditions in the dance formation was considered. With that, Tsuchida et al. (2013) concluded that the sense of dancing with a projected video of a person were the closest to dance with a real person and the trajectory of dance with a self-propelled robot were the closest to the trajectory of a dancer. Additionally, Tsuchida et al. (2013) only applied traditional statistics (e.g. ANOVA) to characterise dance movements.

Another aspect of movement variability in the context of human-humanoid interaction is the generation of robotic dance. Recently, Peng et al. (2015) reviewed an hierarchical taxonomy of four categories of robotic dance (cooperative human-robot dance, imitation of human dance motions, synchronisation for music and creation of robotic choreography). Peng et al. (2015) pointed out that the creation of robotic dances is still an open research question because dance motions should generally be both interesting and exiting for users. According to Peng et al. (2015), the creation of robotic dances can be accomplished with any of the following methodologies: (i) random generation where robots can be preprogrammed with series of predefined algorithms that can be chosen randomly, (ii) mapping rule where robots can react,

Introduction

and therefore dance, to different factors such as colours, sounds, speech, temperature or human activity, (iii) chaotic dynamics which systems are sensitive to initial conditions and therefore create various dance styles from periodic and couple to rhythm to jumping styles, resulting in innovative and consistent dance patterns, (iv) interactive reinforcement learning where the robot can automatically choose motions based on rewards of participants' preferences of graceful motions, (v) evolutionary computation in which multiple iterations of generations of dance motions can create graceful robotic dance motions, and finally (vi) using a Markov chain model, a discrete time stochastic chain, where each sequence of dance motions is considered as a state in the Markov chain producing dance that synchronise with music and emotions. Therefore, while the research questions of this thesis are not fully related to the creation of good robotic dances (e.g, being innovative or having accordance with human aesthetics) (Peng et al., 2015), it is important to note that one of the methodologies to create robotic dance motions is the use of chaotic dynamics which consider initial conditions to generate movements that are neither deterministic or stochastic.

Although, movement variability in the context of human-humanoid interaction has not been directly investigated in recent years, it can be noted that movement variability is indeed applied in exercise, rehabilitation or dance. Hence, it can be noted that the previous works that has analysed gestures, movements or dance activities with only traditional statistics, for which (i) it is not only clear how Görer et al. (2013) performed the evaluation of synchronisation for gestures between participants and the humanoid but also what methods of evaluation, apart from the visual, has been applied to classify correct gestures trajectories, whereas (ii) little has been investigated with regards to the differences in movement of the invited physiotherapists in the work of Guneysu et al. (2014) and Guneysu et al. (2015), (iii) in the results of Tsuchida et al. (2013), it is not clear, for their results, why the distribution of trajectories for subject 1

1.3 Research questions

were more uniform than the trajectories of subject 2, and (iv) even thought, the robot movements for the experiments of this thesis are simple, Peng et al. (2015) noted that generation of robotic dance movements can be done with chaotic dynamics.

Therefore, it is generally highlighted that applying nonlinear analyses instead of traditional statistics in the context of human-humanoid interaction might provide a better quantification and understanding of human movements since these are generally both deterministic and stochastic. Similarly, little research has been done in this context with regards to the reliability of nonlinear tools when using real-data time series (e.g. window length, post-processing techniques, noise contamination, nonstationarity, chaotic deterministic, etc).

1.3 Research questions

A number of questions regarding movement variability has been investigated in the last decade (Stergiou and Decker, 2011; Stergiou et al., 2006) such as: how is variability controlled while learning a new skill? (Bartlett et al., 2007; Seifert et al., 2011; Wagner et al., 2012), is variability associated with disease or health? (Stergiou and Decker, 2011; Stergiou et al., 2006), what are the sources of variability and how do they interact in the production of observed variation of movement? (Preatoni, 2007; Preatoni et al., 2010, 2013). Nonetheless, little has been recently investigated with regards to the reliability of nonlinear tools to quantify movement variability (Iwanski and Bradley, 1998; Yao and Lin, 2017) when dealing with real-world data (Bradley and Kantz, 2015; Caballero et al., 2014). Therefore, this thesis explores the effects on three nonlinear tools (e.g. Reconstructed State Space (RSS), Recurrence Plots (RP) and Recurrence Quantification Analysis (RQA)) with different features of time series such as structure, levels of smoothness and window lengths. To perform such exploration, two experiments were conducted with twenty right-handed healthy participants: one for human-image

Introduction

imitation activities and another in the context of human-humanoid imitation activities. For the experiments participants were asked to imitate simple arm movements and participants and humanoid robot were attached with inertial sensors that collected time series. Hence, three research questions are investigated in this thesis.

- What are the effects on RSSs, RPs, and RQA metrics for different embedding parameters, different recurrence thresholds and different characteristics of time series (window length size, smoothness and structure)?
- How sensitive or robust are RQA metrics when quantifying MV?
- Is it fine to smooth raw time series for the quantification of MV?

1.4 Outline of the thesis

This thesis is organised as follow. Chapter 1 presents a background for the quantification of Movement Variability(MV) for which three research questions are raised. Chapter 2 presents an introduction to fundamentals of time series analysis then it is reviewed (i) what to measure in Movement Variability(MV)? and (ii) which nonlinear tools are appropriate to measure MV? and finalised with a review for nonlinear analyses with real-world data. We then present in Chapter 3 a review of the state space reconstruction that includes an explanation for uniform time delay embedding and a description of the techniques to estimate of minimum embedding parameters (e.g. false nearest neighbour and average mutual information), an introduction to Recurrence Plots (RPs), structures of RPs and different metrics to perform Recurrence Quantification Analysis (RQA) as well as the weakness and strengthens of RPs and RQAs. In Chapter 4, the experiments for human-image imitation and human-humanoid imitation are presented as well as the aims, participants, description of the activities in the experiments, participants, data collection from inertial measurement unit sensors, preprocessing

techniques (e.g raw data, normalised data, smoothed data and windowing) equipments, ethics and preparations of the time series. Chapter 6 and 7 present the results with regards to the two experiments showing the computation of minimum embedding parameters, reconstructed state space using uniform time-delay embedding, recurrence plots, recurrence quantification analysis metrics and its weaknesses and strengths. Finally, Chapter 7 presents the conclusions, the answer for the research questions, the contribution to knowledge and future work for this thesis.

1.5 Publications

Partial work of this thesis has been published in the following peer-reviewed conferences.

- Xochicale M., Baber C., and Oussalah M., Understanding Movement Variability of Simplistic Gestures Using an Inertial Sensor, in Proceedings of the 5th ACM International Symposium on Pervasive Displays, Oulu, Finland, June 2016, pages 239–240. <https://github.com/mxochicale/perdis2016>
- Xochicale M., Baber C., and Oussalah M., Analysis of the Movement Variability in Dance Activities Using Wearable Sensors, in Wearable Robotics: Challenges and Trends, Segovia, Spain, October 2016, pages 149–154.
<https://github.com/mxochicale/werob2016>
- Xochicale M., Baber C., and Oussalah M., Towards the Quantification of Human-Robot Imitation Using Wearable Inertial Sensors, in Proceedings of the Companion of the 2017 ACM/IEEE International Conference on Human-Robot Interaction, Vienna, Austria, March 2017, pages 327–328.
<https://github.com/mxochicale/hri2017>
- Xochicale M., and Baber C., Towards the Analysis of Movement Variability in Human-Humanoid Imitation Activities, in Proceedings of the 5th International

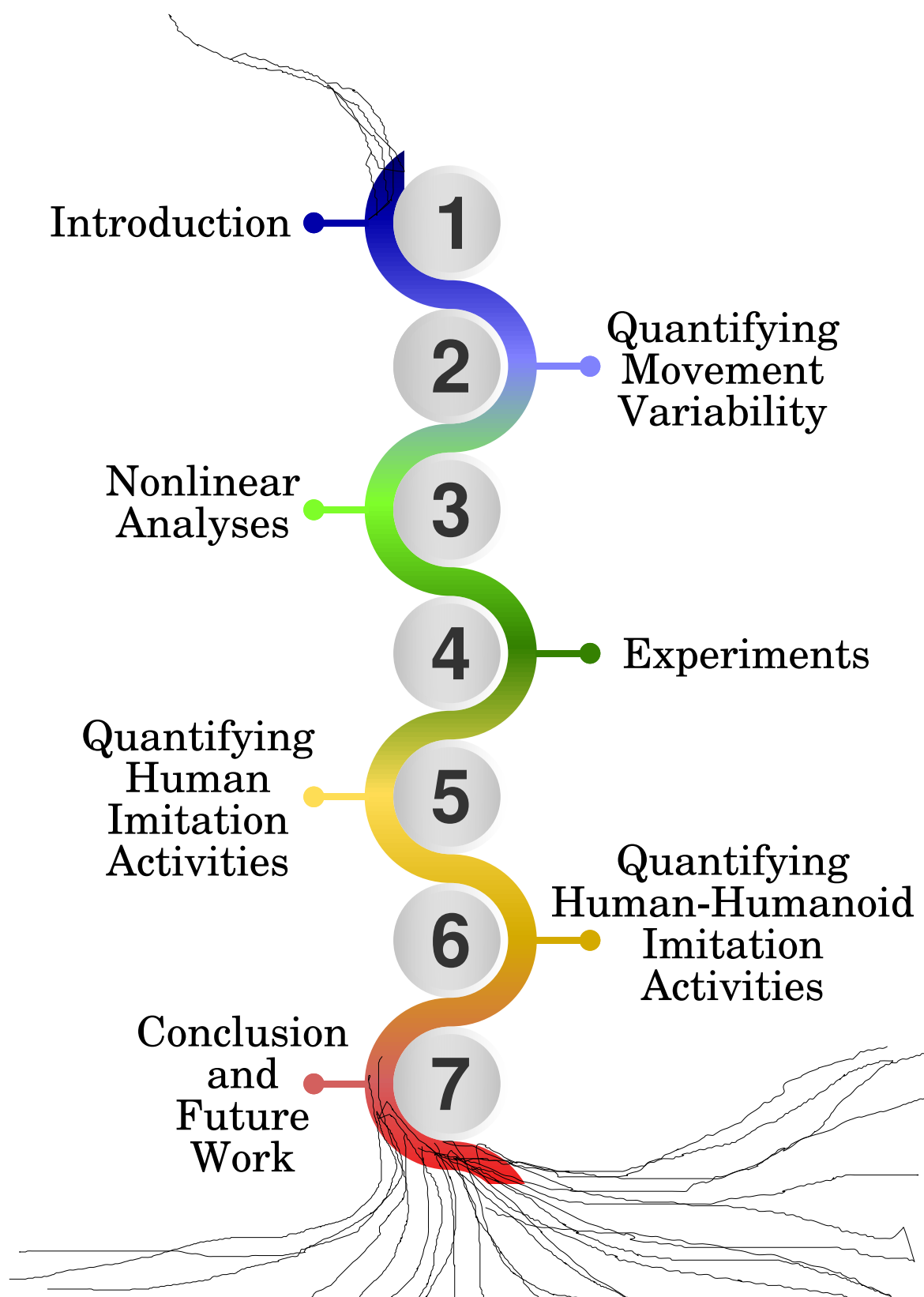


Fig. 1.1 Thesis structure. Chapter numbers and its titles.

1.5 Publications

Conference on Human Agent Interaction, Bielefeld, Germany, October 2017,
pages 371–374. <https://github.com/mxochicale/hai2017>

Chapter 2

Quantifying Movement Variability

2.1 Introduction

It has been stated in Chapter 1 that movement variability can be modelled and quantified using nonlinear tools mainly because the structures of the human physiology (lungs, neurons, etc.) suggest that many of their dynamics are controlled by nonlinear dynamics (Goldberger et al., 1990) and data from human movement is essentially chaotic deterministic, meaning that it is neither deterministic nor stochastic (Hatze, 1986; Preatoni et al., 2010, 2013; Stergiou et al., 2006). Additionally, data from the human body is generally noisy, deterministic, stochastic or nonstationary (Newell and Slifkin, 1998). Therefore, in this chapter fundamentals of time series, nonlinear tools and nonlinear tools with real-data will be reviewed.

2.2 Fundamentals of time-series analysis

Biosignals from living systems can typically be nonstationary, nonlinear, deterministic chaotic and noisy (Caballero et al., 2014; Gómez-García et al., 2014; Harbourne and Stergiou, 2009; Hatze, 1986; Klonowski, 2007; Newell and Slifkin, 1998; Stergiou and

Quantifying Movement Variability

Decker, 2011; Stergiou et al., 2006; Wijnants et al., 2009). Therefore, it is important to provide fundamental definitions of time series which will be used thought the thesis.

2.2.1 Linear and nonlinear systems

Linear systems are proportional or additive. For example, the interaction between variables of a linear system are negligible whereas for a nonlinear system such interaction of variables can produce emergent properties due to the initial conditions of the system (Klonowski, 2007).

2.2.2 Stationary and nonstationary signals

Stationary signals have the same mean and variance as time progress (e.g. a sinusoidal signal), however such stationary signal can also be changeable (e.g. alternative sinusoidal signal). In contrast, when statistics of the time series change with time then such signal is known as nonstationary signal. Nonstationary signals are therefore characterised by having transients and drifts over time. Examples of nonstationary signals are the time series of seasonal trends and changes (Kitagawa and Gersch, 1984), Electroencephalography (EEG) signals which present different and changeable intensity over time (Klonowski, 2007).

2.2.3 Deterministic and stochastic systems

A deterministic systems means that is predictable. Deterministic systems have the characterising to have small number of variables of importance in the system. Deterministic systems are modelled with linear ordinary differential equations and their initial conditions and constants. In contrast, stochastic systems are nonpredictable and therefore have bigger number of variables of equal importance and stochastic systems are modelled with probability theory (Klonowski, 2007).

2.2.4 Deterministic chaotic time series

Deterministic signals can dramatically change with a slight change of initial conditions and then after a long time-scale, the signal can appear to be stochastic (Amato, 1992). Similarly, Klonowski 2007, p. 11 pointed out that "chaotic systems behave like they were stochastic but they are also deterministic", meaning that chaotic systems are predictable for a short time-scale but nonpredictable in a long time-scale because of the initial conditions of the systems. Then, Preatoni et al. 2013, p. 78, in experiments in sport science, mentioned that "variability is likely to have both deterministic and a stochastic origin". Therefore, it can be concluded that time series for human body movement are neither independent nor stochastic but deterministic chaotic (Harbourne and Stergiou, 2009; Stergiou and Decker, 2011; Stergiou et al., 2006).

2.3 Quantifying Movement Variability with Non-linear Dynamics

2.3.1 Introduction

Previous studies have shown that movement variability is not considered as a undesired factor that creates errors but a signature for assessment of healthiness (associated with unhealthy pathological states) or skillfulness (associated with the functionality of movement) (Stergiou and Decker, 2011). Fundamentally, movement variability can be either quantified based on magnitude of the variability or the dynamics and complexity of the variability (Caballero et al., 2014). However, finding the right tools to quantify movement variability is still an open problem.

For instance, Preatoni et al. (2010, 2013) pointed out that conventional statistics (e.g. standard deviation, coefficient of variation, intra-class correlation coefficient) only

Quantifying Movement Variability

quantify the overall variability. Also, Stergiou and Decker (2011) stated that statistical tools (e.g. mean, standard deviation and the range) are a measure of centrality, meaning such metrics are compared around a central point. Similarly, Coffey et al. (2011) pointed out that the use of means and standard deviations led to reduction of data and information is therefore discarded.

Additionally, one can apply frequency-domain tools to quantify movement variability. For example, Hatze (1986) proposed a measure of dispersion to quantify the deviation of motion from a certain reference using the Fourier series. However, deviations of motion are from angular coordinates (radians) and linear coordinates (meters) which made them an unacceptable fusion of variables. Vaillancourt et al. (2001) pointed out that it is rare for frequency and amplitude to differ in postural tremor of patients with Parkinson's disease but differences in time-dependent structures are apparent, and associated with a change of regularity of postural tremor. Then, (Klonowski, 2002, 2007, 2009) stated that frequency-domain tools require to have stationary data, otherwise using other type of data might create misleading results.

Therefore, applying either statistical tools or frequency-domain tools to quantify movement variability might create misleading results, specially when dealing with signals that are deterministic chaotic (Amato, 1992; Dingwell and Cusumano, 2000; Dingwell and Kang, 2007; Miller et al., 2006), considering that the subtle changes in the neuromuscular-skeletal system are caused by influences of environmental changes, training procedures or latent pathologies (Preatoni et al., 2010, 2013) and that movement variability involves evolution of human movement and exploratory nature of movement (Caballero et al., 2014; Stergiou and Decker, 2011). Hence, Caballero et al. (2014); Preatoni et al. (2010); Stergiou and Decker (2011) highlighted that movement variability can be better described and quantified with different nonlinear dynamics tools such as: largest Lyapunov exponent (Bruijn et al., 2009; Donker et al., 2007; Kurz et al.,

2.3 Quantifying Movement Variability with Nonlinear Dynamics

2010; Yang and Wu, 2011), fractal analysis (Delignlères et al., 2003), entropy rate (Cavanaugh et al., 2010), Sample Entropy (SampEn) (Donker et al., 2007; Liao et al., 2008; Richman and Moorman, 2000; Stins et al., 2009; Vaillancourt et al., 2004), Approximate Entropy (ApEn) (Cavanaugh et al., 2010; Kurz and Hou, 2010; Pincus, 1991; Sosnoff et al., 2006; Sosnoff and Voudrie, 2009), Fuzzy Entropy (FuzzyEn) (Chen et al., 2007), Multiscale Entropy (MSE) (Costa et al., 2002), Permutation Entropy (PE) (Bandt and Pompe, 2002; Vakharia et al., 2015), Quadratic Sample Entropy (QSampEn) (Lake and Moorman, 2011), Amplitude-aware permutation entropy (AAPE) (Azami and Escudero, 2016), Detrended Fluctuation Analysis (DFA) (Gates and Dingwell, 2007, 2008; Hausdorff, 2009) and Recurrence Quantification Analysis (RQA) (Marwan, 2008; Trulla et al., 1996; Zbilut and Webber, 1992).

Having got many nonlinear tools to measure movement variability (MV) made Caballero et al. 2014, p. 67 to raise the following question: "Is there a best tool to measure variability?" which leads us to formulate a further set of questions for this thesis on what to measure in MV?, how to measure MV? and which tools are appropriate to measure MV?

2.3.2 What to measure in MV?

Vaillancourt and Newell (2002, 2003) stated that there is no universal increase or decrease in complexity for MV as a function of age or disease but a dependency with the task dynamics. For example, in a constant-force task (where the task dynamics is of low dimension), generally older adults present less complexity due their inability to introduce additional degrees of freedom in the neuromuscular system. However, there is an increase of complexity in older adults or unhealthy adults when the task dynamic is oscillatory because these type of adults have more difficulty to reduce the dimension output to a lower dimension which are the intrinsic dynamics of their resting state.

Quantifying Movement Variability

In contrast, inspired by Tononi et al. (1998) who modelled complexity in neural networks considering complexity versus regularity variables, Stergiou et al. (2006) proposed a model of complexity versus predictability variables for optimal human movement variability. The model of Stergiou et al. (2006) stated that higher complex movements are associated with rich behaviour of movements while lower complex movements are associated with poor behaviours of movements being too rigid or too unstable. Hence, higher complex movements are therefore characterised by chaotic systems, while lesser complexity of movements are characterised either as noisy systems or periodic systems (having either low amounts of predictability or hight amounts of predictability) (Stergiou et al., 2006).

2.3.3 Which nonlinear tools are appropriate to measure MV?

Considering the model of Stergiou et al. (2006) for movement variability, where complexity and predictability variables of a system can characterise and quantify movement variability, it is important to find, to understand and to apply the right tools that measure such variables.

Originally, Pincus (1995, 1991) proposed Approximate Entropy (ApEn) to quantify regularity of time series. Then, Richman and Moorman (2000) found that the algorithm of ApEn match itself to avoid the occurrence of $\ln(0)$ which made ApEn dependant on the available data for which Sample Entropy (SampEn) were proposed as an algorithm that does not consider self-matching. Hence, SampEn values are independent of the length of time series and its algorithm is simpler than ApEn. Then, instead of using single statistics, Costa et al. (2002) proposed Multiscale Entropy (MSE) algorithm which computes SampEn of consecutive coarse-grained time series of the original time series defined by the scale factor, τ . With MSE algorithm, (Costa et al., 2002) noted that pathology dynamics for time series of heartbeat intervals are associated with

2.3 Quantifying Movement Variability with Nonlinear Dynamics

reduction of complexity. Therefore, Costa et al. 2002, p. 3 concluded that physiologic complexity is associated to the adaptive capacity of the organism, diseases states and aging which "may be defined by a sustained breakdown of long-term correlations and loss of information". Essentially, entropy measures (ApEn and SampEn), quantify regularity and complexity of time series (Preatoni et al., 2013). However, Goldberger (1996) mentioned that the increase of irregularity in time series is not a synonymous of increase of physiologic complexity. Similarly, an increase of ApEn or SampEn, "implying increase of irregularity and decrease in predictability" (Goldberger et al., 2002, p. 25), is not synonymous of an increase of dynamical complexity when analysing physiology signals (Costa et al., 2002). Hence, Goldberger et al. (2002) demonstrated that ApEn as a regularity statistic is not a direct index of physiologic complexity where, for example, a randomised time series of a healthy heartbeat with multi-scale and complex patterns of variability show a higher value of ApEn being that the time series is less complex. Therefore, Goldberger et al. 2002, p. 24 concluded that the loss of physiologic complexity can be "better assessed using other measures which can detect and quantify the presence of long-range correlations in nonstationary series." Hence, Costa et al. (2002); Goldberger et al. (2002); Vaillancourt and Newell (2002) concluded that ApEn and SampEn do not necessarily show the right representation of what they are intent to measure.

Therefore, considering the previous cons of ApEn, SampEn and MSE, Detrended Fluctuation Analysis (DFA), which is based on analysing fractal features, can quantify long-term correlations of time series (Peng et al., 1995). DFA is calculated as the root mean square fluctuation of an integrated and detrended time series and it is represented by a scaling exponent, α , which is an indicator for roughness of time series, e.g. "the larger the value of α , the smoother the time series (Peng et al., 1995, p. 83). However, only using DFA can result in a false conclusion for long term correlations

Quantifying Movement Variability

in the time series (Rangarajan and Ding, 2000, p. 5001), therefore DFA "can falsely classify certain type of time series as fractals" (Wijnants et al., 2009, p. 80). With that in mind, Wijnants et al. (2009) proposed the use of RQA as a technique that does not present any constraints with regards to length size, stationary or statistical distribution of the time series. Nonetheless, Wijnants et al. (2009) highlighted that SampEn index is calculated over the sequential values of the time series, whereas Shannon entropy in RQA which is computed over the distribution of deterministic lines in the Recurrence Plots (RP) (Marwan, 2008; Trulla et al., 1996; Zbilut and Webber, 1992). Similarly, Rhea et al. (2011) highlighted that algorithms to compute entropy measures are different since ApEn and SampEn are approximations of the Kolmogorov-Sinai Entropy computing the likelihood that a template pattern repeats in the time series while RQAE is derived from Shannon entropy and is computing number of line segments of varying length in the RP. Even though with those difference in the algorithms, smaller values of recurrence percentage of the RQA shown the increase of practice of movement dynamics, concluding that such recurrence percentage is indicator of increase of system stability (Wijnants et al., 2009).

Another tool to measure variability is the largest Lyapunov exponent (LyE) which "quantify the exponential separation of nearby trajectories in the reconstructed state space of a time series" (Stergiou, 2004, p. ??). For instance, "LyE from a stable system with little to no divergence will be zero (e.g. sine wave)" and "LyE for an unstable system that has highest amount of divergence will be positive and relative hight in value (e.g. 0.469 for random noise)" and for chaotic systems like the Lorenz system, LyE is in between the two of the previous extremes ($\text{LyE} \approx 0.1$) (Miller et al., 2006, p. 2874). However, LyE requires to be validated using surrogation (Dingwell and Cusumano, 2000; Miller et al., 2006).

2.4 Nonlinear analyses with real-world data

Measuring human movement variability requires a combination of the pros and cons of many of the previous tools that analysis either (i) the dynamic complexity or (ii) the degree of regularity, stability or predictability in a system (Goldberger et al., 2002; Harbourne and Stergiou, 2009; Stergiou and Decker, 2011). For instance, Rangarajan and Ding (2000) stated the use of both spectral analysis and random walk analysis, the base of DFA, is a better approach than only using one tool which can lead to false conclusion for long term correlations in the time series. Similarly, Wijnants et al. (2009) selected different tools (spectral analysis, standard dispersion analysis, DFA, RQA and SampEn) to quantify movement variability that can complement the strengths of some of them and also compensate the weakness of others. Recently, Caballero et al. (2014) proposed the unification of different tools to address every aspect of the dynamics of a systems and the characterisation of the variability.

Although, there is no best tool to measure movement variability and an unification of tools to quantify human movement variability is still an open question, finding the right tool to measure movement variability for an specific problem, and knowing its strengths and weakness of such tool is one of the research questions for this thesis.

2.4 Nonlinear analyses with real-world data

Recently, Huffaker et al. (2017) only highlighted that one of the caveats when applying nonlinear time series analysis tools is its unreliability when the estimated metrics come from real-world data which is generally short, noisy and nonstationary. Similarly, Preatoni et al. (2013) mentioned the limitations of the use of nonlinear analyses in sport activities where data required to be large (e.g. number of trials, duration of the experiment and sampling frequency). Whereas Caballero et al. (2014), providing further a investigation, stated the weaknesses of different nonlinear tools regarding the characteristics of the time series such as nonstationarity, length data size, noisy,

Quantifying Movement Variability

sampling rate. However, in the work of Huffaker et al. (2017), Preatoni et al. (2013) and Caballero et al. (2014) no further exploration of the metrics with real-world data is presented.

2.4.1 Nonsationarity

Nonstationarity of time series signals might create spurious increase or decrease in the metrics of nonlinear tools. For instance, Costa et al. (2007) noted that nonsatiornary in the signals might alter the increase of irregularity of signals for the shortest scales when applying MSE. Also, Dingwell and Cusumano (2000) reported nonstationary in time series when using LyE, which required to be validated using surrogation to ensure the robustness of the metric. Hence, Caballero et al. (2014) reported three options when dealing with nonstaionary data: (i) remove nonsatiornary data, (ii) use empirical mode decomposition (EMD), and (iii) apply nonlinear tools, such as DFT and RQA, which are less sensitive to nonstationary data.

To remove nonstationary data, for example, Carroll and Freedman (1993) suggested to remove the trends or to eliminate the first 20 seconds of samples to ignore the trend of time series. Hence, van Dieën et al. (2010), in experiments with center of pressure movements in seated balancing, discarded the first 5 seconds of the time series in the start of the measurement to avoid nonstationary of the data.

Also, nonstatioinary time series can be treated with Empirical Mode Decomposition (EMD) method which decompose nonlinear, nonstatioanry signals into their intrinsic frequency components (Huang et al., 1998; Wu and Huang, 2004, 2009). Hence, Costa et al. (2007); Flandrin et al. (2004) tested that EMD is a robust method for detrending and denoising time series and highlighted that EMD does not require selection of input parameters. However, the reliability of EMD methods is still an open problem, for instance, an extension of EMD called Multivariate Empirical Mode Decomposition

(MEMD) has been proposed to analyse multiple time series (Mandic et al., 2013; Rehman and Mandic, 2010). See (Bonnet et al., 2014; Costa et al., 2007; Daubechies et al., 2011; Mert and Akan, 2018; Wu and Hu, 2006) for applications of EMD.

Finally, one can use of nonlinear tools that are unaffected by nonstationary of time series such as Detrended Fluctuation Analysis (DFA) (Hausdorff et al., 1995) and Recurrence Quantification Analysis (RQA) (Marwan, 2008; Trulla et al., 1996; Zbilut and Webber, 1992). However, Bryce and Sprague (2012) reported negatives of DFA such as the introduction of uncontrolled bias, computational expensiveness and mainly highlighting that DFA cannot provide a generic protection against the nonstationarities of the signals.

2.4.2 Data length

Many of the nonlinear tools are sensitive to time series length (Caballero et al., 2014). For example, given that Multiscale Entropy (MSE) is considered as statistical measure, the data lengths are recommended to be larger to ensure enough samples for the analysis (Costa et al., 2007). Also, LyE (Wolf et al., 1985) and DFA (Peng et al., 1995) metrics are sensitive to data length, while SampEn (Rhea et al., 2011) and FuzzyEn (Chen et al., 2007; Richman and Moorman, 2000) are less sensitive the time series length. However, the metrics of RQA (Riley et al., 1999; Webber and Zbilut, 1994; Wijnants et al., 2009) and PE (Zunino et al., 2009) are less sensitive to data length.

2.4.3 Sampling rate

One solution when dealing with data length problems is the increase or decrease of sampling rate (Caballero et al., 2014). However, Duarte and Sternad 2008, p. 267 stated "the increase of sampling rate frequency would only increase artificially the data points without adding information" which therefore is raise the problem of oversampling

Quantifying Movement Variability

signals. Then, Rhea et al. (2011) investigated the influence of sampling rate in three entropy measures (ApEn, SampEn and RQAEn) concluding that Ap and RQAEn were robust across to the increase of sampling frequency, while SampEn presented significant difference across all sampling frequencies. Rhea et al. (2011) noted that SampEn is more sensitive to coliniarities than Ap and RQAEn at higher frequencies which lead to a decrease of SampEn. Hence, Rhea et al. (2011) concluded that because signals at higher frequencies appear to be more regular due to the increase of data, therefore producing erroneous entropy results. Then, Caballero et al. (2013) showed the robustness of SampEn and DFA tools when using different sampling rate frequencies, stating that frequencies near the dynamics of the activity create a more reliable analysis of the dynamics using DFA values and tested the statement of Duarte and Sternad (2008) that increasing the sampling rate do not increase the gain of information. Caballero et al. (2013) also stated that the decrease of sampling rate frequency is recommended because it presents less consumption of computational power.

2.4.4 Noise

Another point to consider is the noise of the signals and how such noise affects nonlinear tools metrics (Caballero et al., 2014). For instance, Rosenstein et al. (1993) tested the robustness of LyE against three levels of noise (lowest, moderate and highest) noting the unreliability of LyE exponents in hight-noise environments. However, such case of unreliability of the LyE is unreal as the reported values of signal-to-noise ratios are substantially slower than the used at the experiments of Rosenstein et al. (1993). Another examples is the work of Chen et al. (2009) who compared the robustness FuzzEn, ApEn and SampEn metrics against different levels of noise, concluding that for a large value of the parameter r of ApEn and SampEn, these two metrics can work fine with highest level of noise, however when noise increase, ApEn and SampEn

fail to distinguish time series with different level of noise, whereas FuzzEn probe to be robust to such highest levels of noise. Also, Bandt and Pompe (2002) by proposing the Permutation Entropy metric (PeEn) showed the robustness of PeEn against observational noise and dynamical noise.

Regardless of the source of noise which can be either mechanical (due to recording equipment) or physiological (due to different neural noise), Rhea et al. (2011) highlighted the importance of the effects of noise in three entropy measures (ApEn, SampEn and RQAEn) which resulted in different results. For instance, values for AnEn and SampEn tended to increase as noise was added to the signals, while RQAEn showed an inverse effect, e.g. RQAEn values decreased as noise in the signal was increased. Similar results for synthetic data were also reported by Pellecchia and Shockley (2015) where RQAEn values decreased from ($RQAEn \approx 5$) for Lorenz system to a ($RQAEn \approx 2$) for a periodic signal with a further decrease ($RQAEn \approx 0.3$) for a sinusoid signal with superimposed noise. Therefore, RQA can also be affected by noise (Rhea et al., 2011). However, the effects with regard to noise and also nonstationarity can be mitigated with the selection of the right parameters to perform RQA, particularly, using embedding dimension from 10 to 20 for biological systems (Webber and Zbilut, 2005).

Another solution in order to deal with noisy time series is the use of tradition filtering methods, however the attenuation of all frequencies of the signal along the with the noise, given a cutoff frequency, can cut out information that might be useful for nonlinear time-series. Another option is apply DFA, which additionally to the remove of local trends, it also reduces the noise of the signal (Hausdorff et al., 1995). Alternatively, filtering strategies for nonlinear time-series data can be applied which tailor in a more effective way the properties of nonlinear dynamics (see Bradley and Kantz 2015 and references therein).

Chapter 3

Nonlinear Analyses

3.1 Introduction

The method of state space reconstruction was originally proposed by Packard et al. (1980) and formalised by Takens (1981). Since then, various investigations and disciplines relative to nonlinear time series analysis have benefited from it (Aguirre and Letellier, 2009; Frank et al., 2010; Samà et al., 2013; Stergiou and Decker, 2011). The method of state space reconstruction is based on uniform time-delay embedding which is a simple matrix implementation considering the embedding parameters (m and τ), therefore, matrix represents the reconstruction of an unknown d -dimensional manifold M from a scalar time series (e.g. one-dimensional time series in \mathbb{R}). A manifold, in this context, is a multidimensional curved surface within a space (e.g. a saddle) (Guastello and Gregson, 2011). Henceforth, The method of state space reconstruction using a scalar time series can preserve dynamic invariants such as correlation dimension, fractal dimension, Lyapponov exponents, Kolmogorov-Sinai entropy and detrended fluctuation analysis (Bradley and Kantz, 2015; Krakovská et al., 2015; Quintana-Duque and Saupe, 2013; Quintana-Duque, 2012, 2016). However, selecting appropriate embedding parameters is still an open challenge.

In the following subsections, we describe in more detail the state space reconstruction theorem (RSSs), uniform time-delay embedding theorem (UTDE), the methods to compute embedding parameters: false nearest neighbours (FNN) and average mutual information (AMI). We also introduce the fundamentals of Recurrence plots(RPs) and Recurrence quantification analysis (RQA).

3.2 State Space Reconstruction Theorem

Following the notation employed in Casdagli et al. (1991); Garland et al. (2016); Gibson et al. (1992); Takens (1981); Uzal et al. (2011); Uzal and Verdes (2010), the method of state space reconstruction is defined by:

$$s(t) = f^t[s(0)], \quad (3.1)$$

where $s, s : A \rightarrow M$ given that $A \subseteq \mathbb{R}$ and $M \subseteq \mathbb{R}^d$, represents a trajectory which evolves in an unknown d -dimensional manifold M , $f : M \rightarrow M$ is an evolution function and f^t , with time evolution $t \in \mathbb{N}$, is the t -th iteration of f that corresponds to an initial position $s(0) \in M$ (Takens, 1981). Then, a point of a scalar time series $x(t)$ in \mathbb{R} , can be obtained with

$$x(t) = h[s(t)], \quad (3.2)$$

where h is a function, $h : M \rightarrow \mathbb{R}$, defined on the trajectory $s(t)$.

Reconstructed state space can then be described as an n -dimensional state space defined by $y(t) = \Psi[\mathbf{X}(t)]$ where $\mathbf{X}(t) = \{x(t), x(t - \tau), \dots, x(t - (m - 1)\tau)\}$ is the uniform time-delay embedding with a dimension embedding m and delay embedding τ and $\Psi : \mathbb{R}^m \rightarrow \mathbb{R}^n$ is a further transformation of dimensionality (e.g. Principal

3.3 Uniform Time-Delay Embedding (UTDE)

Component Analysis, Singular Value Decomposition, etc) being $n \leq m$. With that in mind, uniform time-delay embedding, $\mathbf{X}(t)$, defines a map $\Phi : M \rightarrow \mathbb{R}^m$ such that $\mathbf{X}(t) = \Phi(s(t))$, where Φ is a diffeomorphic map (Takens, 1981) whenever $\tau > 0$ and $m > 2d_{box}$ and d_{box} is the box-counting dimension of M (Garland et al., 2016). Then, if Φ is an embedding of an attractor (i.e. evolving trajectories) in the reconstructed state space, a composition of functions represented with F^t is induced on the reconstructed state space:

$$\mathbf{X}(t) = F^t[\mathbf{X}(0)] = \Phi \circ f^t \circ \Phi^{-1}[\mathbf{X}(0)]. \quad (3.3)$$

Hence, an embedding is defined as "a smooth one-to-one coordinate transformation with a smooth inverse" (Casdagli et al., 1991, p. 54). Figure 3.1 illustrates the state space reconstruction.

3.3 Uniform Time-Delay Embedding (UTDE)

Frank et al. (2010) and Samà et al. (2013) refer to the state space reconstruction outlined in 3.2 as "time-delay embeddings" or "delay coordinates", respectively. However, we consider the term "uniform time-delay embedding" as more descriptive and appropriate terminology for this thesis.

The uniform time-delay embedding is represented as a matrix of uniform delayed copies of the time series $\{\mathbf{x}_n\}_{n=1}^N$ where N is the sample length of $\{\mathbf{x}_n\}$ and n is index for the samples of $\{\mathbf{x}_n\}$. $\{\mathbf{x}_n\}_{n=1}^N$ has a sample rate of T . The delayed copies of $\{\mathbf{x}_n\}$ are uniformly separated by τ and represented as $\{\tilde{\mathbf{x}}_{n-i\tau}\}$ where i goes from $0, 1, \dots, (m - 1)$ (Fig 3.2). $\{\tilde{\mathbf{x}}_{n-i\tau}\}$ contains information of unobserved state variables and encapsulates the information of the delayed copies of the available time series in

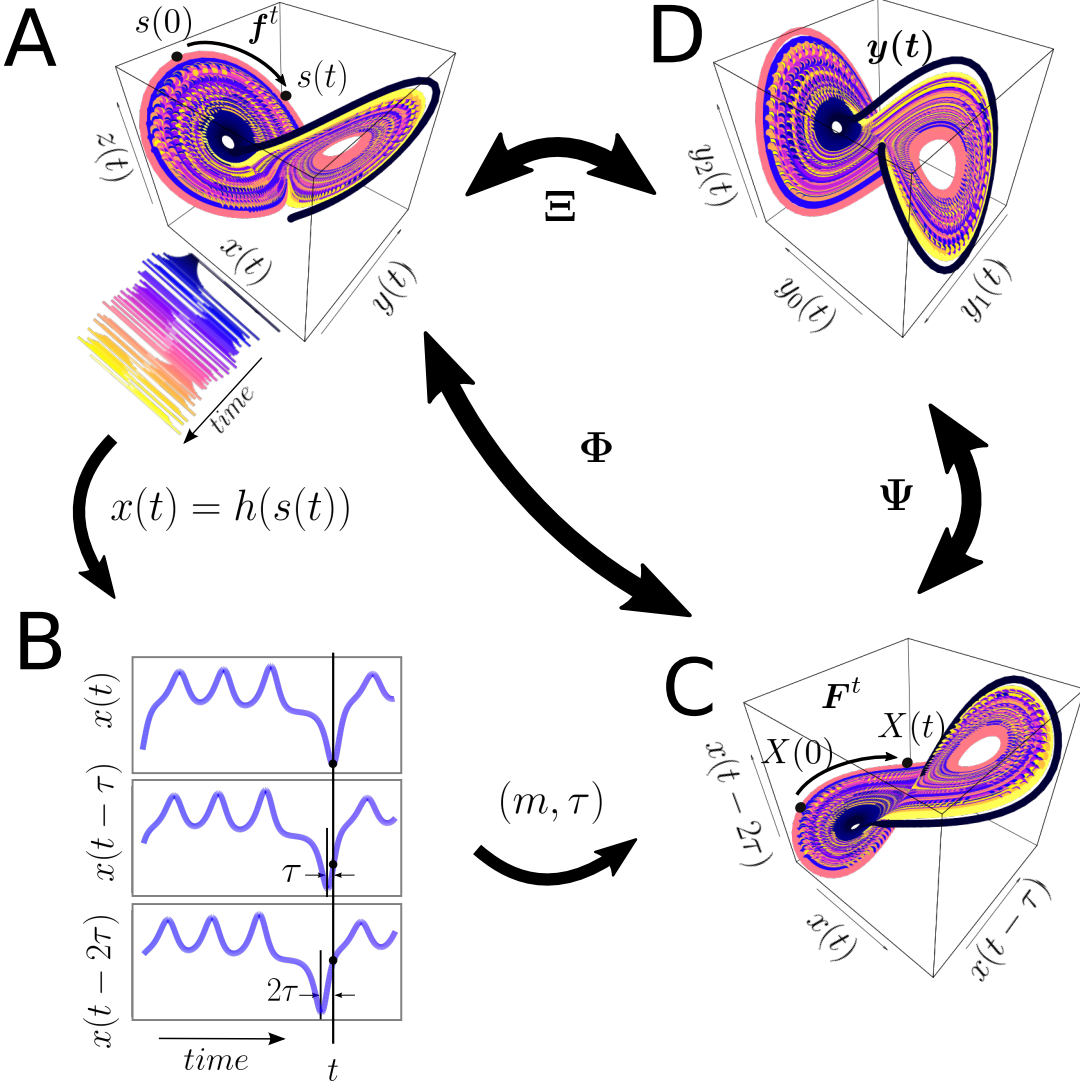


Fig. 3.1 State space reconstruction methodology. State space reconstruction is based on $x(t) = h[s(t)] = h[f^t[s(0)]]$ where $h[\cdot]$ is a function $h : M \rightarrow \mathbb{R}$, defined on the trajectory $s(t)$. f is the true dynamical system, $f : M \rightarrow M$, defined as evolution function and f^t , with time evolution $t \in \mathbb{N}$ which is the t -th iteration of f that corresponds to an initial position $s(0) \in M$. The time-delay embedding represented as the Φ , maps the original d -dimensional state $s(t)$ into the m -dimensional uniform time-delay embedding matrix $\mathbf{X}(t)$. The transformation map Ψ maps $\mathbf{X}(t)$ into a new state $y(t)$ of dimensions $n < m$. (A) M -dimensional state space (e.g. Lorenz system); (B) Delayed copies of 1-dimensional $x(t)$ from the Lorenz system; (C) m -dimensional reconstructed state space with m and τ , and (D) $y(t)$ is the n -dimensional reconstructed state space. The total reconstruction map is represented as $\Xi = \Psi \circ \Phi$ where Φ is the delay reconstruction map and Ψ is the coordinate transformation map. This figure is adapted from the work of Casdagli et al. (1991); Quintana-Duque (2012); Uzal et al. (2011) and R code to reproduce the figure is available from Xochicale (2018).

3.4 Estimation of Embedding Parameters

the uniform time-delay embedding matrix \mathbf{X}_τ^m , $\mathbf{X}_\tau^m \in \mathbb{R}^{m \times N}$, defined as

$$\mathbf{X}_\tau^m = \begin{pmatrix} \tilde{\mathbf{x}}_n \\ \tilde{\mathbf{x}}_{n-\tau} \\ \tilde{\mathbf{x}}_{n-2\tau} \\ \vdots \\ \tilde{\mathbf{x}}_{n-(m-1)\tau} \end{pmatrix}^\top, \quad (3.4)$$

where m is the embedding dimension, τ is the embedding delay and $^\top$ denotes the transpose. m and τ are known as embedding parameters. The matrix dimension of \mathbf{X}_τ^m is defined by $N - (m - 1)\tau$ rows and m columns and $N - (m - 1)\tau$ defines the length of each delayed copy of $\{\tilde{\mathbf{x}}_n\}$ in \mathbf{X}_τ^m . A graphical representation of uniform time-delay embedding is shown in Figure 3.2. For further details and explicit examples of uniform time-delay embedding methodology, we refer the reader to the appendix A.

3.4 Estimation of Embedding Parameters

The estimation of the embedding parameters (m and τ) is an essential step for the state space reconstruction in order to apply the method of uniform time-delay embedding (UTDE). Hence, we review two of the most common algorithms, which will be used in this thesis, to compute the embedding parameters: the false nearest neighbour (FNN) and the average mutual information (AMI).

3.4.1 False Nearest Neighbours (FNN)

To select the minimum embedding dimension m_0 , Kennel et al. (1992) used the method of false neighbours which can be understood as follows: on one hand, when the embedding dimension is too small to unfold the attractor (i.e. evolving trajectories in

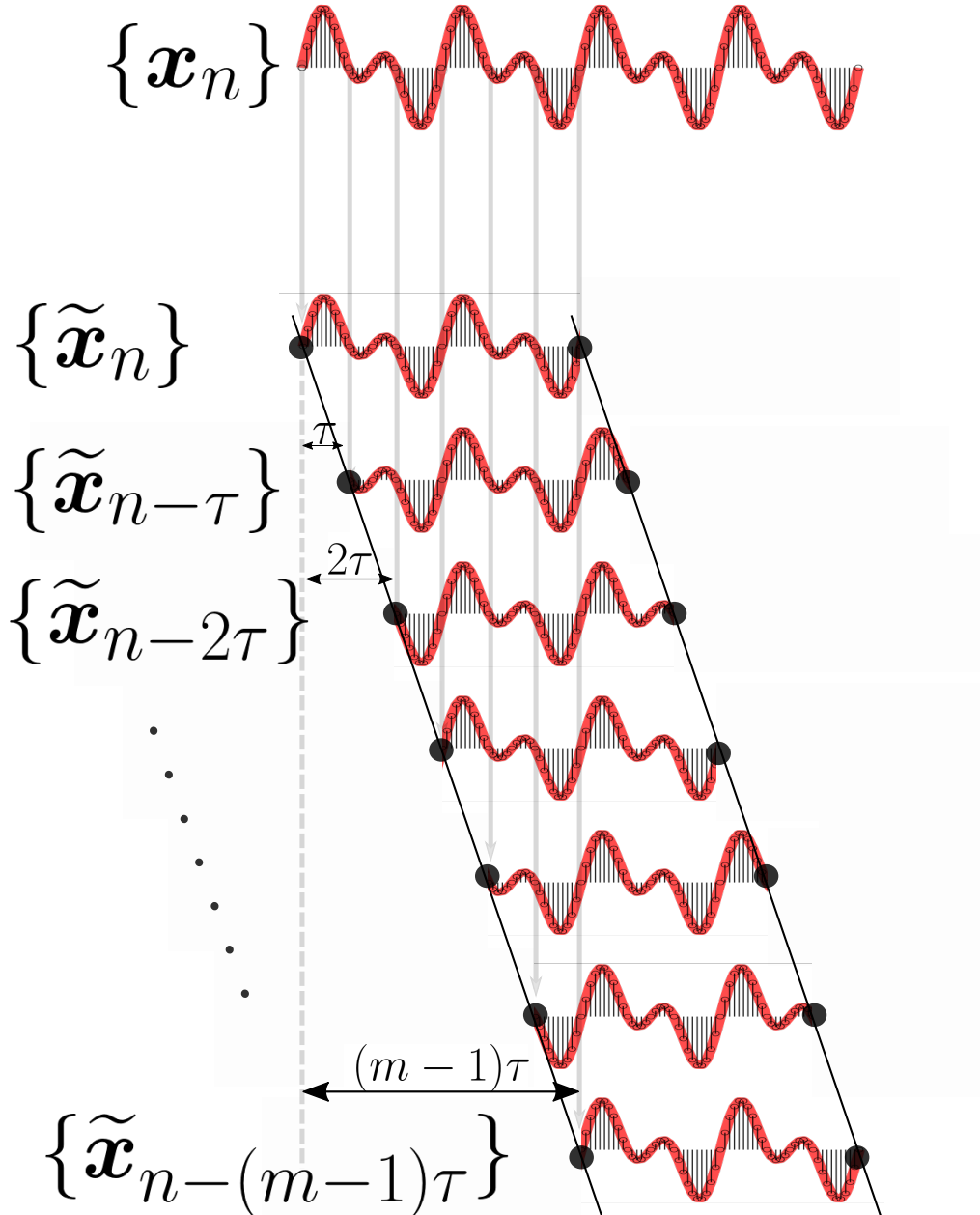


Fig. 3.2 Uniform time-delay embedding. UTDE is illustrated as $m - 1$ delayed copies of $\{x_n\}$, uniformly separated by τ and represented as $\{\tilde{x}_n, \dots, \tilde{x}_{n-(m-1)\tau}\}$ (Eq. 3.4). R code to reproduce the figure is available Xochicale (2018).

3.4 Estimation of Embedding Parameters

a state space) "not all points that lie close to each other will be neighbours and some points appear as neighbours as a result of the attractor being projected down into an smaller space", on the other hand, when increasing the embedding dimension "points that are near to each other in the sufficient embedding dimension should remain close as the dimension increase from m to $m + 1$ " (Krakovská et al., 2015, p. 3).

From a mathematical point of view, state space reconstruction is done when the attractor is unfolded with either the minimum embedding dimension, m_0 , or any other embedding dimension value where $m \geq m_0$ (Kennel et al., 1992). In contrast, any large value of m_0 leads to excessive computations (Bradley and Kantz, 2015). Hence, Cao (1997) proposed an algorithm based on the false neighbour method where only the time-series and one delay embedding value are necessary to select the minimum embedding dimension. Cao's algorithm is based on $E(m)$ which is the mean value of all $a(i, m)$, both defined as:

$$\begin{aligned} E(m) &= \frac{1}{N - m\tau} \sum_{i=1}^{N-m\tau} a(i, m) \\ &= \frac{1}{N - m\tau} \sum_{i=1}^{N-m\tau} \frac{\|\mathbf{X}_i(m+1) - \mathbf{X}_{n(i,m)}(m+1)\|}{\|\mathbf{X}_i(m) - \mathbf{X}_{n(i,m)}(m)\|} \end{aligned} \quad (3.5)$$

where $\mathbf{X}_i(m)$ and $\mathbf{X}_{n(i,m)}(m)$ are the time-delay embeddings with $i = 1, 2, \dots, N - (m - 1)\tau$ and $n(i, m) = 1 \leq n(i, m) \leq N - m\tau$. From Eq. 3.5 $E(m)$ is only dependent on m and τ for which $E_1(m)$ is defined as

$$E_1(m) = \frac{E(m+1)}{E(m)}. \quad (3.6)$$

$E_1(m)$ is therefore proposed to investigate the variation from m to $m + 1$ in order to find the minimum embedding dimension m_0 (Eq. 3.6). As Cao 1997, p. 44 described: " $E_1(m)$ stops changing when m is greater than some m_0 , if the time series comes from a multidimensional state space then $m_0 + 1$ is the minimum dimension". Additionally,

Nonlinear Analyses

Cao (1997) proposed $E_2(m)$ to distinguish deterministic signals from stochastic signals. $E_2(m)$ is defined as

$$E_2(m) = \frac{E^*(m+1)}{E^*(m)}, \quad (3.7)$$

where

$$E^*(m) = \frac{1}{N - m\tau} \sum_{i=1}^{N-m\tau} |\mathbf{X}_i(m+1) - \mathbf{X}_{n(i,m)}(m+1)|. \quad (3.8)$$

For instance, when the signal comes from random noise (values that are independent from each other), all $E_2(m)$ values are approximately equal to 1 (e.g. $E_2(m) \approx 1$). However, for deterministic data $E_2(m)$ is not constant for all m (e.g. $E_2(m) \neq 1$).

As an example of the use of $E_1(m)$ and $E_2(m)$ values, we consider two time series: the solution for the x variable of the chaotic deterministic Lorenz system (Figure 3.3E), and a Gaussian noise time series with zero mean and a variance of one (Figure 3.3F). We then compute $E_1(m)$ and $E_2(m)$ values for each time series. The $E_1(m)$ values for the chaotic time series appear to be constant after the dimension is equal to six. The determination of six is given that any value of m can be used as $E_1(m)$ values are within the threshold of 1 ± 0.05 (Fig 3.3A). Although the $E_2(m)$ values for the chaotic time series tend to be closer to one as m increases, these are different to one (Fig 3.3C), for which, it can be concluded that the chaotic time series comes from a chaotic deterministic signal. With regard to the noise time series, $E_1(m)$ values appeared to be constant when m is close to thirteen which is defined by the same threshold of 1 ± 0.05 (Figure 3.3B). Then, contrary to the $E_2(m)$ values for a chaotic Lorenz time series, all values of $E_2(m)$ for a noise time series are approximately equal to one (Figure 3.3D). Hence, $E_1(m)$ values then indicate the minimum embedding dimension of the noisy time series is thirteen, however all of the $E_2(m)$ values are approximately equal to one (Figure 3.3D) for which it can be concluded that noise time series is a stochastic signal.

3.4 Estimation of Embedding Parameters

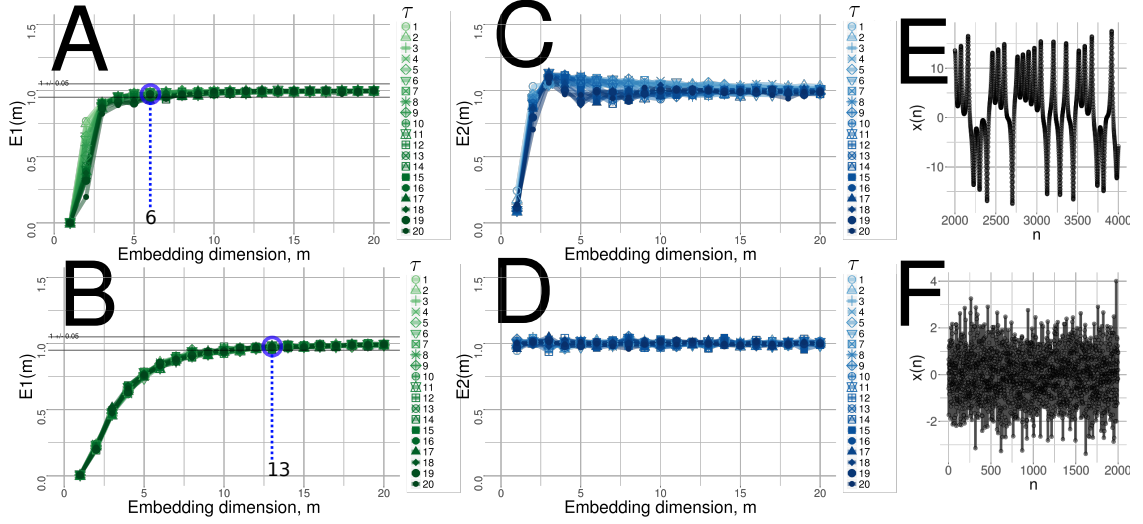


Fig. 3.3 Minimum dimension embedding values with Cao’s method. (A, B) $E_1(m)$ values and (C, D) $E_2(m)$ values with variations of τ values from one to twenty for (E) chaotic and (F) random time series. R code to reproduce the figure is available from Xochicale (2018).

It is important to note that for this thesis not only the values for $E_1(m)$ and $E_2(m)$ are computed but also a variation of τ from 1 to 20 (Figure 3.3A,B,C and D) has been presented. The purpose of the increasing variation for τ is to show its independence with regard to the $E_1(m)$ and $E_2(m)$ (Figure 3.3A,B,C, and D). Although Cao (1997) mentioned that no parameters are required to find the minimum embedding dimension, we found that it is required to define a new threshold for which $E_1(m)$ values appear to be constant. Hence, for the given examples and the reported results for this thesis, we defined a threshold to be 0.05.

3.4.2 Average Mutual Information (AMI)

When selecting the delay dimension parameter, τ , one can consider the following two cases: (i) when τ is too small, the elements of time-delay embedding will be along the bisectrix of the phase space and the reconstruction is generally not satisfactory, (ii) when τ is too large the elements of the uniform time-delay embedding will become

Nonlinear Analyses

spread and uncorrelated which makes recovering the underlying attractor (i.e. evolving trajectories in a state space) difficult if not impossible (Casdagli et al., 1991; Emrani et al., 2014; Garcia and Almeida, 2005).

There are many approaches to compute the embedding parameters (Bradley and Kantz, 2015), for instance, geometry-based methodologies where the amount of space filled in the reconstructed state is the metric to compute the delay embedding (Rosenstein et al., 1994) or theoretical approaches to estimate an optimal parameter for τ Casdagli et al. (1991). However, the autocorrelation function and the average mutual information (AMI) are the two most commonly used algorithms to compute the minimum delay embedding parameter τ_0 . Emrani et al. (2014) used the autocorrelation function in which the first zero crossing is considered as the minimum delay embedding parameter. However, the autocorrelation function is a linear statistic whereas AMI considers the nonlinear dynamical correlations (Fraser and Swinney, 1986; Krakovská et al., 2015). With that in mind, the AMI algorithm is described below to estimate the minimum delay embedding parameter, τ_0 .

To compute the AMI, an histogram of $x(n)$ using n bins is calculated and then a probability distribution of data is computed (Kantz and Schreiber, 2003). AMI is therefore denoted by $I(\tau)$ which is the average mutual information between the original time series, $x(n)$, and the delayed time series, $x(n - \tau)$, delayed by τ (Kabiraj et al., 2012). AMI is defined by

$$I(\tau) = \sum_{i,j}^N p_{ij} \log_2 \frac{p_{ij}}{p_i p_j}. \quad (3.9)$$

Probabilities are defined as follows: p_i is the probability that $x(n)$ has a value inside the i -th bin of the histogram, p_j is the probability that $x(n + \tau)$ has a value inside the j -th bin of the histogram and $p_{ij}(\tau)$ is the probability that $x(n)$ is in bin i and $x(n + \tau)$ is in bin j . The AMI is measured in bits (base 2, also called shannons) (Garcia and Sawitzki, 2016; Kantz and Schreiber, 2003). For small τ ($\tau < 3$), AMI will be large (

3.4 Estimation of Embedding Parameters

$I(\tau) > 6$) and as m increase AMI will then decrease rapidly. Hence, as τ increase and goes to a large limit, $x(n)$ and $x(n + \tau)$ have nothing to do with each other and $p(ij)$ is factorised as $p_i p_j$ for which AMI is close to zero. Then, in order to obtain τ_0 , "it has to be found in the first minimum of $I(\tau)$ where $x(n + \tau)$ adds maximal information to the knowledge from $x(n)$ " meaning that the redundancy between $x(n + \tau)$ and $x(n)$ is the least (Kantz and Schreiber, 2003, p. 151).

For example, we compute the AMI for two time series: (i) the x solution of the deterministic chaotic Lorenz system, and (ii) a noise time series using a normal distribution with mean zero and standard deviation equal to one. The AMI plots are shown in Figure 3.4, where the minimum delay embedding parameter for the chaotic time series is $\tau_0 = 17$ and for the noise time series is $\tau_0 = 1$. Hence, it can be concluded that the amount of knowledge for any noise time series is zero for which the first minimum embedding parameter is equal to one. On the contrary, the first minimum of the AMI for the chaotic time series is $\tau_0 = 17$ which is the value that maximize the independence in the reconstructed state space (Bradley and Kantz, 2015).

3.4.3 Overall minimum embedding parameters

The method to select minimum embedding parameters (m_0 and τ_0) for this thesis is firstly to compute m_0 with FNN algorithm (considering a threshold of 0.05 for $E_1(m)$ values), secondly to compute τ_0 with AMI which does not need any extra parameters. Hence, from the previous example of the chaotic deterministic Lorenz system, Fig 3.3(A) is used to determine the minimum dimension embedding with a value of seventeen ($m_0 = 6$) and Fig 3.4(A) is used to determine the minimum delay embedding with a value of seventeen ($\tau_0 = 17$). Therefore with the selection of the minimum embedding parameters, the reconstructed attractor is created in order to

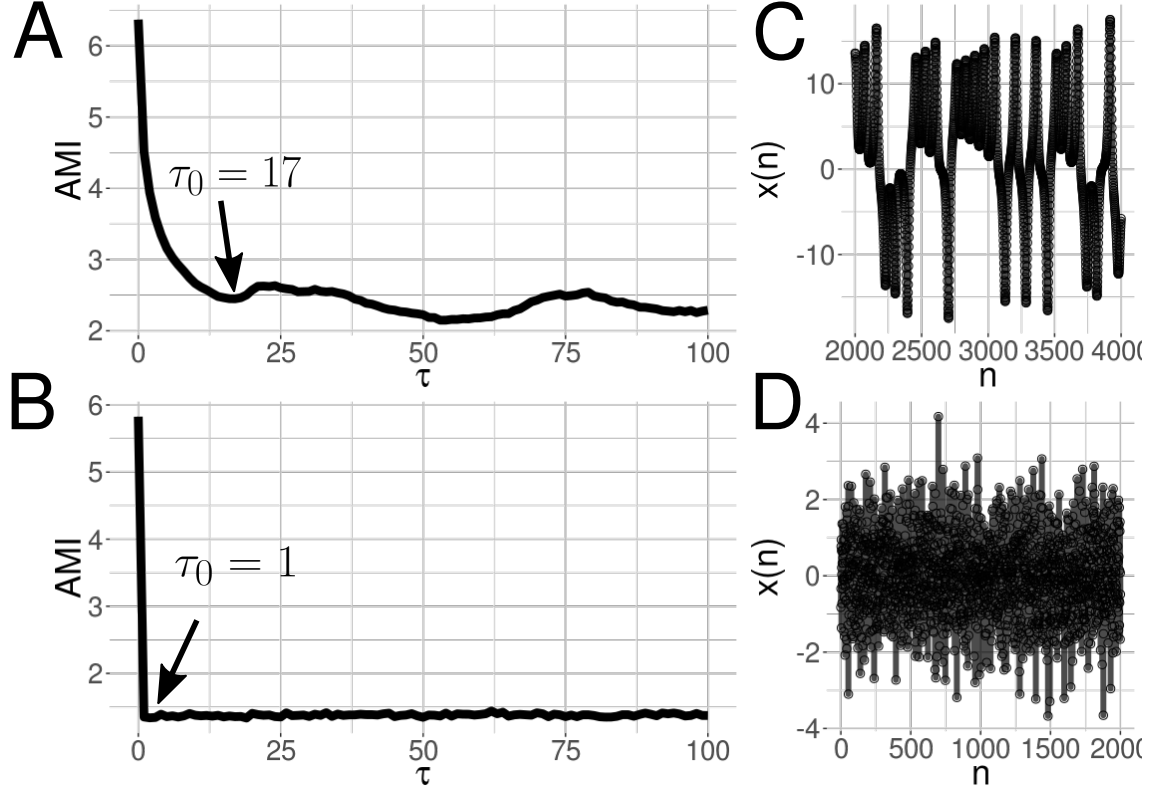


Fig. 3.4 Minimum delay embedding values with AMI's method. (A, B) AMI values where its first minimum value in the curve is the minimum time delay embedding (τ_0), for (C) a chaotic and (D) noise time series. R code to reproduce the figure is available from Xochicale (2018).

ensure with τ_0 the maximum independence between $x(t)$ and $x(t + \tau_0)$ and with m_0 allowing the trajectories in the reconstructed state space to be unfolded.

We use sample mean for an overall value of embedding minimum embedding parameters $(\bar{m}_0, \bar{\tau}_0)$ in which minimum values (m_{0_i}, τ_{0_i}) are averaged over N which is the total number of minimum embedding values:

$$\bar{m}_0 = \frac{1}{N} \sum_{i=1}^N m_{0_i}, \quad (3.10)$$

$$\bar{\tau}_0 = \frac{1}{N} \sum_{i=1}^N \tau_{0_i}. \quad (3.11)$$

3.5 Reconstructed State Space with UTDE

Given a time series $x(n)$, the UTDE matrix is computed with its minimum embedding parameters and then PCA is applied in order to select the first three axis of the rotated data to create the reconstructed state spaces (Frank et al., 2010; Samà et al., 2013).

3.6 Recurrence Plots (RP)

Henri Poincaré in 1890 introduced the concept of recurrences in conservative systems, however the discovery was not put into practice until the development of faster computers (Marwan et al., 2007), for which Eckmann et al. (1987) introduced a method where recurrences in the dynamics of a system can be visualised using Recurrence Plots (RP). The intention of Eckmann et al. Eckmann et al. (1987) was to propose a tool, called Recurrence Plot (RP), that provides insights into high-dimensional dynamical systems where trajectories are very difficult to visualise. Hence, "RP is a tool that helps us to investigate the m -dimensional phase space trajectories through a two-dimensional representation of its recurrences" (Marwan and Webber, 2015, p. 7). Similarly, Marwan and Webber (2015) pointed out that in addition to the methodologies of the state space reconstruction and other dynamic invariants (e.g. Lyapunov exponent, Kolmogorov-Sinai entropy), the recurrences of the trajectories in the phase space can provide important clues to characterise the underlying process for periodicities (as Milankovitch cycles) or irregular cycles (as El Niño Southern Oscillation). Such recurrences can not only be visualised using Recurrence Plots (RP) but also be quantified with Recurrence Quantification Analysis (RQA) metrics, which leads to applications of these tools in various areas such as Economics, Physiology, Neuroscience, Earth Science, Astrophysics and Engineering (Marwan et al., 2007).

A recurrence plot based on time series $\{\mathbf{x}_n\}$ is computed from the state space reconstruction with uniform time-delay embedding method $X(i) = \{\tilde{\mathbf{x}}_n, \dots, \tilde{\mathbf{x}}_{n-(m-1)\tau}\}$ where $i = 1, \dots, N$, N is the number of considered states of $X(i)$ and $X(i) \in \mathbb{R}^m$ (Eckmann et al., 1987). The recurrence plot is therefore a two-dimensional $N \times N$ square matrix, \mathbf{R} , where a black dot is placed at (i, j) whenever $X(i)$ is sufficiently close to $X(j)$:

$$\mathbf{R}_{i,j}^m(\epsilon) = \Theta(\epsilon_i - \|X(i) - X(j)\|), \quad X(i) \in \mathbb{R}^m, \quad i, j = 1, \dots, N, \quad (3.12)$$

where N is the number of considered states of $X(i)$, ϵ is a threshold distance, $\|\cdot\|$ a norm, and $\Theta(\cdot)$ is the Heaviside function (i.e. $\Theta(x) = 0$, if $x < 0$, and $\Theta(x) = 1$ otherwise) (Fig 3.5) (Eckmann et al., 1987; Marwan et al., 2007; Marwan and Webber, 2015). RP is also characterised with a line of identity (LOI) which is a black main diagonal line due to $R_{i,j} = 1$ ($i, j = 1, \dots, N$).

3.6.1 Structures of Recurrence Plots

Pattern formations in RPs can be designated either as topology for large-scale patterns or texture for small-scale patterns. In the case of topology, the following pattern formations are presented: (i) homogeneous where uniform recurrence points are spread in the RP e.g., uniformly distributed noise (Figure 3.6A), (ii) periodic and quasi-periodic systems where diagonal lines and checkerboard structures represent oscillating systems, e.g., sinusoidal signals (Figure 3.6B), (iii) drift where paling or darkening recurrence points away from the LOI is caused by drifting systems, e.g., logistic map (Figure 3.6C), and (iv) disrupted where recurrence points are presented white areas or bands that indicate abrupt changes in the dynamics, e.g. Brownian motion (Figure 3.6D) (Eckmann et al., 1987; Marwan and Webber, 2015). Texture, for small-scale patterns, can be categorised as: (i) single or isolated recurrence points that

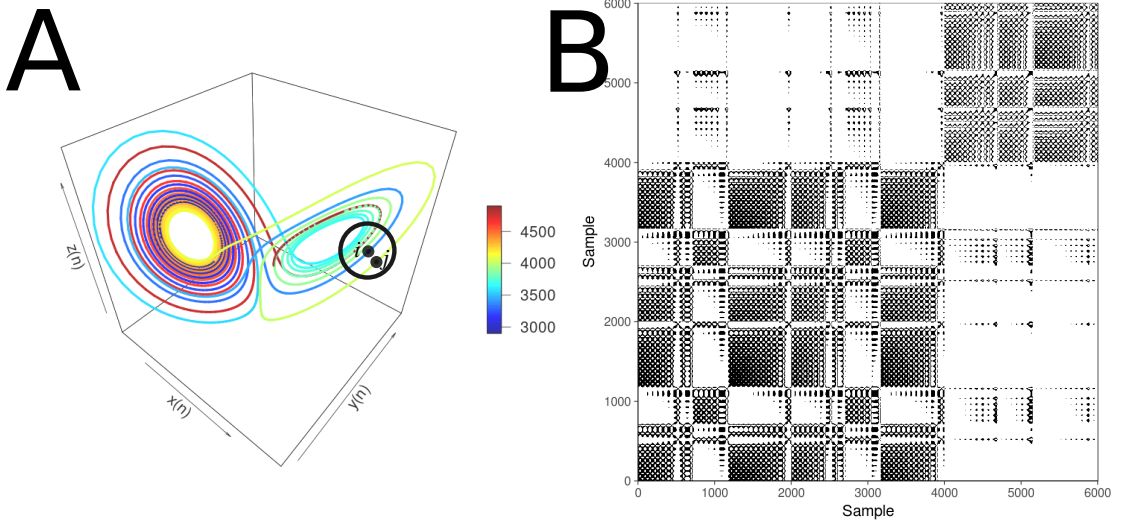


Fig. 3.5 Recurrence Plots. (A) State space of the Lorenz system with controlling parameters ($\rho = 28, \sigma = 10, \beta = 8/3$). A point, j , in trajectory $X()$ which falls into the neighborhood (black circle) of a given point at i is a recurrent point and is represented as a black dot in the recurrence plot at location (i, j) or white otherwise. (B) Recurrence plot using the three components of the Lorenz system and the RP with no embeddings and threshold $\epsilon = 5$. This figure is adapted from Marwan and Webber (2015) and R code to reproduce it is available from Xochicale (2018).

represent rare occurring states, do not persist for any time or fluctuate heavily, (ii) dots forming diagonal lines where the length of the small-scale parallel lines in the diagonal are related to the ratio of determinism or predictability in the dynamics of the system, and (iii) dots forming vertical and horizontal lines where the length of the lines represent a time length where a state does not change or change very slowly and the patterns formation represent discontinuities in the signal, and (iv) dots clustering to inscribe rectangular regions which are by related to laminar states or singularities (Marwan and Webber, 2015).

Although, each of the previous pattern descriptions of the structures in the RP offer an idea of the characteristics of dynamical systems from time-series, these descriptions might be misinterpreted and conclusions might tend to be subjective as these require the interpretation of a researcher(s). Because of that, recurrence quantification analysis

Nonlinear Analyses

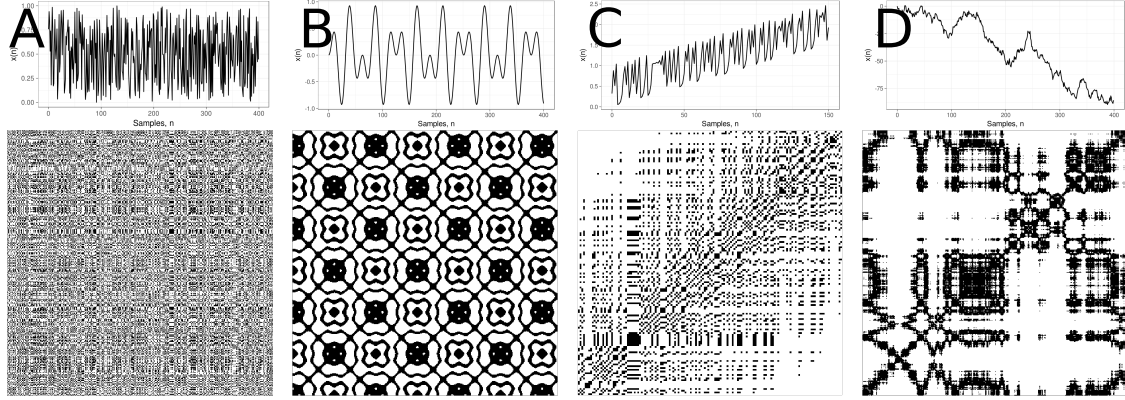


Fig. 3.6 Patterns in Recurrence Plots. Time-series with its respective recurrence plots for: (A) uniformly distributed noise, (B) super-positioned harmonic oscillation ($\sin(\frac{1}{5} * t) * \sin(\frac{5}{100} * t)$), (C) drift logistic map ($x_{i+1} = 4x_i(1 - x_i)$) corrupted with a linearly increase term ($0.01 * i$), and (D) disrupted brownian motion ($x_{i+1} = x_i + 2 * rnorm(1)$). Figure is adapted from Marwan and Webber (2015) and R code to reproduce the figure is available from Xochicale (2018).

(RQA) offer objective metrics to quantify the visual characteristics of recurrent pattern structures in the RP (Zbilut and Webber, 1992).

3.7 Recurrence Quantifications Analysis (RQA)

Zbilut and Webber (1992) proposed metrics to investigate the density of recurrence points in RPs, then histograms of lengths for diagonal lines in RPs were studied by Trulla et al. (1996), then Marwan (2008) introduced the term Recurrence Quantification Analysis (RQA). RQA metrics are percentage of recurrence, percentage of determinism, ratio, Shannon entropy of the frequency distributions of the line lengths, maximal line length and divergence, trend and laminariy (Marwan et al., 2007; Marwan and Webber, 2015).

3.7 Recurrence Quantifications Analysis (RQA)

3.7.1 Measures of RP based on the recurrence density

The percentage of recurrence (REC) or recurrence rate (RR) is defined as

$$REC(\epsilon, N) = \frac{1}{N^2 - N} \sum_{i \neq j=1}^N \mathbf{R}_{i,j}^m(\epsilon), \quad (3.13)$$

which enumerates the black dots in the RP excluding the line of identity. RR is a measure of the relative density of recurrence points in the sparse matrix (Marwan and Webber, 2015).

3.7.2 Measures of RP based on diagonal lines

The percent determinism (DET) is defined as the fraction of recurrence points that form diagonal lines and it is determined by

$$DET = \frac{\sum_{l=d_{min}}^N l H_D l}{\sum_{i,j=1}^N \mathbf{R}_{i,j}(\epsilon)}, \quad (3.14)$$

where

$$H_D(l) = \sum_{i,j=1}^N (1 - \mathbf{R}_{i-1,j-1}(\epsilon))(1 - \mathbf{R}_{i+l,j+l}(\epsilon)) \prod_{k=0}^{l-1} \mathbf{R}_{i+k,j+k}(\epsilon) \quad (3.15)$$

is the histogram of the lengths of the diagonal structures in the RP. DET can be interpreted as the predictability of the system for periodic signals which, in essence, have longer diagonal lines for chaotic signals shorter or absent diagonal lines for stochastic signals (Marwan et al., 2007; Marwan and Webber, 2015). Similarly, DET is considered as a measurement for the organisation of points in RPs (Iwanski and Bradley, 1998).

RATIO is defined as the ratio between DET and REC and it is calculated from the frequency distributions of the lengths of the diagonal lines. RATIO is useful to discover dynamic transitions (Marwan and Webber, 2015).

Nonlinear Analyses

D_{max} is the longest diagonal line in the RP, defined as

$$D_{max} = \arg, \max_l H_D(l). \quad (3.16)$$

D_{max} is an indicator of the divergence of trajectory segments. The smaller D_{max} is, the more divergent the trajectories are (Marwan et al., 2007; Marwan and Webber, 2015). According to Iwanski and Bradley (1998), D_{max} is also related to the inverse of the largest positive Lyapunov exponent, where for example periodic signals tend to have very long lines, as opposed to the chaotic time series where parallel lines are shorter.

The average diagonal line length is defined as

$$\langle D \rangle = \frac{\sum_{l=d_{min}}^N l H_D(l)}{\sum_{l=d_{min}}^N H_D(l)}, \quad (3.17)$$

and it is the average time that two segments of the trajectory are close to each other. $\langle D \rangle$ can be interpreted as a measure for determinism (predictability) of the system (Marwan et al., 2007; Marwan and Webber, 2015).

ENT is the Shannon entropy of the frequency distribution of the diagonal line lengths and it is defined as

$$ENT = - \sum_{l=d_{min}}^N p(l) \ln p(l) \quad \text{with} \quad p(l) = \frac{H_D(l)}{\sum_{l=d_{min}}^N H_D(l)}. \quad (3.18)$$

ENT reflects the complexity of the deterministic structure in the system. For instance, for uncorrelated noise or oscillations, the value of ENT is rather small and indicates low complexity of the system, therefore "the higher the ENT is the more complex the dynamics are" (Marwan and Webber, 2015, p. 15).

3.7 Recurrence Quantifications Analysis (RQA)

Trend (TND) "is a linear regression coefficient over the recurrence point density of the diagonals parallel to the LOI" (Marwan and Webber, 2015, p. 16) and is defined as

$$TND = \frac{\sum_{i=1}^{\tilde{N}} (1 - \tilde{N}/2)(RR_i - \langle RR_i \rangle)}{\sum_{i=1}^{\tilde{N}} (i - \tilde{N}/2)^2}. \quad (3.19)$$

Trend value "provides information about the stationarity versus nonstationarity in the process" (Marwan and Webber, 2015, p. 16). TNT values near to zero represent quasi-stationary dynamics and TNT values far from zero represent nonstationary dynamics that reveal the "drift in the dynamics" (Marwan and Webber, 2015, p. 16). TNT measures how quickly the RP pales away from the main diagonal (Iwanski and Bradley, 1998).

3.7.3 Measures of RP based on vertical lines

The previous RQA metrics are based on length, number and distribution of diagonal lines. However, patterns for horizontal and vertical lines can also be quantified. The following are some examples.

Laminarity (LAM) computes the percentage of recurrence points in vertical lines which is analogous to the DET variable Marwan and Webber (2015).

Trapping time (TT) variable computes the average length of vertical lines. "TT contains information about the amount and length of vertical structures in the RP" which represent "the mean time the system will" stay "at a specific time" (Marwan and Webber, 2015, p. 17).

The maximal length of the vertical structures V_{max} represents "the longest vertical line in the RP" which is analogous to D_{max} . According to Marwan et al. (Marwan and Webber, 2015, p. 17) the dynamical interpretation of this variable is not clear but only as a relationship with "singular states in which the system is stuck in a holding pattern inscribing rectangles in the RP".

3.7.4 The weakness and strengths of RP and RQA.

One of the main advantages of the use of RP is their capacity to detect small modulations in frequency or phase that are not detectable using standard methods e.g. spectral or wavelet analysis (Marwan, 2011). Nonetheless, RP is a very young field in nonlinear dynamics and many questions are still open, for instance, different parameters for window length size of the time series, embedding parameters or recurrence threshold can generate different results in RQA metrics (Eckmann et al., 1987; Marwan, 2011). Additionally, the selection of recurrence threshold, ϵ , can depend on the system that is analysed. For instance, when studying dynamical invariants ϵ require to be very small, for trajectory reconstruction ϵ requires to have a large thresholds or when studying dynamical transition there is little importance about the selection of the threshold (Marwan, 2011). Other criteria for the selection of ϵ is that the recurrence threshold should be five times larger than the standard deviation of the observational noise or the use of diagonal structures within the RP is suggested in order to find the optimal recurrence threshold for (quasi-)periodic process (Marwan, 2011).

Similarly, Iwanski and Bradley (1998) highlighted the importance of choosing the right embedding parameters to perform RQA for which many experiments have to be performed using different parameters in order to have a better intuition of the nature of the time series and how this is represented by using RQA. In the same investigation, Iwanski and Bradley (1998) pointed out that RQA metrics are quantitatively and qualitatively independent of embedding dimension. However, with an example, Iwanski and Bradley (1998) showed that two dissimilar RPs one from the Rössler system and the other from a sine-wave signal of varying period have got equal values of REC (2.1%) and have approximately equal values of DET (42.9%, 45.8%, respectively). Also, Iwanski and Bradley (1998) pointed out the importance of choosing the right parameters to perform RQA, since many experiments must be performed with different

3.7 Recurrence Quantifications Analysis (RQA)

parameters to have a better intuition of the nature of the time series and how this is represented using RQA. Other example to determine embedding parameters for the RQA is the method of Zbilut and Webber (1992) in which 3D surfaces are created with an increase of embedding parameters (m and τ), then, for instance, Zbilut and Webber (1992) explored fluctuations and gradual changes in the 3D surfaces that provide information about the embeddings parameters. Recently, Marwan and Webber (2015) created 3D surfaces for visual selection of not only embedding parameters but also recurrence thresholds.

With that, therefore, it can be stated for this thesis that little has been investigated with regards to: (i) the strengthens and weaknesses of different nonlinear tools when using real-world data which is nonstationarity, noisy and has different sampling rate and length (Section 2.4), (ii) different models for movement variability where, for instance, not only the model of Stergiou et al. (2006) where complexity and predictability variables can characterise movement variability but also it can take into account the dependencies of the task dynamics (Vaillancourt and Newell, 2002, 2003) (Section 2.3.2), and (iii) the selection and application the right tools in order to quantify MV (Section 2.3.3). We, therefore, explore, in this thesis, the weaknesses and strengths of the window size of time series, embedding parameters for RSS with UTDE and recurrence threshold for RP and RQA in order to gain a better insight into the underlying time series collected from inertial sensors in the context of human-humanoid imitation activities.

Chapter 4

Experiments

4.1 Aims

Not only tackling the weaknesses and robustness of RSS, UTDE, embedding parameters, RP and RQA metrics regarding different conditions for time-series (smoothness, windowsizes and structures), but also considering the models of Stergiou et al. (2006) and (Vaillancourt and Newell, 2002, 2003) for movement movement variability, we design two experiments in the context of human-humanoid interaction where participants perform simple arm movements repetitions.

4.2 Participants

For this thesis, twenty-three participants, from now on defined as pN where N is the number of participant, were invited for two experiments of simple arm movements. Although the same number of participants were invited for the experiments, different number of participants were take into account for each of the experiments.

Experiments

4.2.1 Human-Image Imitation Activities

4.2.2 Human-Humanoid Imitation Activities

For the experiment of Human-Humanoid Imitation Activities, data for only twenty participants were analysed since the instructions for *p01*, who was the only left-handed, were mistakenly given in a way that movements were performed different from what had been planned, and for participants *p13* and *p16* data were corrupted because bluetooth communications problems with the sensors. With that in mind, all of the 20 participants were right-handed healthy participants, being four females and sixteen males, with a mean and standard deviation (SD) age of mean=19.8 (SD=1.39) years.

4.3 Equipment

During the experiments, time series were collected with four neMEMSi Inertial Measurement Units (IMUs) using a sampling rate of 50Hz (Comotti et al., 2014). neMEMSi sensors provide tri-axial time series from the accelerometer, gyroscope and magnetometer sensors and quaternions. A further technical information regarding the NeMEMSi IMU sensors is given in Appendix B.1. For the human-humanoid imitation activities, NAO, a humanoid robot from Aldebaran (Gouaillier et al., 2009), were programmed with choreographer to perform horizontal and vertical arm movements. A further technical information regarding NAO and the code of NAO's movements is given in Appendix B.3

4.4 Ethics

For the experiments of this thesis conducted in November 2016, participants confirmed reading and understanding the participant information sheet for the experiments and

were able to withdraw from the experiment at any time without giving any reason. The design of the experiments is adhered to University of Birmingham regulations and data were anonymised and stored only on a personal computer in accordance with the Data Protection Act 1998. For further information about the ethics, online participation information sheets and experiment check list, refer to Appendix C.

4.5 Experiments

4.5.1 Human-Image Imitation Activities

For the human-image imitation (HHI) experiment four wearable IMUs sensors were used and attached to the right hand of the participant (Figure 4.1 A,D). Participants performed two experiments: (i) an unconstrained arm movement imitation activity where participants only receive instructions and look at images of the movement and, (ii) a constrained experiment where participants hear a beat to synchronise their arm movements.

Arm movements following an image while not hearing a beat

Participants received instructions to perform upper arm movements while only looking at an image of:

- ten repetitions of horizontal arm movement at their comfortable speed (Fig. 4.1(A, B, C)),
- ten repetitions of vertical arm movement at their comfortable speed (Fig. 4.1(D, F, E)),
- ten repetitions of horizontal arm movement at a faster speed than the comfortable speed but not at their fastest speed (Fig. 4.1(A, B, C)), and

Experiments

- ten repetitions of vertical arm movement at a faster speed than the comfortable speed but not at their fastest speed (Fig. 4.1(D, F, E)).

Arm movements following an image while hearing a beat

Participants received instructions to perform upper arm movements while listening a beat to constraint their movements.

- ten repetitions of horizontal arm movement at normal speed (Fig. 4.1(A, B, C)),
- ten repetitions of vertical arm movement at normal speed (Fig. 4.1(D, F, E)),
- ten repetitions of horizontal arm movement at faster speed and (Fig. 4.1(A, B, C)), and
- ten repetitions of vertical arm movement at faster speed (Fig. 4.1(D, F, E)).

4.5.2 Human-Humanoid Imitation Activities

For the human-humanoid imitation (HHI) experiment four wearable IMUs sensors were used in which two sensors were attached to the right hand of the participant and two sensors were attached to the left hand of the humanoid robot (Figure 4.2 A,C). Then, in the face-to-face imitation activity each participant was asked to imitate repetitions of simple horizontal and vertical arm movements performed by the humanoid robot in the following conditions:

- ten repetitions of horizontal arm movement at normal (HN) and faster (HF) speed (Fi. 4.2 A), and
- ten repetitions of vertical arm movement at normal (VN) and faster (VF) speed (Fig. 4.2 C).

The normal and faster speed of arm movements is defined by the duration in number of samples of one repetition of NAO's arm movements. We select NAO's arm movements duration to distinguish between normal and faster arm movements as the movements

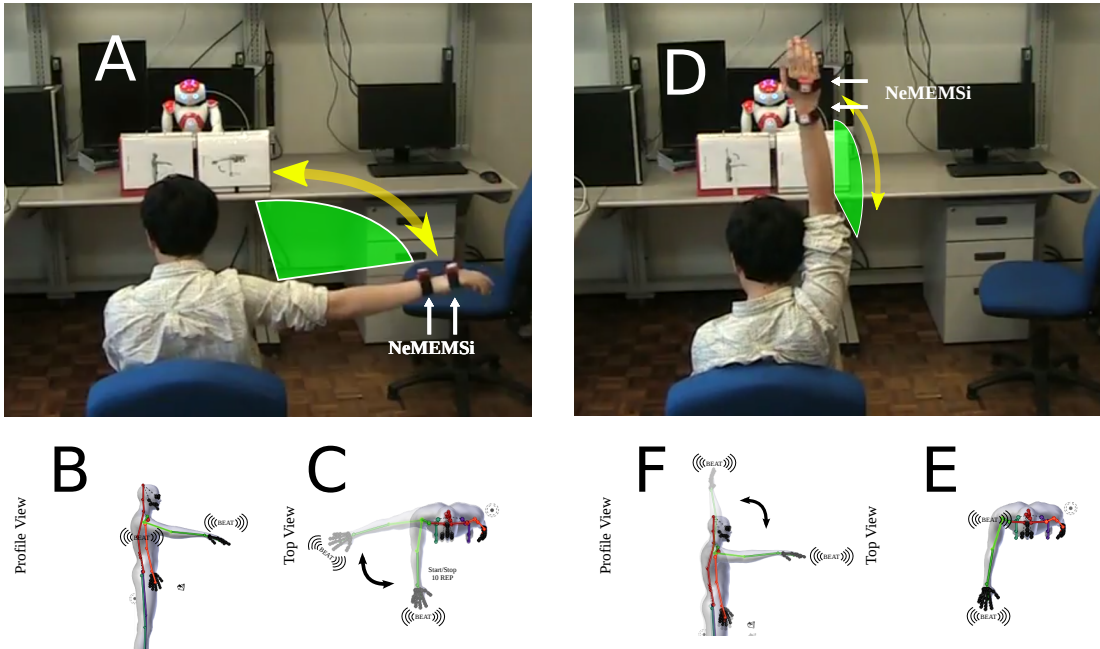


Fig. 4.1 Human-image imitation (HII) activities. (A) HII of horizontal arm movement, (B) image of the profile view for horizontal arm movement, (C) image of the top view for horizontal arm movement, (D) HII of vertical arm movement, (E) image of the profile view for vertical arm movement, and (F) image of the top view for horizontal arm movement. (B, C, F and E) show '(((BEAT)))' to indicate the participants arm movements synchronisation when hearing a beat.

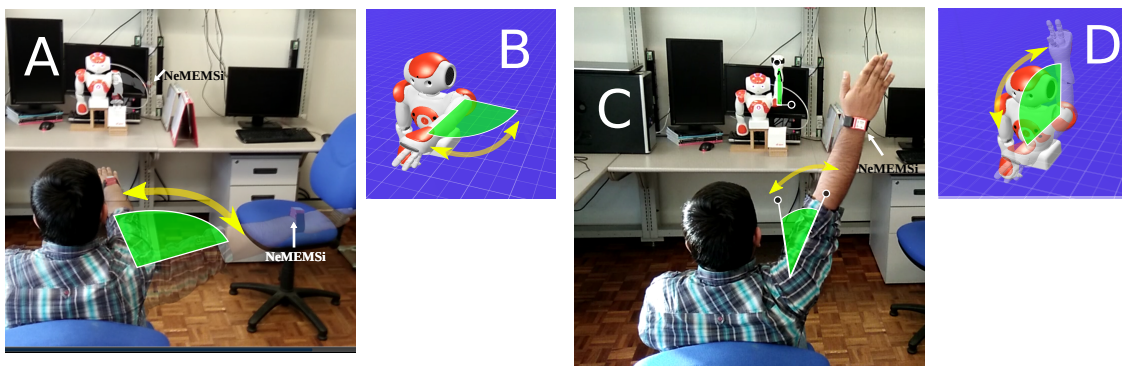


Fig. 4.2 Human-humanoid imitation activities. Face-to-face human-humanoid imitation (HHI) activities for (A) HHI of horizontal arm movement, (B) Humanoid horizontal arm movement, (C) HHI of vertical arm movement, and (D) Humanoid vertical arm movement.

Experiments

from the humanoid robot have less variation between repetition to repetition. The duration for one repetition of the horizontal arm movement at normal speed, HN, is about 5 seconds considering that each repetition last around 250 samples. For horizontal arm movement at faster speed, HF, each repetition were performed in around 2 seconds which correspond to 90 samples of data. The vertical arm movement at normal speed, VN, were performed in 6 seconds which is around 300 samples of data. For vertical arm movement at faster speed, VF, each repetition lasts about 2.4 seconds which correspond to 120 samples of data. To visualise the distinction between normal and faster speed for horizontal and vertical arm movements, Fig 4.3 shows smoothed time series for axes Z and Y of the gyroscope sensors with four window lengths: 2-sec (100-samples), 5-sec (250-samples), 10-sec (500-samples) and 15-sec (750-samples).

4.6 Preparation of time series

4.6.1 Raw time-series

Considering the work of Shoaib et al. (2016) which provided evidence of an improvement in recognition activities when combining data from accelerometer and gyroscope. We focus our analysis for time series of the accelerometer and gyroscope only of the IMU sensors and leave the time series of the magnetometer and quaternions for future investigations because of their possible variations with regard to magnetic disturbances.

Time series from the accelerometer are defined by triaxial time series $A_x(n)$, $A_y(n)$, $A_z(n)$ which forms the matrix \mathbf{A} (Eq. 4.1), and the same for data from the gyroscope which is defined by triaxial time-series of $G_x(n)$, $G_y(n)$, $G_z(n)$ representing the matrix \mathbf{G} (Eq. 4.2). Both triaxial time series of each sensor, a and g , are denoted with its respective axes subscripts x, y, z , where n is the sample index and N is the same maximum length of all axes for the time series. Matrices \mathbf{A} and \mathbf{G} are represented as

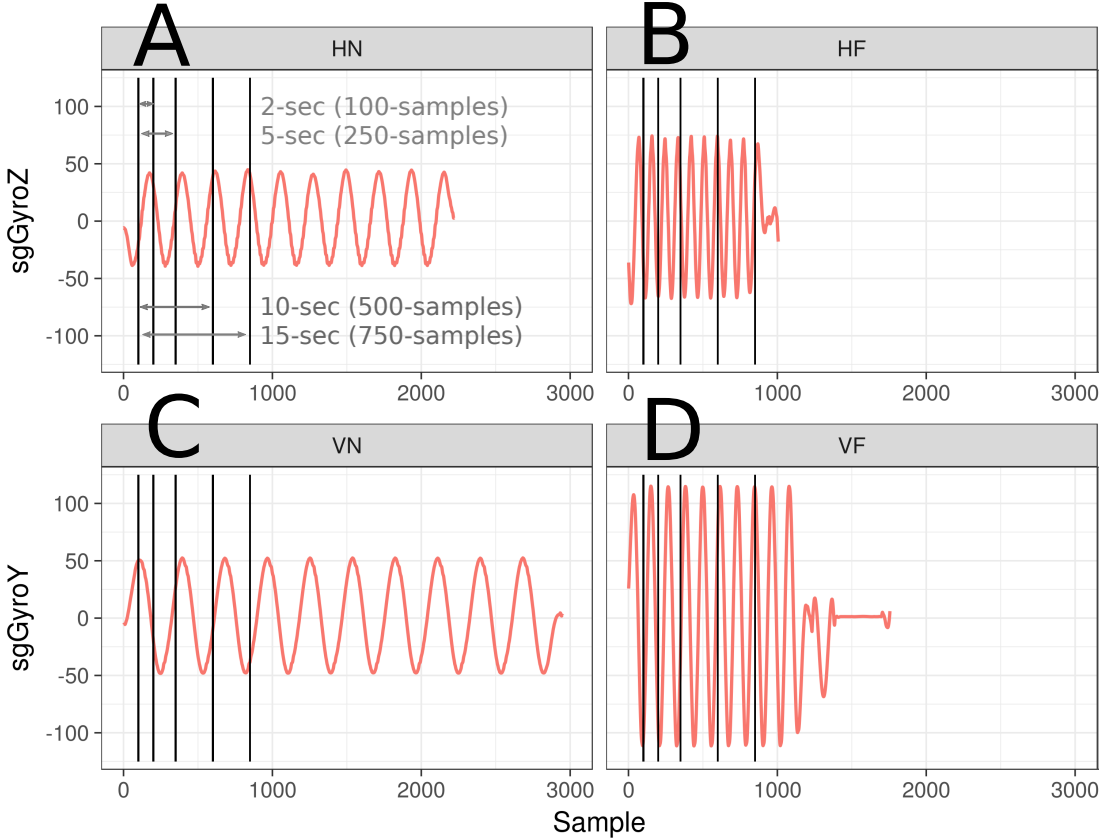


Fig. 4.3 Time series duration of horizontal and vertical arm movements. Time series of smoothed data from gyroscope sensor for different speed arm movements performed by NAO: (A) Horizontal Normal arm movement, HN, (B) Horizontal Faster arm movement, HF, (C) Vertical Normal arm movement, VN, and (D) Vertical Faster arm movement, VF. Additionally, (A) shows window sizes for 2-seconds (100 samples), 5-seconds (250 samples), 10-seconds (500 samples) and 15-seconds (750 samples) which are also presented in (B), (C) and (D). R code to reproduce the figure is available Xochicale (2018).

follow

$$\mathbf{A} = \begin{pmatrix} A_x(n) \\ A_y(n) \\ A_z(n) \end{pmatrix} = \begin{pmatrix} a_x(1), a_x(2), \dots, a_x(N) \\ a_y(1), a_y(2), \dots, a_y(N) \\ a_z(1), a_z(2), \dots, a_z(N) \end{pmatrix}, \quad (4.1)$$

Experiments

$$\mathbf{G} = \begin{pmatrix} G_x(n) \\ G_y(n) \\ G_z(n) \end{pmatrix} = \begin{pmatrix} g_x(1), g_x(2), \dots, g_x(N) \\ g_y(1), g_y(2), \dots, g_y(N) \\ g_z(1), g_z(2), \dots, g_z(N) \end{pmatrix}, \quad (4.2)$$

where n is the sample index and N is the same maximum length of all axes for the time series.

4.6.2 Postprocessing time-series

After the collection of raw time-series from four NeMEMsi sensors, time synchronisation alignment and interpolation were performed in order to create time series with the same length and synchronised time. We refer the reader to Appendix B for technical information about the time synchronisation process and IMU sensors.

4.6.3 Normalization of time-series

Tim series are normalised to have zero mean and unit variance using sample mean and sample standard deviation (Ioffe and Szegedy, 2015). The sample mean and sample standard deviation using $x(n)$ is given by

$$\mu_{x(n)} = \frac{1}{N} \left(\sum_{i=1}^N x(i) \right), \quad \sigma_{x(n)} = \sqrt{\frac{\sum_{i=1}^N (x(i) - \mu_{x(n)})^2}{N-1}}, \quad (4.3)$$

then the normalised data, $\hat{x}(n)$, is computed as follows

$$\hat{x}(n) = \frac{x(n) - \mu_{x(n)}}{\sigma_{x(n)}}. \quad (4.4)$$

4.6.4 Smoothing time-series

Using a low-pass filter is the common way to either capture the low frequencies that represent %99 of the human body energy or to get the gravitational and body motion

components of accelerations (Anguita et al., 2013). However, for this thesis the main focus is on the conservation of the structure of the time series in terms of the width and heights where, for instance, Savitzky-Golay filter can help to accomplish such task (Press et al., 1992). Savitzky-Golay filter is based on the principle of moving window average which preserves the area under the curve (the zeroth moment) and its mean position in time (the first moment) but the line width (the second moment) is violated and that results, for example, in the case of spectrometric data where a narrow spectral line is presented with reduced height and width. The aim of Savitzky-Golay filtering is to find the filter coefficients c_n that preserve higher momentums which are based on local least-square polynomial approximations (Press et al., 1992; Savitzky and Golay, 1964; Schafer, 2011). Hence, Savitzky-Golay coefficients are therefore computed using an R function `sgolay(p,n,m)` where p is the filter order, n is the filter length (must be odd) and m is the m -th derivative of the filter coefficients (signal R developers, 2014). Smoothed signal is represented with a tilde over the original signal: $\tilde{x}(n)$.

4.6.5 Window size of time-series

With regard to the window size, Shoaib et al. (2016) investigated its effects using seven window lengths (2, 5, 10, 15, 20, 25, 30 seconds) and combination of inertial sensors (accelerometer, gyroscope and linear acceleration sensor) in activity recognition performance for repetitive activities (walking, jogging and biking) and less repetitive activities (smoking, eating, giving a talk or drinking a coffee). Similarly, Shoaib et al. (2016) experimented with different window size effect to conclude that the increase of window size improved the recognition of complex activities because these required a large window to learn the repetitive motion patterns. Also, Shoaib et al. (2016) concluded that the use of large window size improve the recognition performance of less repetitive activities which mainly involve random hand gestures.

Experiments

For the activities in this thesis which are mainly repetitive, we selected only four window sizes: 2-s window (100 samples), 5-s window (250 samples), 10-s (500 samples) and 15-s window (750 samples) (Figure 4.3).

Chapter 5

Quantifying Human Imitation Activities

5.1 Introduction

5.2 Time series

5.3 Minimum Embedding Parameters

5.4 Reconstructed state spaces with UTDE

5.5 Recurrences Plots

5.6 Recurrence Quantification Analysis

5.6.1 REC values

5.6.2 DET values

5.6.3 RATIO values 66

5.6.4 ENTR values

Chapter 6

Quantifying Human-Humanoid Imitation Activities

6.1 Introduction

We investigated the robustness and weaknesses of the reconstructed state spaces (RRSs) using the uniform time-delay embedding technique (UTDE) and recurrence plots (RPs) for recurrent quantification analysis (RQA) methodologies in the following conditions:

- Three levels of smoothness for the normalised data (`sg0zmuv`, `sg1zmuv` and `sg2zmuv`), computed from two different filter lengths (29 and 159) with the same polynomial degree of 5 using the function `sgolay(p,n,m)` signal R developers (2014),
- Four velocities arm movement activities: horizontal normal (HN), horizontal faster (HF), vertical normal (VN), and vertical faster (VF), and
- Four window lengths: 2-sec (100 samples), 5-sec (250 samples), 10-sec (500 samples) and 15-sec (750 samples).

Further details about the preparations of time series are presented in Section 4.6.

6.2 Time series

To make comparison easier, we only present 10-sec (500 samples) window length time series for three participants (p01, p01 and p03) performing horizontal arm movements (axis GyroZ) and vertical arm movements (axis GyroY) (Figs 6.1 and 6.2), other data is then presented in Appendix D. We consider different levels of smoothness of the normalised data with two different Savitzky-Golay filter lengths (29 and 159) with the same polynomial degree of 5 using `sgolay(p,n,m)` (signal R developers, 2014).

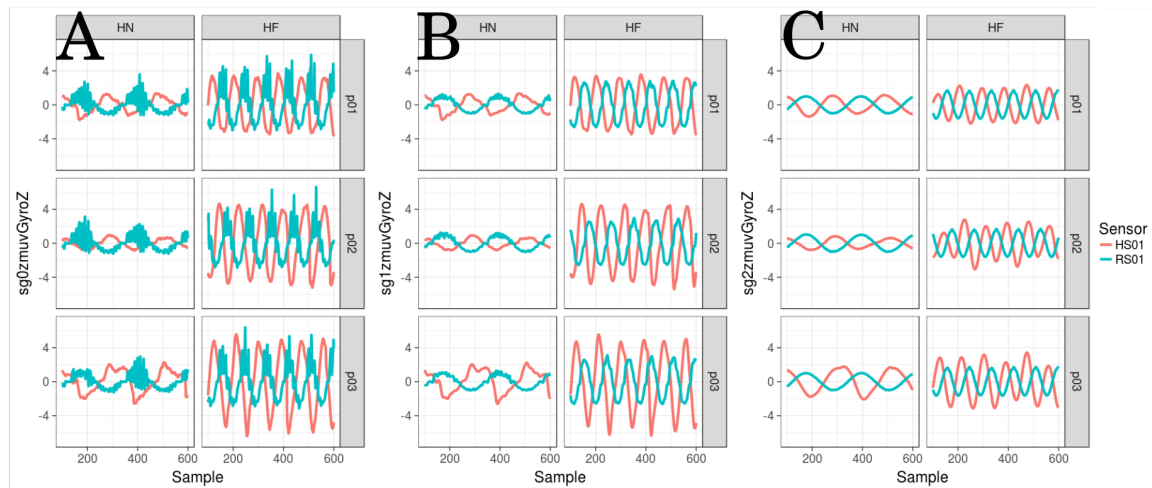


Fig. 6.1 **Time series for horizontal arm movements.** (A) raw-normalised ($sg0zmuvGyroZ$), (B) normalised-smoothed 1 ($sg1zmuvGyroZ$) and (C) normalised-smoothed 2 ($sg2zmuvGyroZ$). Time series are only for three participants (p01, p02, and p03) for horizontal movements in normal and faster velocity (HN, HF) with the normalised GyroZ axis ($zmuvGyroZ$) and with one sensor attached to the participant (HS01) and other sensor attached to the robot (RS01). R code to reproduce the figure is available from Xochicale (2018).

6.3 Minimum Embedding Parameters

The first step to create RSSs with the use of UTDE is to compute the average minimum embedding parameters for all participants, sensors and activities using False Nearest Neighbour (FNN) and Average Mutual Information algorithms (AMI).

6.3 Minimum Embedding Parameters

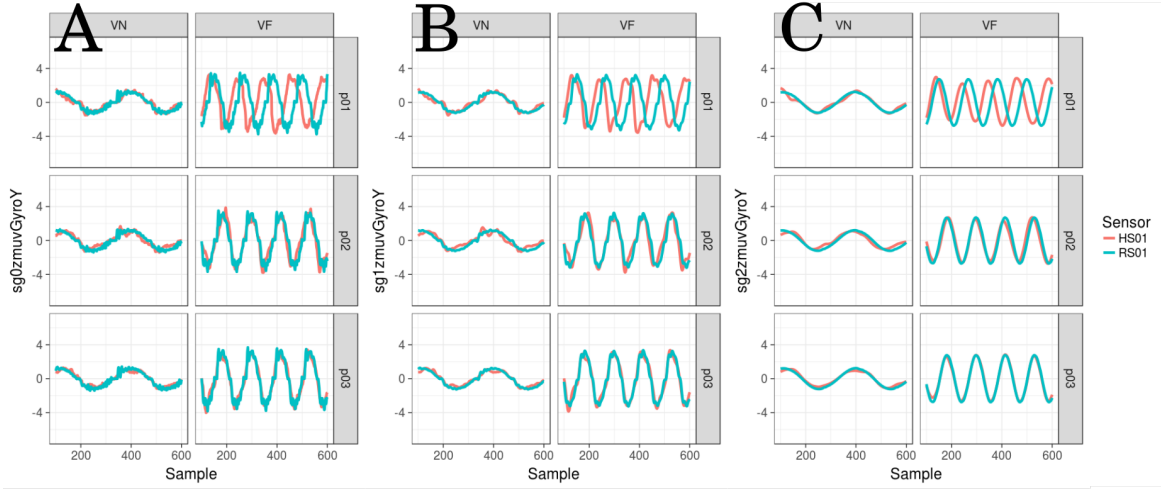


Fig. 6.2 Time series for vertical arm movements. (A) raw-normalised ($sg0zmuvGyroY$), (B) normalised-smoothed 1 ($sg1zmuvGyroY$) and (C) normalised-smoothed 2 ($sg2zmuvGyroY$). Time series are only for three participants (p01, p02, and p03) for vertical movements in normal and faster velocity (VN, VF) with the normalised GyroY axis ($zmuvGyroY$) and with one sensor attached to the participant (HS01) and other sensor attached to the robot (RS01). R code to reproduce the figure is available from Xochicale (2018).

Hence, for the average minimum embedding dimension, Figs 6.3 and 6.4 show the minimum embedding dimension for twenty participants for the horizontal and vertical arm movements at normal and faster velocity (HN, HF, VN, and VF) with the human attached sensor (HS01) and robot attached sensor (RS01). Generally, Figs 6.3 and 6.4 show that the minimum embedding values appear to be more constant for sensor RS01 than the slightly variations for embedding values for sensor HS01. It can also be seen in Figs 6.3 and 6.4 that there is a minor decrease of minimum embedding values as smoothness of time series increase.

Similarly, the first minimum values of the Average Mutual Information (AMI) for participants (p01-p20), activities (HN, HF, VN, and VF) and sensors (HS01, RS01) is shown in Figs 6.5 and 6.6. Hence, Fig 6.5(A) shows that the first minimum values of AMI, for normal horizontal arm movements, tend to be more spread as the smoothness of the time series is increasing while AMI values for faster horizontal arm movements

Quantifying Human-Humanoid Imitation Activities

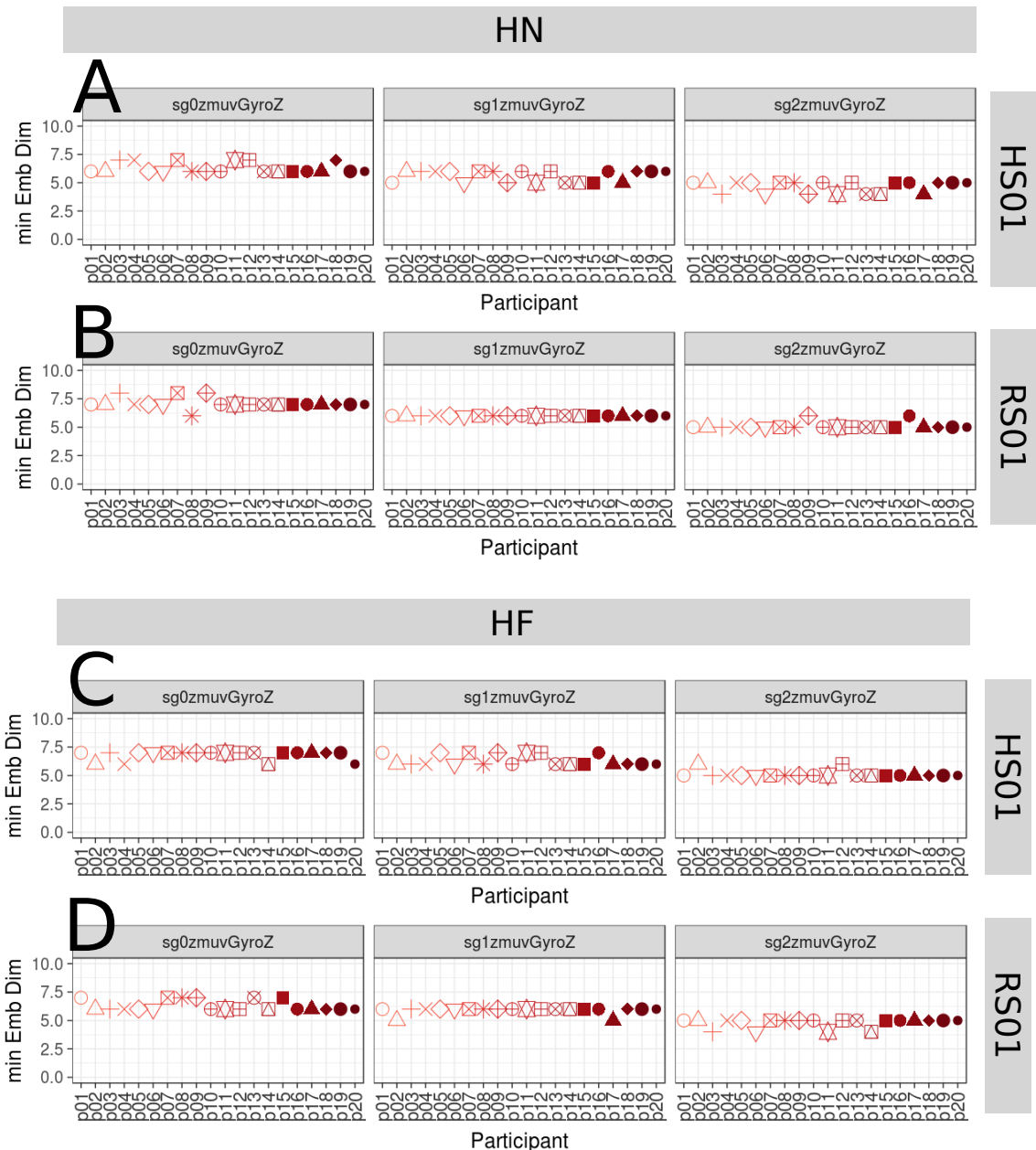


Fig. 6.3 Minimum embedding dimensions for horizontal arm movements. (A, B) Horizontal Normal (HN), (C, D) Horizontal Faster (HF) movements, (A, C) sensor attached to participants (HS01), and (B, D) sensor attached to robot (RS01). Minimum embedding dimensions are for twenty participants (p01 to p20) with three smoothed signals (sg0zmuvGyroZ, sg1zmuvGyroZ and sg2zmuvGyroZ) and window lenght of 10-sec (500 samples). R code to reproduce the figure is available from Xochicale (2018).

6.3 Minimum Embedding Parameters

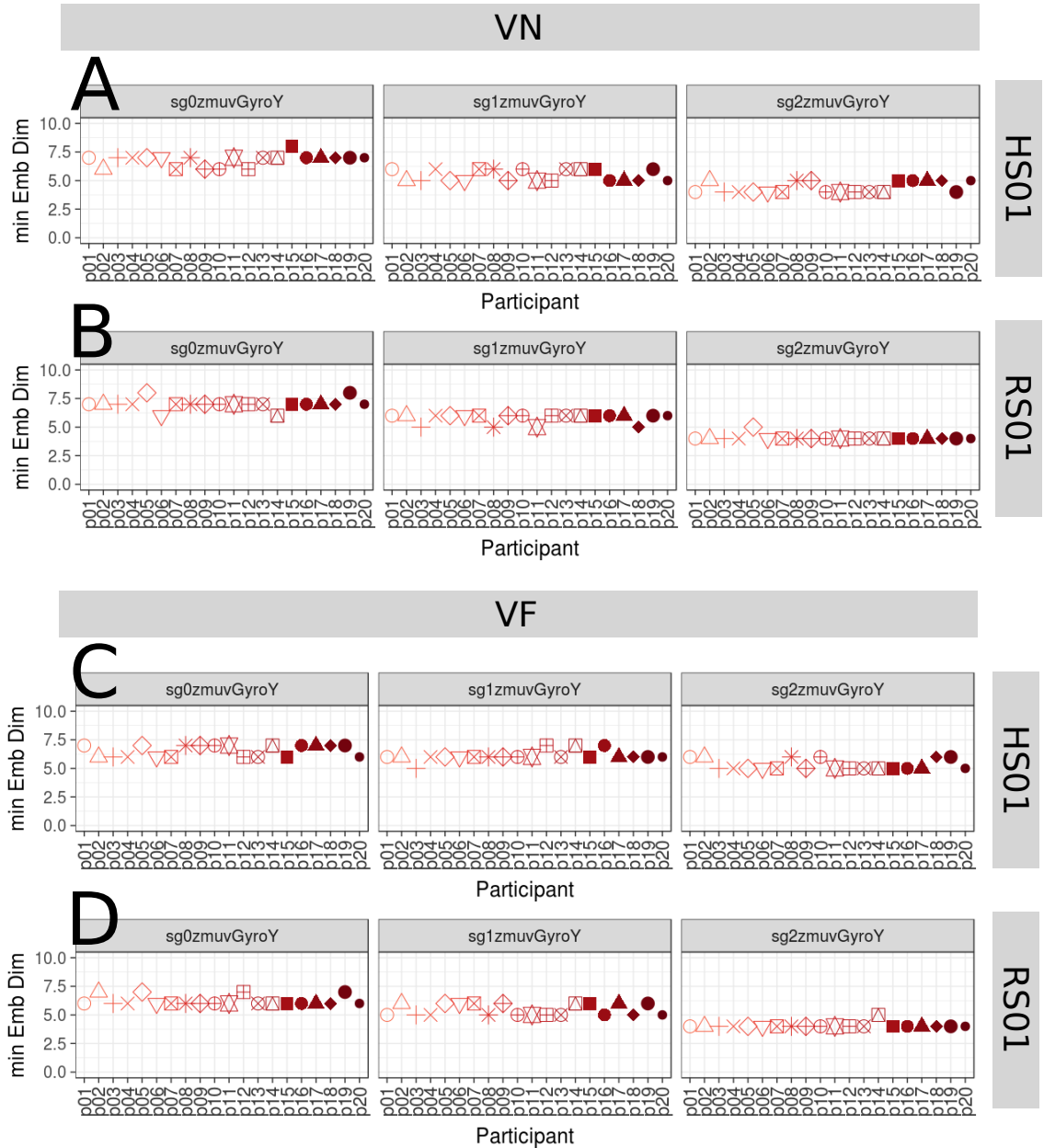


Fig. 6.4 Minimum embedding dimensions for vertical arm movements. (A, B) Vertical Normal (VN), (C, D) Vertical Faster (VF) movements, (A, C) sensor attached to participants (HS01), and (B, D) sensor attached to robot (RS01). Minimum embedding dimensions are for twenty participants (p01 to p20) with three smoothed signals (sg0zmuvGyroY, sg1zmuvGyroY and sg2zmuvGyroY) and window length of 10-sec (500 samples). R code to reproduce the figure is available from Xochicale (2018).

Quantifying Human-Humanoid Imitation Activities

in Fig 6.5(C) show little effect with regards to its fluctuation as the smoothness of time series increase. Fig 6.5(B) shows that minimum values of AMI are less spread as smoothness is increasing. However, values for horizontal faster movements in Fig 6.5(D) tend to be more spread as smoothness is increasing. With regard to vertical arm movements, the minimum values of AMI in Figs 6.6(A) and 6.6(C) show a slightly increase of the spread values as the smoothness is increasing and minimum AMI values in Fig 6.6(B) appear to have less fluctuations as the smoothness of the time series is increasing, however, that do not happen for the second smoothed values (sg2zmuvGyroY) in Fig 6.6(D) which appear to be constant. It can be noted that the increase of fluctuations of minimum AMI values in Figs 6.5 and 6.6 is due to the smoothed curves in the AMIs as the smoothness of time series is increasing.

6.4 Reconstructed state spaces with UTDE

Although the implementation of Uniform Time-Delay Embedding matrix (UTDE) is simple, the main challenge in this regard is to select embedding parameters to reconstruct the state spaces for each time series, considering that time series are unique in terms of its structure (modulation of amplitude, frequency and phase) (Bradley and Kantz, 2015; Frank et al., 2010; Samà et al., 2013). With that in mind, the problem is not to compute individual embedding parameters for each of the time series but to deal with the selection of two parameters that can represent all the time series. Our solution for that problem was, therefore, to compute a sample mean over all values that represents all participants, sensors and activities (Section 3.4.3). Hence, the sample mean for the minimum values of $E_1(m)$ from Figs 6.3 and 6.4 is $\bar{m}_0 = 6$ and the sample mean for minimum values of AMIs from Figs 6.5 and 6.6 is $\bar{\tau}_0 = 8$, for which the average minimum embedding parameters is ($\bar{m}_0 = 6$, $\bar{\tau}_0 = 8$).

6.4 Reconstructed state spaces with UTDE

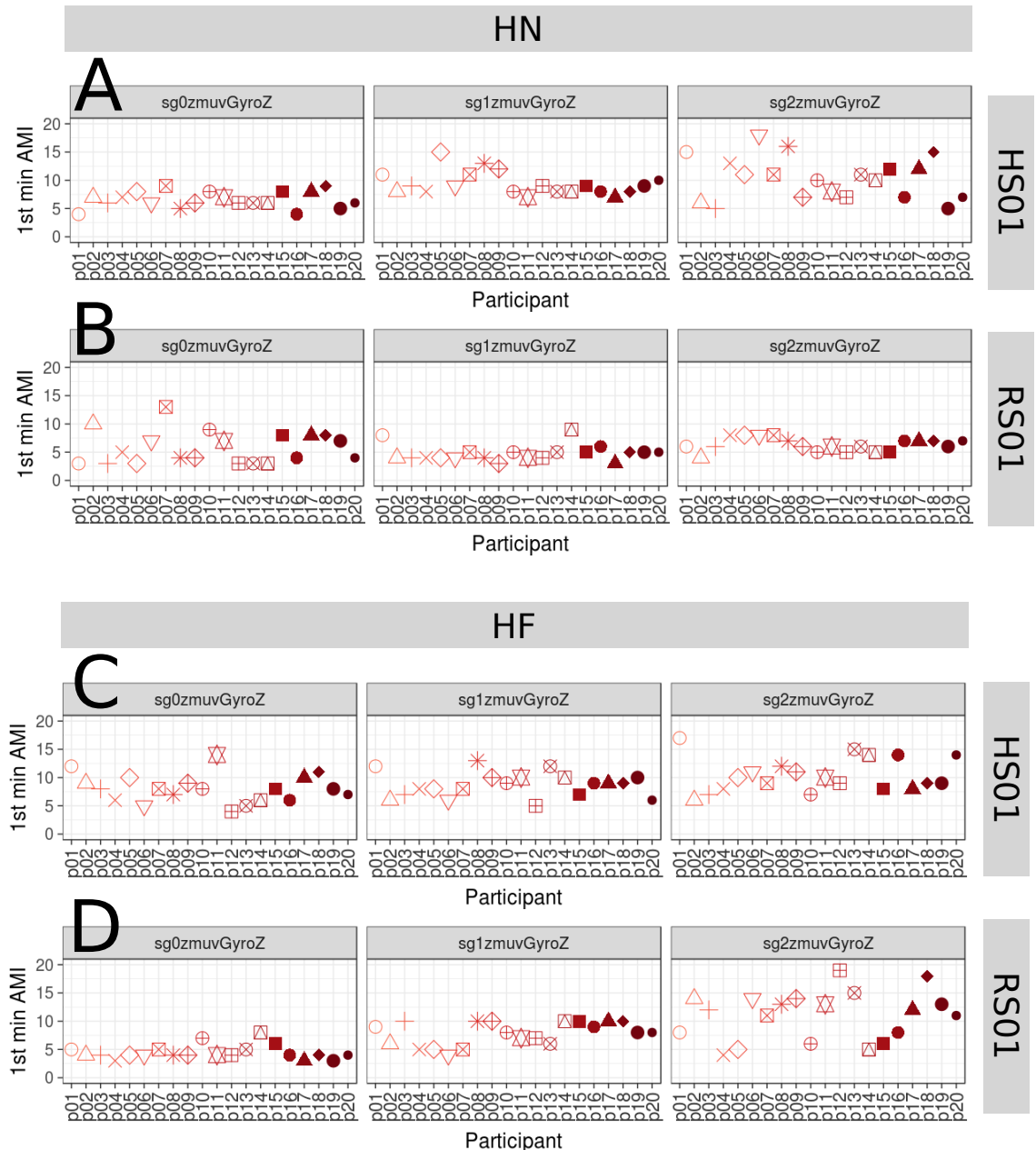


Fig. 6.5 First minimum AMI values for horizontal arm movements. (A, B) Horizontal Normal (HN), (C, D) Horizontal Faster (HF) movements, (A, C) sensor attached to participants (HS01), and (B, D) sensor attached to robot (RS01). First minimum AMI values are for twenty participants (p01 to p20) with three smoothed signals (sg0zmuvGyroZ, sg1zmuvGyroZ and sg2zmuvGyroZ) and window lenght of 10-sec (500 samples). R code to reproduce the figure is available from Xochicale (2018).

Quantifying Human-Humanoid Imitation Activities

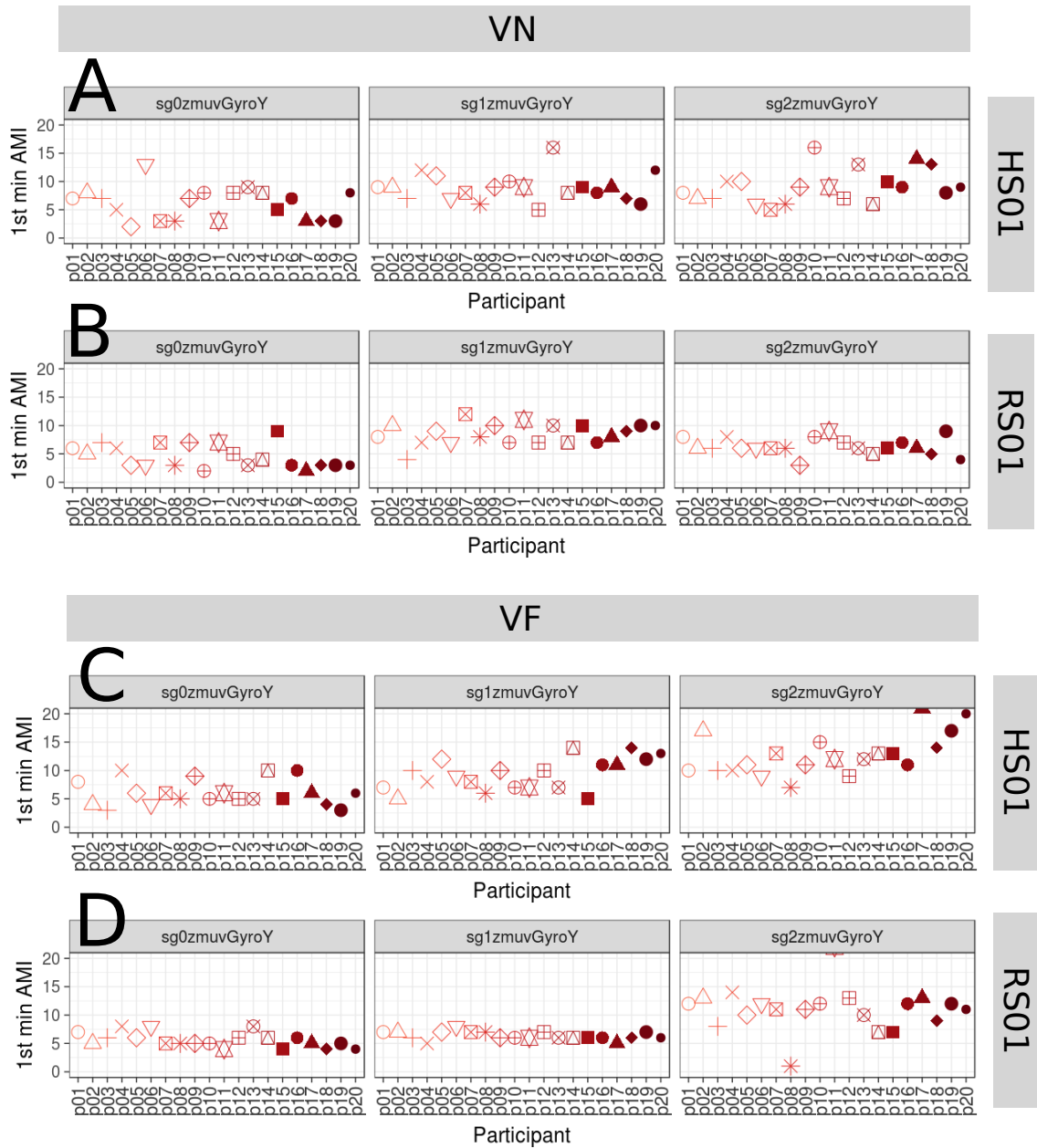


Fig. 6.6 First minimum AMI values for vertical arm movements. (A, B) Vertical Normal (VN), (C, D) Vertical Faster (VF) movements, (A, C) sensor attached to participants (HS01), and (B, D) sensor attached to robot (RS01). First minimum AMI values are for twenty participants (p01 to p20) with three smoothed signals ($sg0zmuvGyroZ$, $sg1zmuvGyroZ$ and $sg2zmuvGyroZ$) and window lenght of 10-sec (500 samples). R code to reproduce the figure is available from Xochicale (2018).

6.4 Reconstructed state spaces with UTDE

Therefore, considering time series for participant 01 (Figs 6.1, 6.2) the reconstructed state spaces for horizontal arm movements (Figs 6.7) and vertical arm movements (Figs 6.8) are computed with $\bar{m}_0 = 6$ and $\bar{\tau}_0 = 8$ (Section 3.5).

The trajectories of the RSSs for horizontal normal and faster from the human sensors (HS01) are slightly smoothed as the time-series smoothness increase (Figs 6.7(A,C)). Similarly, the smoothness of the trajectories in the RSSs for robot sensor (RS01) is increasing as the time series smoothness increase (Figs 6.7(B,D)). Although the frequency of the movement increase from normal to faster velocity, the trajectories RSSs in Figs 6.7(B) show higher oscillations specially for a maximum values of smoothness (sg2zmuvGyroZ), while the trajectories in the RSS for HF in Figs 6.7(D) show a lower and smoothed oscillations as the smoothness increase.

In contrast, the time series for vertical movements are less noisy and well structured (Figs 6.2) for which the trajectories in the RSSs seem to be less organised, specially for Fig 6.8(A,C), while time series for vertical faster movements (VF) which have more periods (Figs 6.2), this created trajectories in the RSS with well defined patterns (6.8(C,D)). It is important to note that the smoothness of time series also create an effect on smoothness in the trajectories of the RSS, being the RS01 more organised and more persistent while trajectories for HS01 are more changeable (Figs. 6.7, 6.8).

Therefore, one can observe by eye the differences in each of the trajectories in the reconstructed state spaces (Figs 6.7, 6.8), however one might be not objective when quantifying those differences since such observations might vary from person to person. With that in mind, in our early experiments, we tried to objectively quantify those differences using euclidean distances between the origin to each of the points in the trajectories in the trajectories of the RSSs, however these created suspicious metrics, specially for trajectories which looked very messy. Hence, we considered to apply

Quantifying Human-Humanoid Imitation Activities

Recurrence Quantification Analyses in order to have a more objective quantification of the differences in each of the cases of the time series.

6.5 Recurrences Plots

With the time series of Figs 6.1 and 6.2, we computed its Recurrence Plots for horizontal arm movements (Fig 6.9) and vertical arm movements (Fig 6.10) using the average embedding parameters ($m = 6$, $\tau = 8$) and a recurrence threshold of $\epsilon = 1$. For the selection of the recurrence threshold, Marwan (2011) pointed out that choosing an appropriate recurrence threshold is crucial to get meaningful representations in the RPs, however, for this thesis where quantifying movement variability is our aim, we give little importance to the selection of the recurrence threshold for the RPs as long as it is able to represent the dynamical transitions in each of the time series.

Generally, the increase of smoothness in time series results in ticker and more well defined diagonal lines in the RPs (Figs 6.9, 6.10). Regarding the low and hight frequencies in the time series due to the changes in velocities of the movements, the patterns in the RPs show both an increase of diagonal lines and a decrease of its thickness (Figs 6.9(A,B), 6.10(C,D)). Although, the patterns of RPs show consistency with the movements type and velocities changes, it can be noticed that patterns of the RPs for HS01 are not entirely well defined while patterns of the RPs for RS01 shown a more consistent pattern (Fig 6.9, 6.10).

It is important to note that only RPs for participant 01 are presented in (Fig 6.10, 6.9), however other RPs for all participants are presented in Appendix D.4. With that in mind, we can highlight that, as similar as, the Reconstructed State Spaces (Figs 6.7, 6.8), the patterns in the RPs can be easily noticed by eye for different conditions of the time series (Figs 6.9, Fig 6.10), however these characteristics in the patterns of the RPs are subjective for the person who analysed them and might vary from person to

6.6 Recurrence Quantification Analysis

person. That lead us to apply Recurrence Quantification Analysis in order to have a more objective quantification for the movement variability for each of the conditions of the time series.

6.6 Recurrence Quantification Analysis

Considering the RPs for 20 participants performing four activities (HN, HF, VN and VF) with sensors attached to the human (HS01) and to the humanoid robot (RS01) and with the increase of smoothness ($sg0zmuvGyroZ$, $sg1zmuvGyroZ$ and $sg2zmuvGyroZ$), we hence compute four metrics of RQA metrics (REC, DET, RATIO and ENTR) with embedding parameters $m = 6$, $\tau = 8$ and recurrence threshold $\epsilon = 1$ shown in the following subsections.

6.6.1 REC values

It can be seen in Figs 6.11 and 6.12 that REC values, representing the % of black dots in the RPs, are more spread for HN than HF movements with time series coming from HS01 sensor. In contrast, REC values appear to be constant and present little variation for both HN and HF movements with time series from the sensor attached to the humanoid robot RS01. With regard to the increase of smoothness of time series ($sg0zmuvGyroZ$, $sg1zmuvGyroZ$ and $sg2zmuvGyroZ$), REC values present little variation as the smoothness is increasing for time series from HS01 and REC values more similar as the smoothness is increasing for data from RS01.

6.6.2 DET values

DET values, representing predictability and organisation of the RPs, change very little even for type of movement and type of sensor (Figs 6.13 and 6.14). With regard to the

Quantifying Human-Humanoid Imitation Activities

smoothness of time series, DET values appear to be more similar as the smoothness of the time series is increasing.

6.6.3 RATIO values

RATIO values, representing dynamic transitions, for both horizontal and vertical movements (Figs 6.15 and 6.16) vary less for HN movements than HF movements for HS01 sensor which is a similar behaviour of RATIO values for RS01 sensor. It can also noticed a decrease of variation in RATIO values as the smoothness of the time series is increasing.

6.6.4 ENTR values

ENTR values, representing the complexity of the deterministic structure of the time series, for both horizontal and vertical movements (Figs 6.17 and 6.18) show more variation for HS01 sensor than ENTR values for RS01 sensor which appear to be more constant. Generally, it can also be said that the smoothness of time series affects little to the variation of ENTR values.

6.7 The weaknesses and strengths of RQA

Considering the raised points in Section 3.7.4 regarding the weaknesses and strengths of RQA, we computed RQA metrics (REC, DET, RATIO and ENTR) and plotted 3D surfaces using an unitary increase of pair embedding parameters ($0 > m \leq 10$, $0 > \tau \leq 10$) and a decimal increase of 0.1 for recurrence thresholds ($0.2 \geq \epsilon \leq 3$) (Fig. 6.19). Hence, the 3D surface for REC values, representing the percentage of black dots in the RP, in Fig. 6.19(A) shows an increase for REC values as the recurrence threshold increase, while the variation for embedding parameters creates

6.7 The weaknesses and strengths of RQA

slightly decrease of REC values as the dimension m increase and even a more slighter decrements of REC values for the increase of τ . For the 3D surface of DET values (Fig. 6.19(B)), representing predictability and organisation of the RPs, can be noted a plateau for DET values near to 1 for embedding dimension parameters of less than 5 and recurrence threshold values of greater than 2. It can also be noted that the increases of delay embedding made the DET values increase so as to make an cascade effect in the surface along with the increase of dimension embedding m . For RATIO values (Fig. 6.19(C)), representing dynamic transitions, the 3D surface show a plateau of RATIO values near to zero for recurrence thresholds greater than 1.0, while fluctuations are more evident for recurrence thresholds of less than 1.0, particularly it can also be noted an increase in the fluctuations of RATIO values as the embedding dimension is increasing. For ENTR values in Fig. 6.19(D), representing the complexity of the deterministic structure in time series, it can be noted that the increase of recurrence threshold is, not strictly linearly, proportional to the increase of ENTR values. It can also be seen that the increase of delay embeddings affects little the ENTR values for embedding dimensions of 1, while for higher values of embedding dimensions there is a decrease of ENTR values as the increase of the embedding dimension, besides the decrease of ENTR values as delay dimension value is increasing.

We also computed 3D surfaces of RQA metrics for different sensors and different activities (Figs. 6.20, 6.21), where it can generally be noted similar 3D surface patterns for RQA metrics as the ones in Fig. 6.19.

The 3D surfaces for REC values (Fig. 6.20(A)) show slightly differences with regard to vertical or horizontal activities however there are notable differences for normal and faster velocities, specially for the faster movements where the 3D surfaces shown a maximum REC value for embedding dimension values near to 1 and for recurrence thresholds near to 3. The 3D surfaces for DET values (Fig. 6.20(B)) and RATIO

Quantifying Human-Humanoid Imitation Activities

values (Fig. 6.20(C)) show slightly notable variations across the type of activities. For 3D surfaces of ENTR values it can be noted a slightly variation for the surfaces of normal and faster velocities (Fig 6.20(D)).

As similar as Fig 6.20, the 3D surfaces patters for RS01 in Fig 6.21 show the differences between the activities performed at normal and faster velocities specially for REC and ENTR values (Fig 6.20(A, D)), while 3D surfaces for DET and RATIO values show slightly variations (Fig 6.20(B, C)).

3D surfaces for RQA metrics with four window size lengths of 100, 250, 500 and 750 samples are shown in Fig. 6.22. In general, the increase of samples in the time series creates 3D surface patterns with better resolution (Figs. 6.22).

Considering three levels of smoothness of the time series (sg0, sg1, sg2) to compute the 3D surfaces of the RQA metrics, it can be noted that such smoothness have a direct effect on the smoothness of the 3D surfaces. Especially for dimension embeddings lower than 2 with the increase of delay embedding which is more evident for REC and ENTR values (Fig. 6.23(A, D)). The 3D surfaces of DET values are smoothed to a degree that the plateau is increase, while RATIO values appear to be less affected to the level of smoothness (Fig. 6.23(C)).

3D surfaces of RQA metrics were also computed for three participants (Fig. 6.24). Differences of the 3D surfaces across participants are more notable with REC (Fig. 6.24(A)) and ENTR values (Fig. 6.24(D)), while minor differences of 3D surfaces across participants are presented in DET (Fig. 6.24B)) and RATIO vales (Fig. 6.24(C)).

Generally, it can be noted the changes for RQA metrics are evident with both the increase of embedding dimension parameters and the recurrence threshold which were expected results because of different structures, window size, levels of smoothness of the time series. It is also important to highlight that the patterns in the 3D surfaces of the RQA metrics (REC, DET, RADIO and ENTR) (Fig 6.19) are certainly similar to

6.7 The weaknesses and strengths of RQA

its corresponded metrics for the different characteristics of the time series (Figs. 6.20, 6.21, 6.22, 6.23, 6.24).

Quantifying Human-Humanoid Imitation Activities

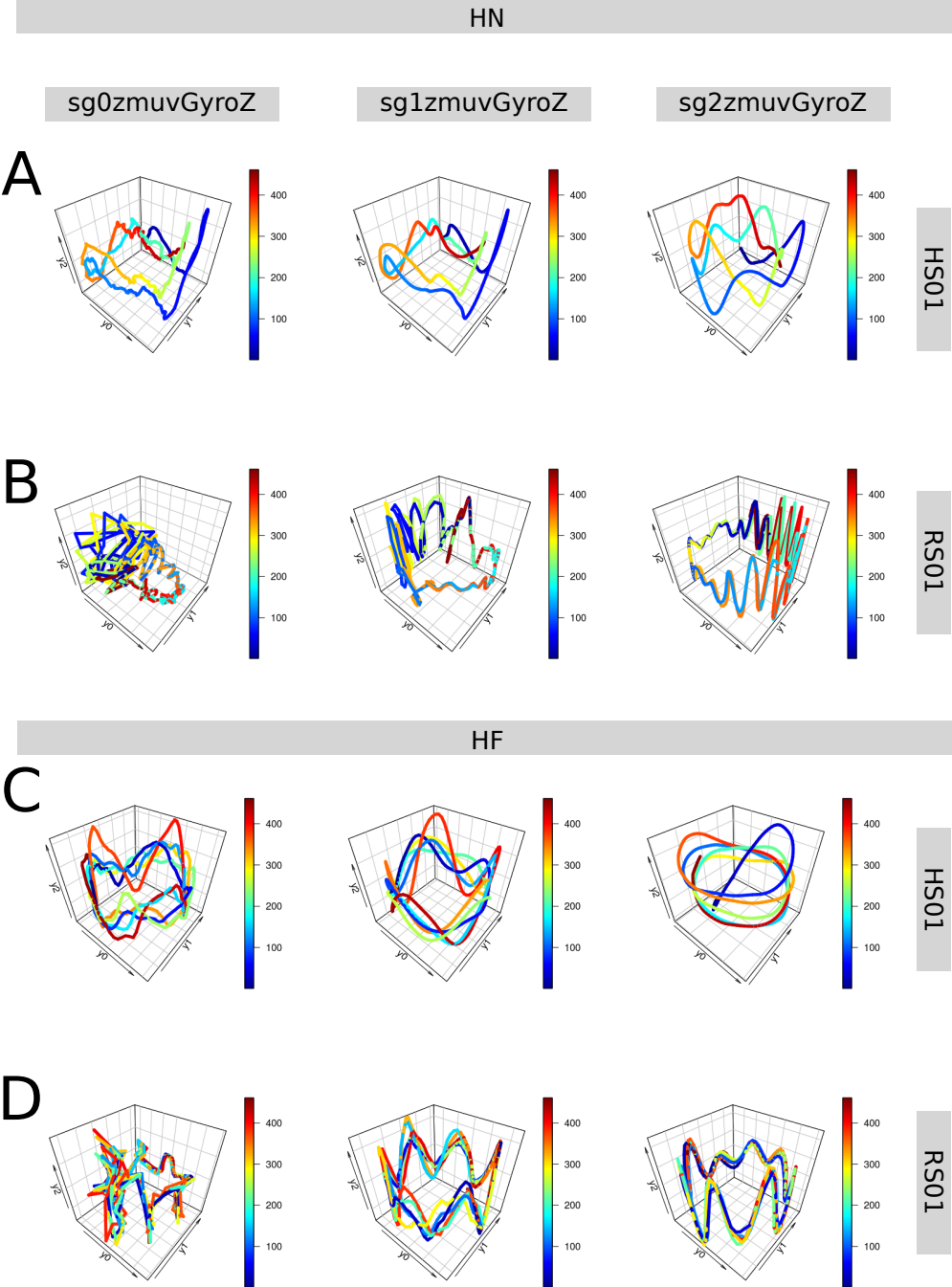


Fig. 6.7 RSSs for horizontal arm movements. Reconstructed state spaces of participant p01 for horizontal movements in normal and faster velocity (HN, HF) with raw-normalised ($sg0zmuvGyroZ$), normalised-smoothed 1 ($sg1zmuvGyroZ$) and normalised-smoothed 2 ($sg2zmuvGyroZ$) time series of the sensors attached to the participant (HS01) and other sensor attached to the robot (RS01). Reconstructed state spaces were computed with embedding parameters $m = 6$, $\tau = 8$. R code to reproduce the figure is available from Xochicale (2018).

6.7 The weaknesses and strengths of RQA

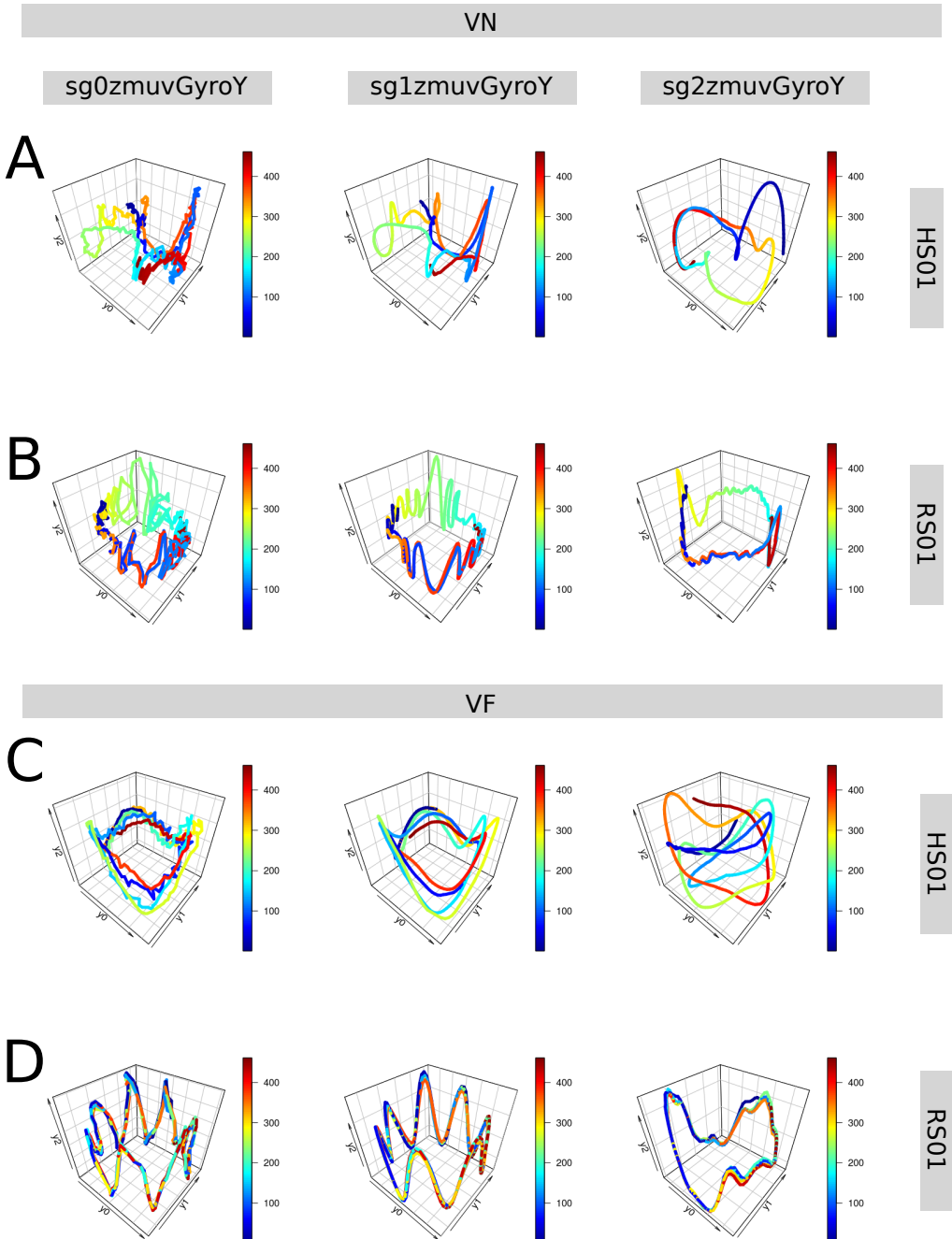


Fig. 6.8 RSSs for vertical arm movements. Reconstructed state spaces of participant p01 for vertical movements in normal and faster velocity (VN, VF) with raw-normalised (sg0zmuvGyroZ), normalised-smoothed 1 (sg1zmuvGyroZ) and normalised-smoothed 2 (sg2zmuvGyroZ) time series of the sensors attached to the participant (HS01) and other sensor attached to the robot (RS01). Reconstructed state spaces were computed with embedding parameters $m = 6$, $\tau = 8$. R code to reproduce the figure is available from Xochicale (2018).

Quantifying Human-Humanoid Imitation Activities

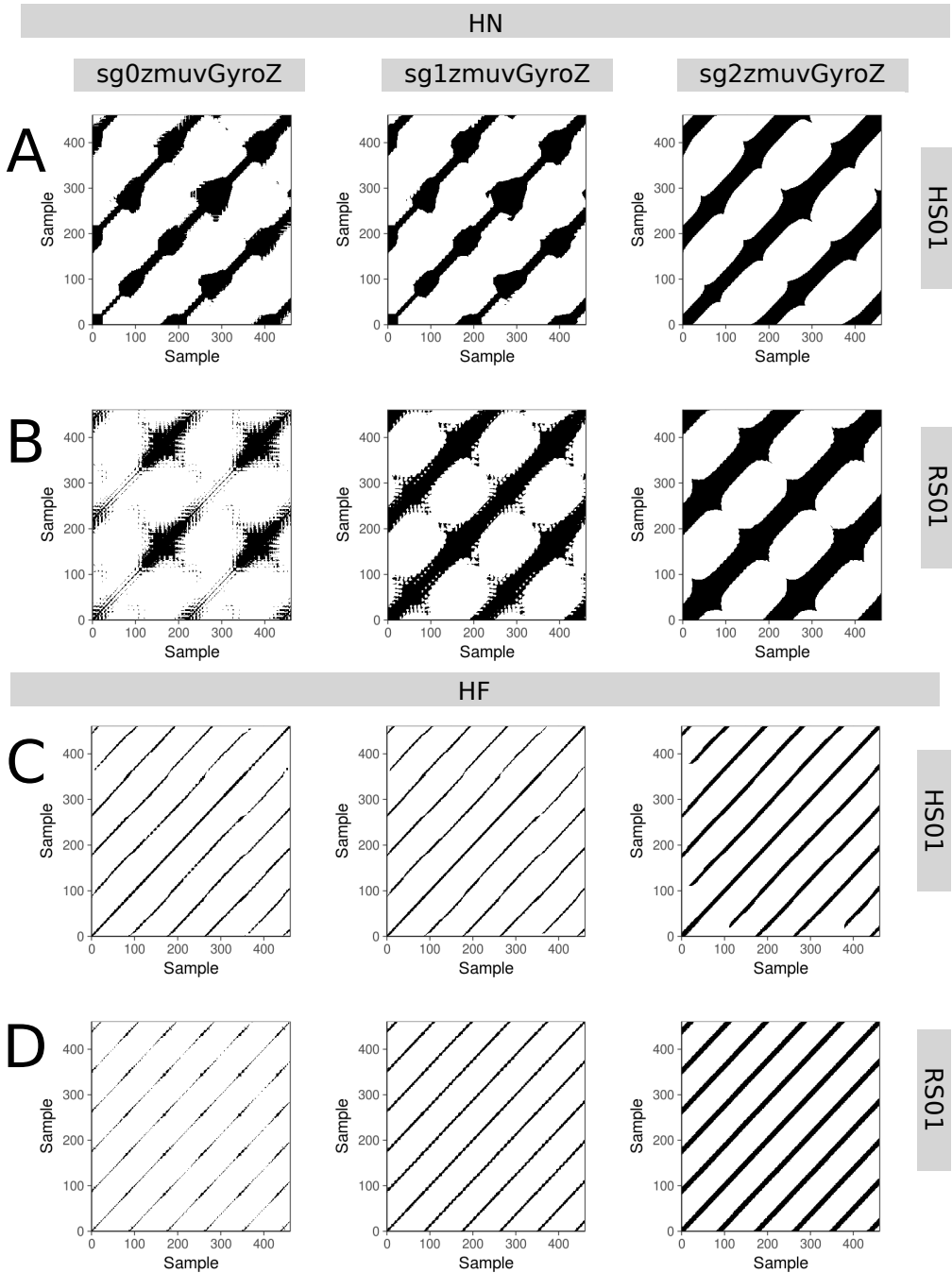


Fig. 6.9 RPs for horizontal arm movements. Recurrence plots of participant p01 for horizontal movements in normal and faster velocity (HN, HF) with raw-normalised ($sg0zmuvGyroZ$), normalised-smoothed 1 ($sg1zmuvGyroZ$) and normalised-smoothed 2 ($sg2zmuvGyroZ$) time series of the sensors attached to the participant (HS01) and other sensor attached to the robot (RS01). Recurrence plots were computed with embedding parameters $m = 6$, $\tau = 8$ and $\epsilon = 1$. R code to reproduce the figure is available from Xochicale (2018).

6.7 The weaknesses and strengths of RQA

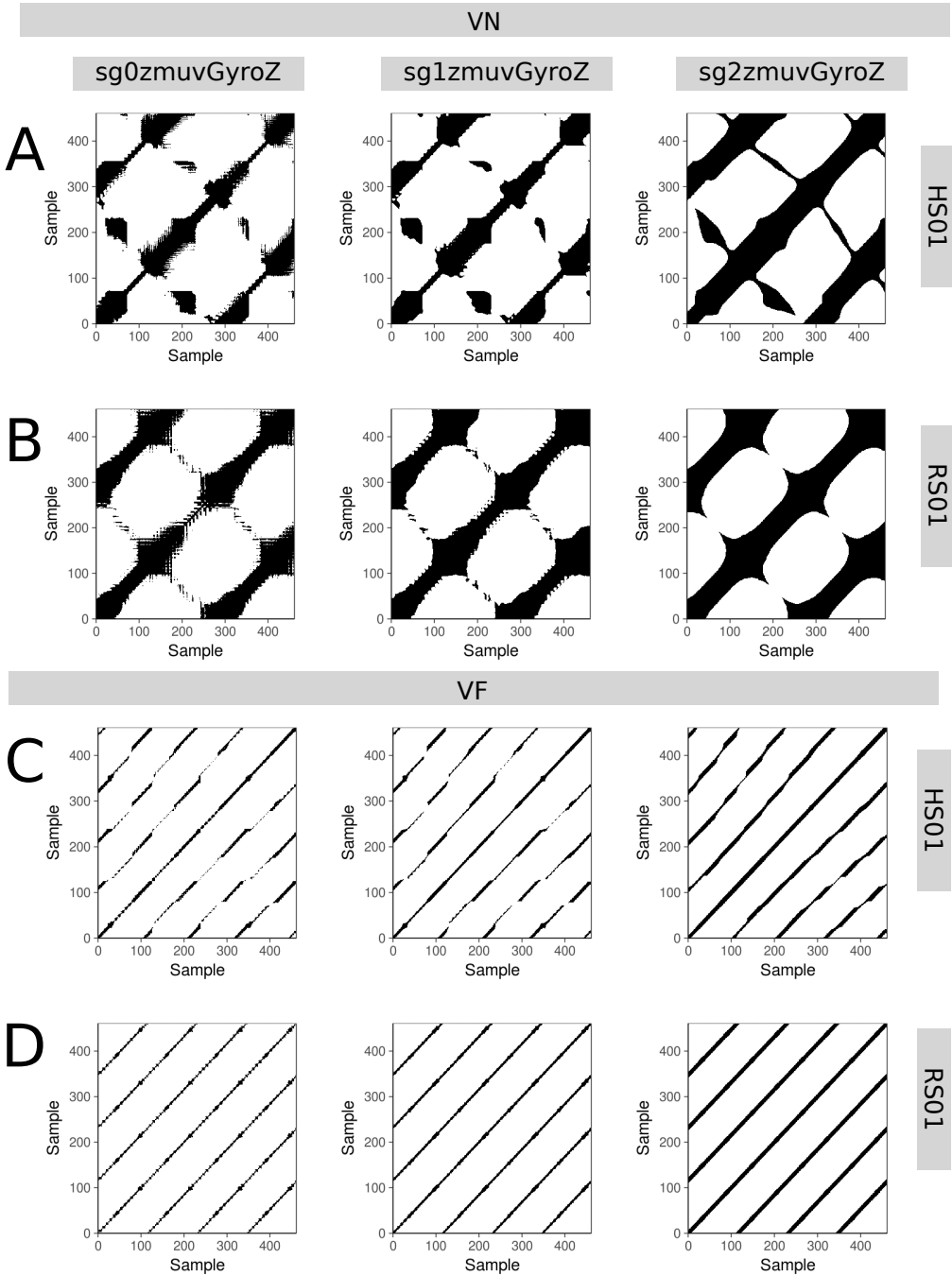


Fig. 6.10 RPs for vertical arm movements. Recurrence plots of participant p01 for vertical movements in normal and faster velocity (VN, VF) with raw-normalised ($sg0zmuvGyroZ$), normalised-smoothed 1 ($sg1zmuvGyroZ$) and normalised-smoothed 2 ($sg2zmuvGyroZ$) time series of the sensors attached to the participant (HS01) and other sensor attached to the robot (RS01). Recurrence plots were computed with embedding parameters $m = 6$, $\tau = 8$ and $\epsilon = 1$. R code to reproduce the figure is available from Xochicale (2018).

Quantifying Human-Humanoid Imitation Activities

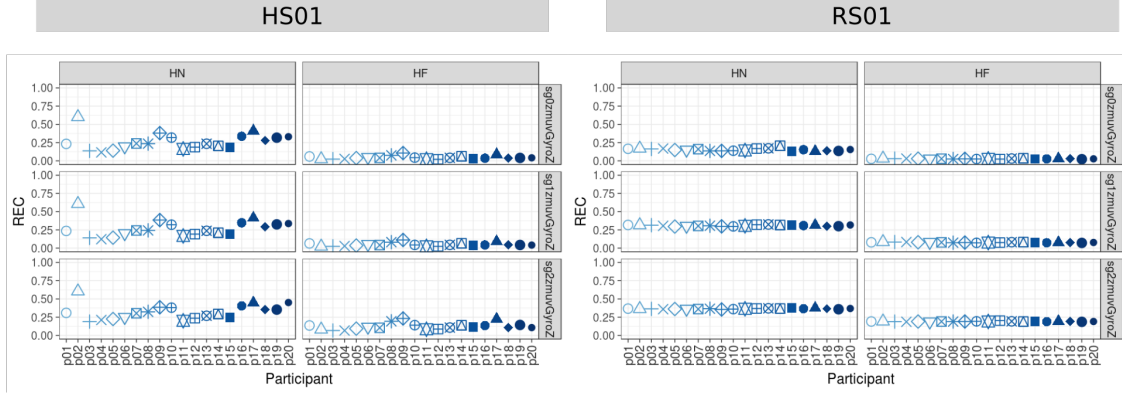


Fig. 6.11 REC values for horizontal arm movements. REC values (representing % of black dots in the RPs) for 20 participants performing HN and HF movements with sensors HS01, RS01 and three smoothed-normalised axis of GyroZ (sg0zmuvGyroZ, sg1zmuvGyroZ and sg2zmuvGyroZ). REC values were computed with embedding parameters $m = 6$, $\tau = 8$ and $\epsilon = 1$. R code to reproduce the figure is available from Xochicale (2018).

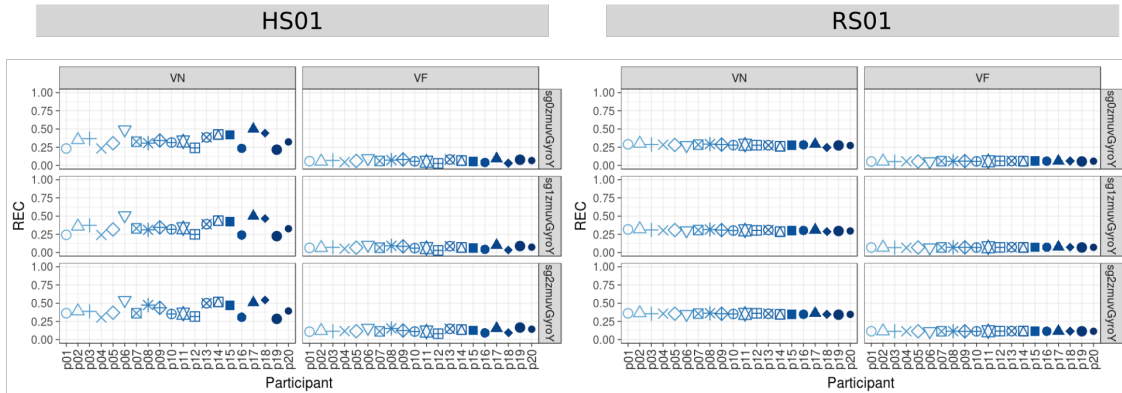


Fig. 6.12 REC values for vertical arm movements. REC values (representing % of black dots in the RPs) for 20 participants performing VN and VF movements with sensors HS01, RS01 and three smoothed-normalised axis of GyroY (sg0zmuvGyroY, sg1zmuvGyroY and sg2zmuvGyroY). REC values were computed with embedding parameters $m = 6$, $\tau = 8$ and $\epsilon = 1$. R code to reproduce the figure is available from Xochicale (2018).

6.7 The weaknesses and strengths of RQA

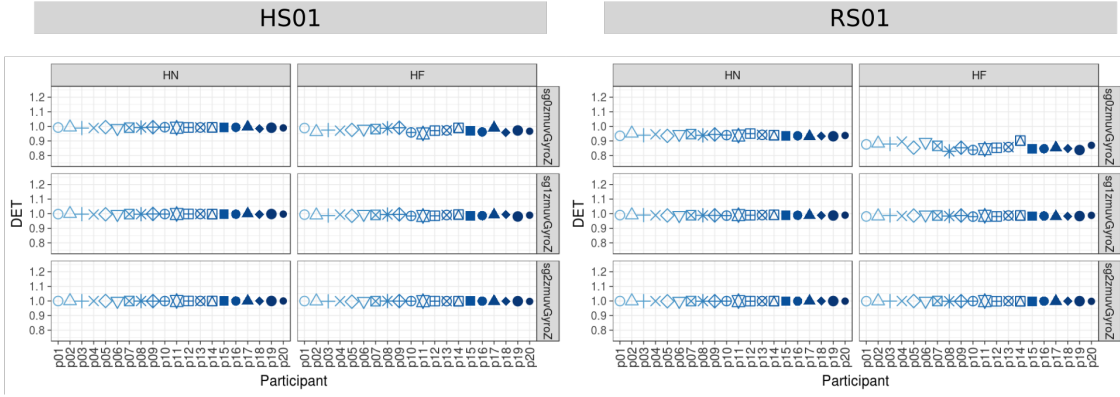


Fig. 6.13 **DET values for horizontal arm movements.** DET values (representing predictability and organisation of the RPs) for 20 participants performing HN and HF movements with sensors HS01, RS01 and three smoothed-normalised axis of GyroZ (sg0zmuvGyroZ, sg1zmuvGyroZ and sg2zmuvGyroZ). DET values were computed with embedding parameters $m = 6$, $\tau = 8$ and $\epsilon = 1$. R code to reproduce the figure is available from Xochicale (2018).

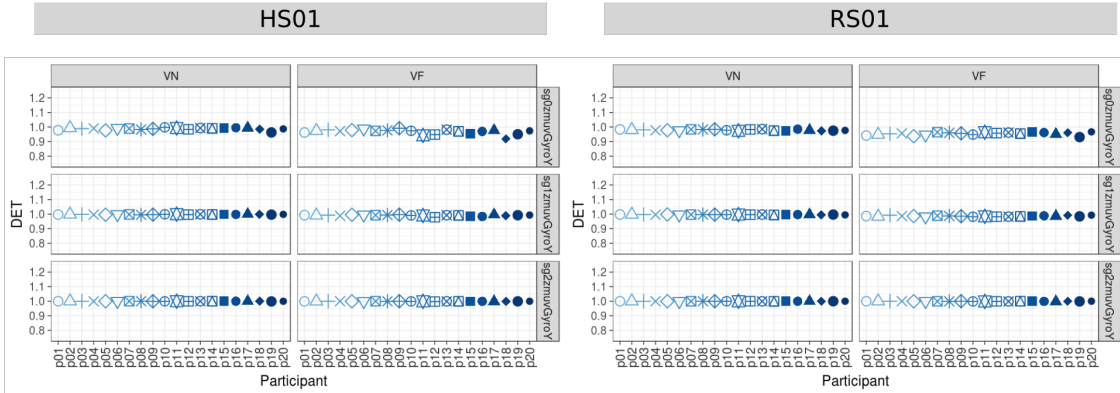


Fig. 6.14 **DET values for vertical arm movements.** DET values (representing predictability and organisation of the RPs) for 20 participants performing VN and VF movements with sensors HS01, RS01 and three smoothed-normalised axis of GyroY (sg0zmuvGyroY, sg1zmuvGyroY and sg2zmuvGyroY). DET values were computed with embedding parameters $m = 6$, $\tau = 8$ and $\epsilon = 1$. R code to reproduce the figure is available from Xochicale (2018).

Quantifying Human-Humanoid Imitation Activities

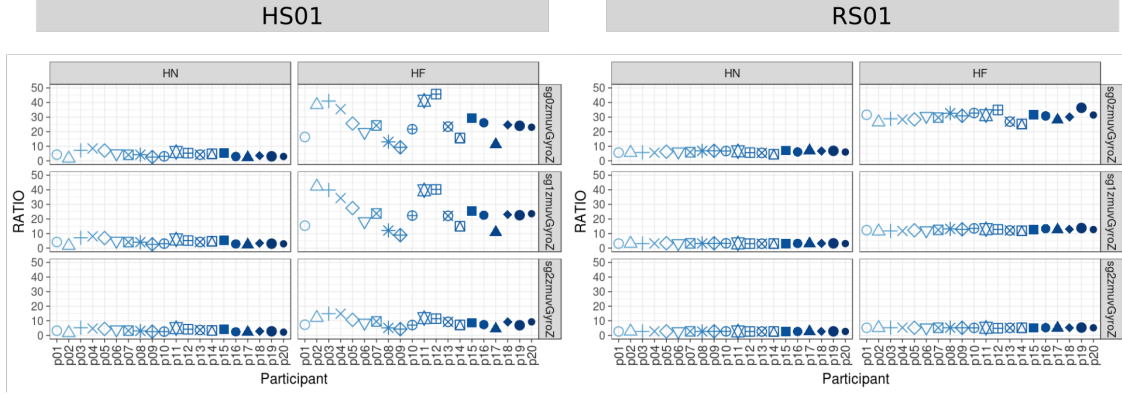


Fig. 6.15 RATIO values for horizontal arm movements. RATIO (representing dynamic transitions) for 20 participants performing HN and HF movements with sensors HS01, RS01 and three smoothed-normalised axis of GyroZ (sg0zmuvGyroZ, sg1zmuvGyroZ and sg2zmuvGyroZ). RATIO values were computed with embedding parameters $m = 6$, $\tau = 8$ and $\epsilon = 1$. R code to reproduce the figure is available from Xochicale (2018).

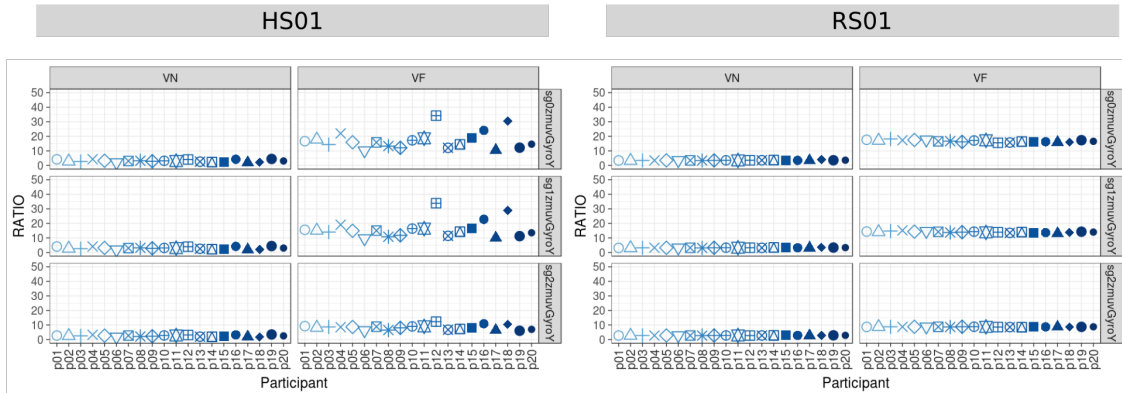


Fig. 6.16 RATIO values for vertical arm movements. RATIO (representing dynamic transitions) for 20 participants performing VN and VF movements with sensors HS01, RS01 and three smoothed-normalised axis of GyroY (sg0zmuvGyroY, sg1zmuvGyroY and sg2zmuvGyroY). RATIO values were computed with embedding parameters $m = 6$, $\tau = 8$ and $\epsilon = 1$. R code to reproduce the figure is available from Xochicale (2018).

6.7 The weaknesses and strengths of RQA

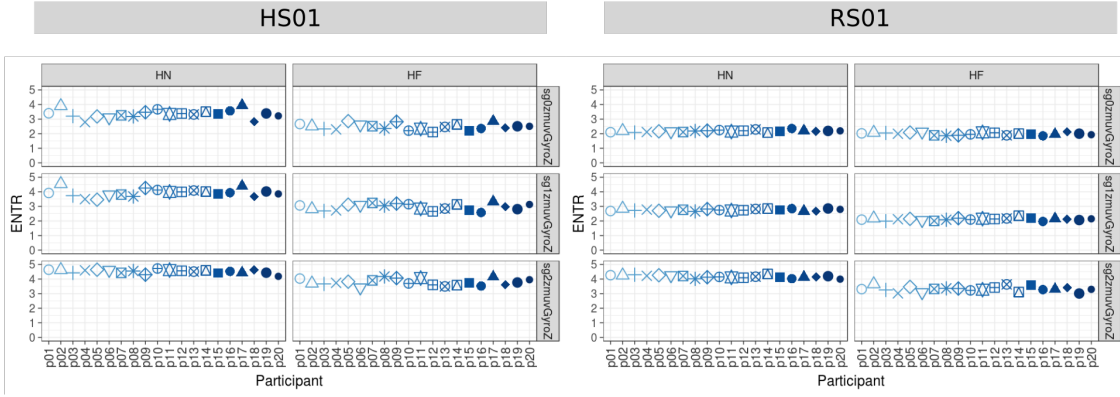


Fig. 6.17 ENTR values for horizontal arm movements. ENTR values (representing the complexity of the deterministic structure in time series) for 20 participants performing HN and HF movements with sensors HS01, RS01 and three smoothed-normalised axis of GyroZ (sg0zmuvGyroZ, sg1zmuvGyroZ and sg2zmuvGyroZ). ENTR values were computed with embedding parameters $m = 6$, $\tau = 8$ and $\epsilon = 1$. R code to reproduce the figure is available from Xochicale (2018).

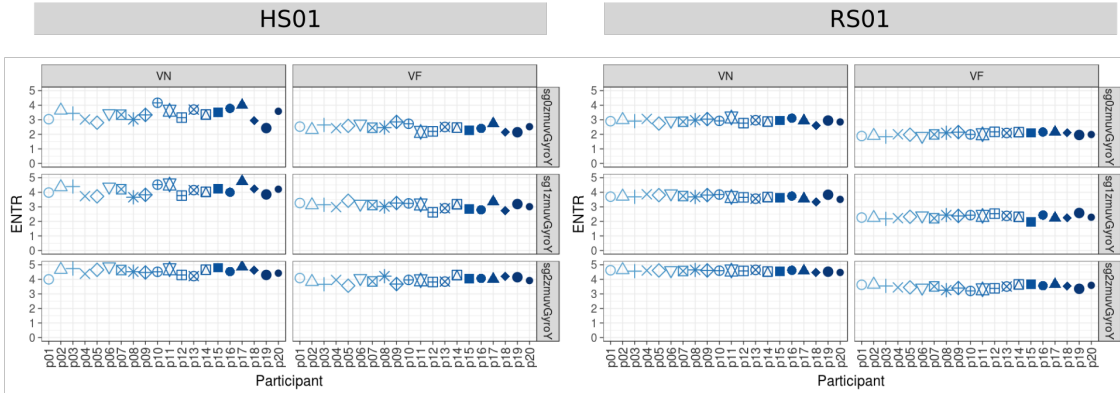


Fig. 6.18 ENTR values for vertical arm movements. ENTR values (representing the complexity of the deterministic structure in time series) for 20 participants performing VN and VF movements with sensors HS01, RS01 and three smoothed-normalised axis of GyroY (sg0zmuvGyroY, sg1zmuvGyroY and sg2zmuvGyroY). ENTR values were computed with embedding parameters $m = 6$, $\tau = 8$ and $\epsilon = 1$. R code to reproduce the figure is available from Xochicale (2018).

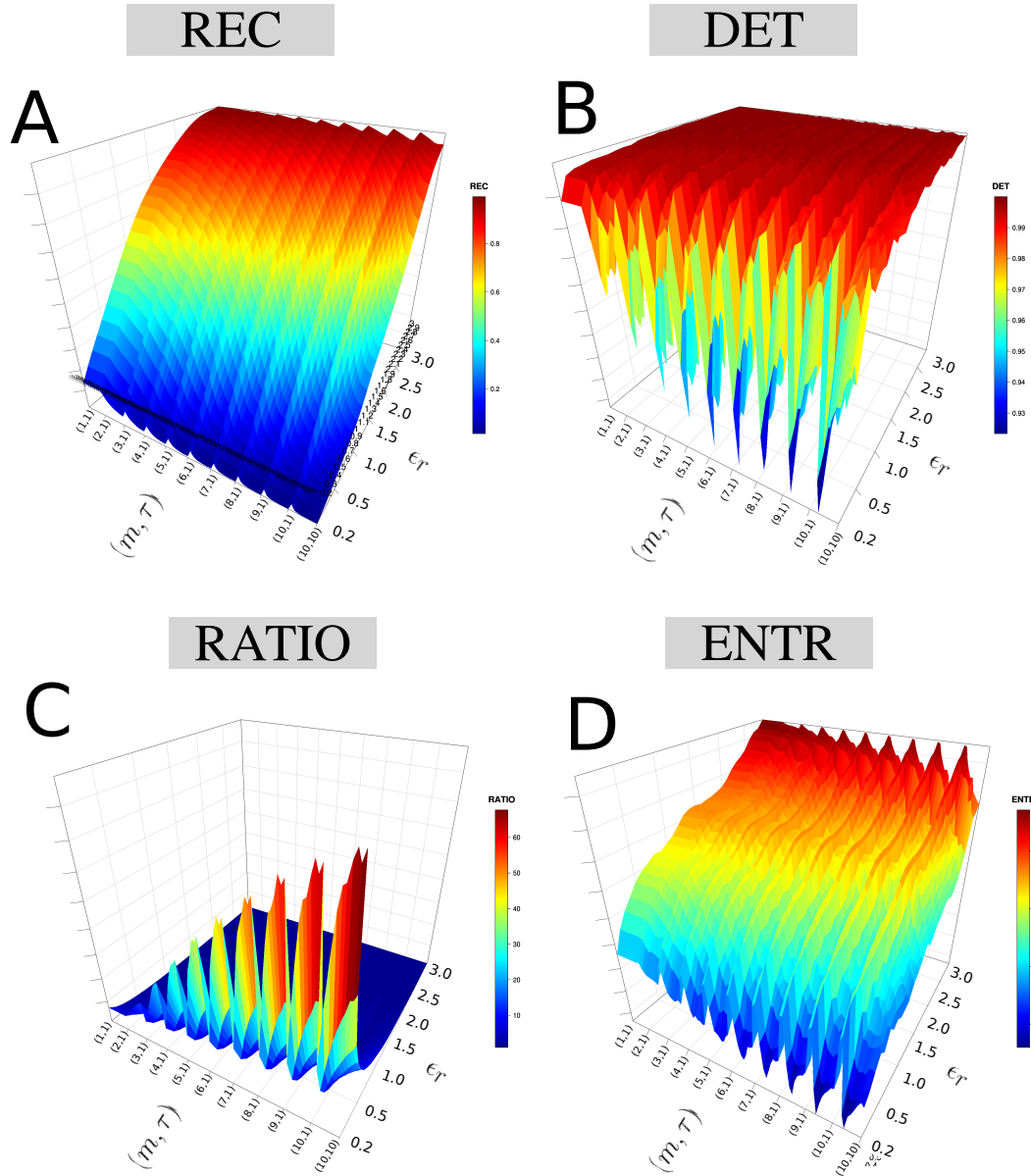


Fig. 6.19 **3D surfaces for RQA metrics.** 3D surfaces for (A) REC, (B) DET, (C) RATIO and (D) ENTR values with increasing pair of embedding parameters ($0 \leq m \leq 10$, $0 \geq \tau \leq 10$) and recurrence thresholds ($0.2 \geq \epsilon \leq 3$). RQA metrics are computed with the time series of participant p01 using HS01 sensor, HN activity, sg0zmuvGyroZ axis and 500 samples for window size length. R code to reproduce the figure is available from Xochicale (2018).

6.7 The weaknesses and strengths of RQA

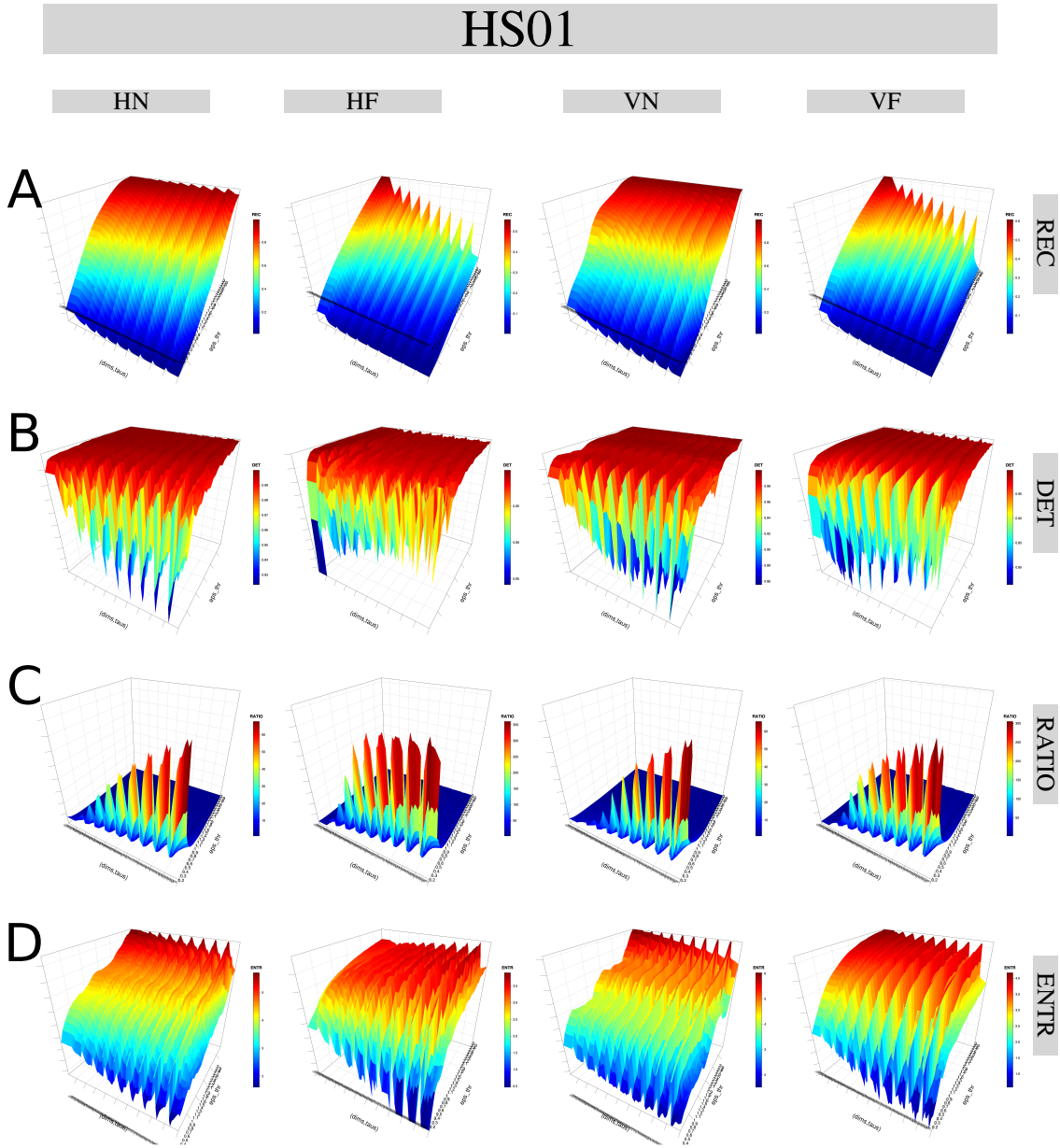


Fig. 6.20 3D surfaces of RQA metrics for HS01 sensor. 3D surfaces of RQA metrics ((A) REC, (B) DET, (C) RATIO, and (D) ENTR) with increasing embedding parameters and recurrence thresholds are for time series of participant p01 for sensors HS01, activities (HN, HF, VN and VF) and sg0zmuvGyroZ axis with 500 samples window size length. R code to reproduce the figure is available from Xochicale (2018).

Quantifying Human-Humanoid Imitation Activities

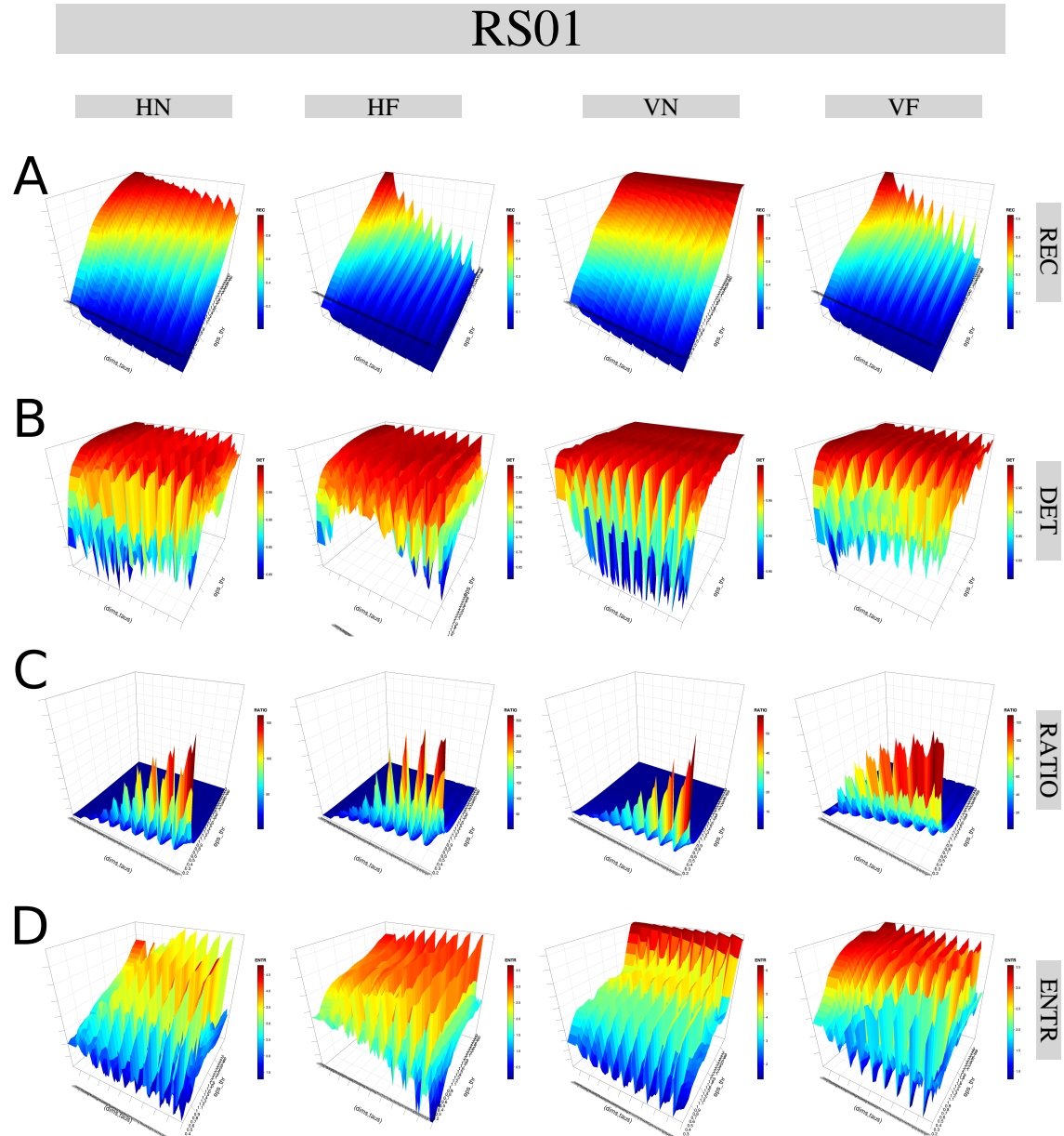


Fig. 6.21 **3D surfaces of RQA metrics for RS01 sensor.** 3D surfaces of RQA metrics ((A) REC, (B) DET, (C) RATIO and (D) ENTR) with increasing embedding parameters and recurrence thresholds are for time series of humanoid robot for sensors RS01, activities (HN, HF, VN and VF) and sg0zmuvGyroZ axis with 500 samples window size length. R code to reproduce the figure is available from Xochicale (2018).

6.7 The weaknesses and strengths of RQA

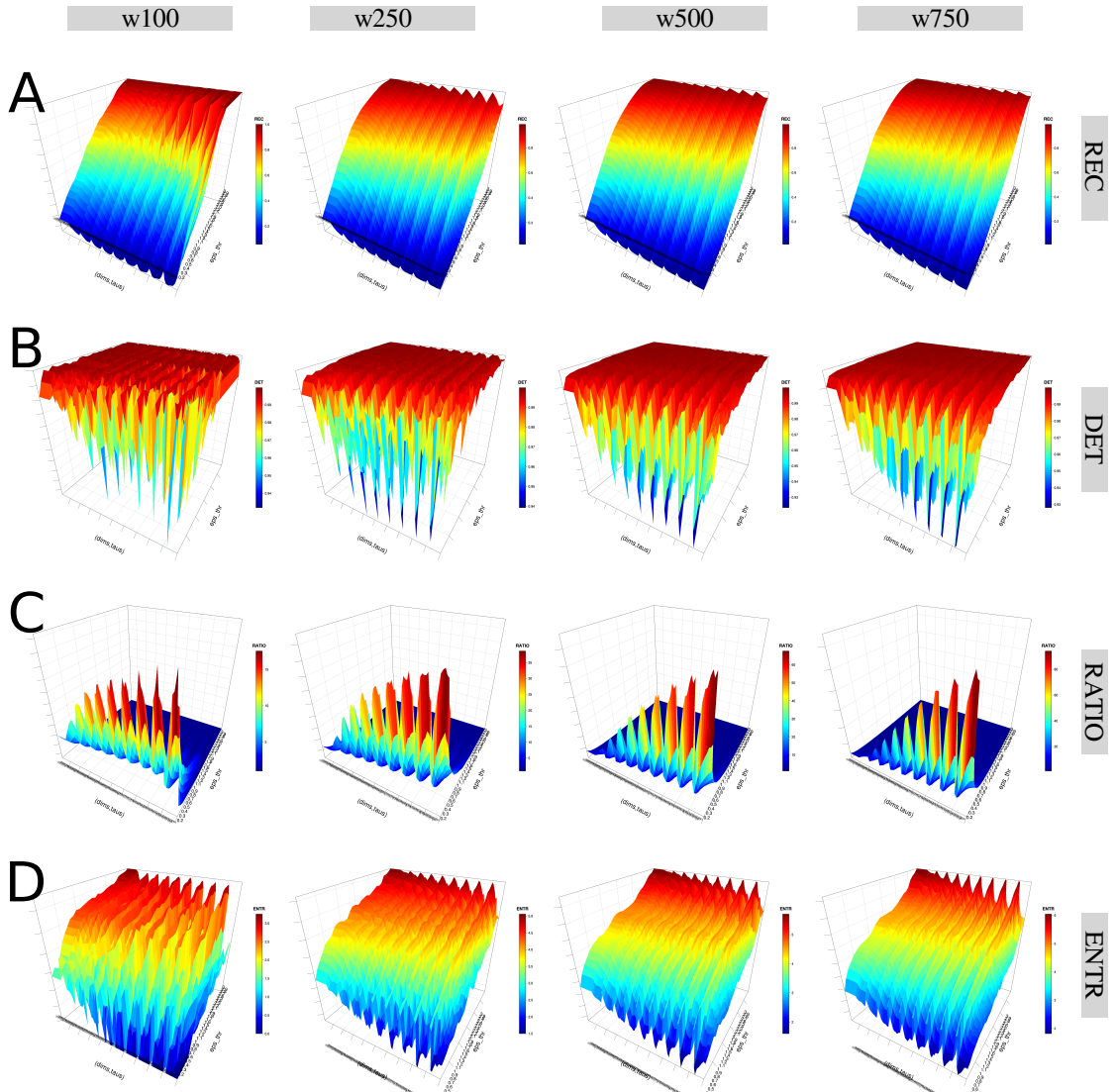


Fig. 6.22 3D surfaces for RQAs metrics with four window lengths. 3D surfaces of RQA metrics ((A) REC, (B) DET, (C) RATIO, and (D) ENTR) with increasing embedding parameters and recurrence thresholds for four window lengths (w100, w250, w500 and w750). RQA metrics values are for time series of participant p01 using HS01 sensor, HN activity and sg0zmuvGyroZ axis. R code to reproduce the figure is available from Xochicale (2018).

Quantifying Human-Humanoid Imitation Activities

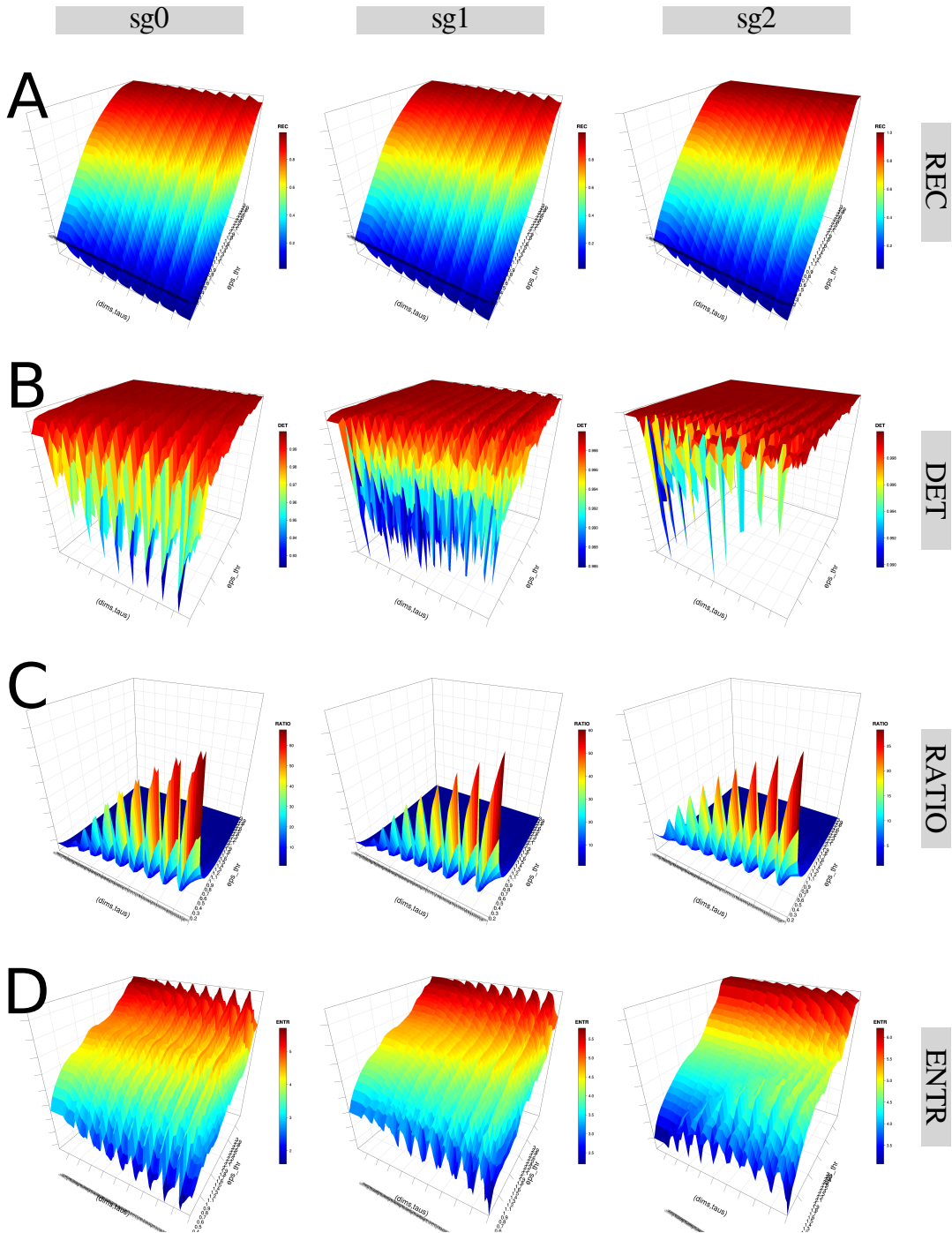


Fig. 6.23 3D surfaces for RQA metrics with three levels of smoothness. 3D surfaces of RQA metrics ((A) REC, (B) DET, (C) RATIO, and (D) ENTR) with increasing embedding parameters and recurrence thresholds for three levels of smoothness (sg0zmuvGyroZ, sg1zmuvGyroZ and sg1zmuvGyroZ). RQA metrics are computed from time series of participant p01 using HS01 sensor, HN activity and 500 samples window length. R code to reproduce the figure is available from Xochicale (2018).

6.7 The weaknesses and strengths of RQA

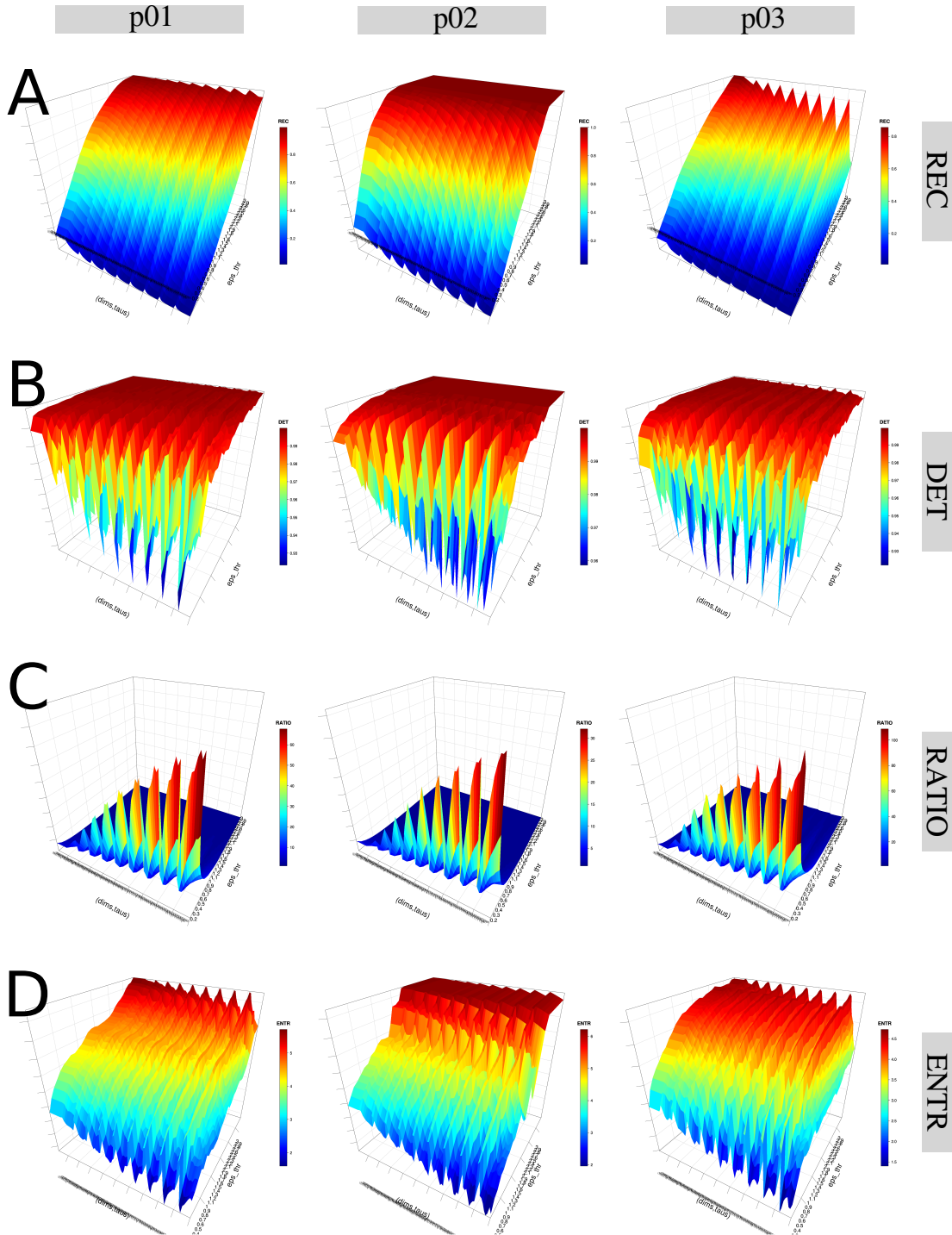


Fig. 6.24 **3D surfaces for RQA metrics with three participants.** 3D surfaces of RQA metrics ((A) REC, (B) DET, (C) RATIO, and (D) ENTR) for participants p01, p02 and p03 with increasing embedding parameters and recurrence thresholds. RQA metrics values are for time series of HS01 sensor, HN activity and 500 samples window length. R code to reproduce the figure is available from Xochicale (2018).

Chapter 7

Conclusions, contributions and future work

7.1 Conclusions

The main conclusion for this thesis is that quantification of MV in the context of human-humanoid interaction using nonlinear analyses with real-world data is possible. However, we will point out some positives and negatives of this thesis by answering the research questions.

7.1.1 What are the effects of different parameters for Nonlinear Tools with different characteristics of time series?

In general, it is evidently that time series from different sources (participants, movements, axis type, window size lengths or levels of smoothness) will present differences for not only the computation time of the embedding parameters but also for the patterns in RRSs, RP, RQAs and 3D surfaces of RQA metrics.

Conclusions, contributions and future work

7.1.2 How sensitive or robust are RQA metrics when quantifying MV?

In general, not only the activity type, window size length and structure of the time series affects the values of RQA metrics but also certain RQA metrics are better to describe the dynamics of a determined type of movement (predictability, organisation of the RPs, dynamics transitions, or complexity and determinism)

RQA metrics with fixed parameters

Considering that RQA metrics were computed with fixed embedding parameters ($m = 6$ and $\tau = 8$) and recurrence thresholds ($\epsilon = 1$), we found the following. REC values, representing the % of black points in the RPs, were more affected with an increase in normal movements (HN and VN) than faster velocity movements (HF and VF) for the sensor attached to the participants (HS01). Such decrease of REC values from normal to faster velocity movements is also presented in the time series from the sensor attached to the robot (RS01), and REC values for RS01 appear to be more constant than those from HS01. Similarly, DET values, representing predictability and organisation in the RPs, present little variation in the any of the time series where little can be said but the effect of smoothing the time series made DET values appear to be more similar and therefore constant. In contrast, RATIO values, which represent dynamic transitions, were more variable for arm movements performed at faster velocity (HF and VF) than normal velocity (HN and VN) for the sensor attached to the participants (HS01). For time series coming from sensor attached to the robot (RS01), RATIO values from horizontal movements (HN, HF) appear to vary more than values coming from vertical movements (VN, VF). With that in mind, it can be said that RATIO values can be represented better than using REC or DET metrics for the variability, particularly their dynamics transitions of imitation activities in each of the

7.1 Conclusions

conditions for time series. In the same way, ENTR values for HN were higher than values for HF and ENTR values varied more for sensor attached to participants (HS01) than ENTR values for sensors of the robot (RS01). It is evidently that the higher the entropy the more complex the dynamics are, however, ENTR values for HN appear a bit higher than HF values, we believe this happens because of the structure the time series which appear more complex for HN than HF movements (presenting a more consistence repetition).

We also explored the effect of smoothness of raw-normalised data for RQA metrics where, for instance, REC and DET values appear to be constant and therefore, they were little affected by the smoothness of time series. However, the effect of smoothness can be well noticed for both RATIO and ENTR values where a slightly decrease of amplitude of the values in any of the time series conditions is presented.

RQA metrics with different parameters

Patterns in RPs and metrics for RQA are independent of embedding dimension parameters (Iwanski and Bradley, 1998), however, that is not the case when using different recurrence thresholds. Hence, 3D surfaces of RQA with increments of embedding parameters and recurrence thresholds were computed to show their variations with respect to different characteristic of the time series such as window size length, participants, sensors and levels of smoothness. In general, it can be noted that the patterns in 3D surfaces of RQA are sensible to the increase of embedding parameters and recurrence threshold, meaning that stability of RQA metrics is dependant on changes of embedding parameters and recurrence thresholds.

Conclusions, contributions and future work

7.1.3 Is it fine to smooth raw time series for the quantification of MV?

The answer depends on what ones needs to measure, for instance, to avoid erratic changes in the metrics, smoothing the raw signals helps to have a more defined metric. In contrast, when using raw data, the metrics might create a closer representation of the variability.

With regard to the nonlinear tools, these are generally affected by the smoothness, showing also a proportional smoothness in the metrics. Also some RQA's metrics (e.g. DET and ENTR) are more robust to the effect of smoothness of time series.

It was also found that using a different levels of smoothness for time series helps to visualise the variations of movements between participants using RSSs, RPs and RQA. Also, it is important to mention that some RQA's metrics (e.g. DET and ENTR) are more robust to the effect of smoothness of time series. However, we believe that further investigation is required to find the right balance between the level of smoothness of the signal and its representations using RSS, RP and RQA. Particularly, where the level of smoothness does not affect the variation of each of the movements' quantification.

7.2 Contributions

This thesis contribute with experimental work to test the weakness and strengths of nonlinear dynamics tools with real-world data in the context of human-humanoid interaction, specially with the use of RQA metrics. Iwanski and Bradley (1998) pointed out that RQA metrics are independent of dimension parameters but through the 3D visualization of RQA patterns in this thesis we found that RQA are not only dependent on dimension parameters but dependent on recurrence thresholds.

7.3 Future work

7.3.1 Inertial sensors

To have more fundamental understanding of nature of signals collected through inertial sensors in the context of human-robot interaction, future experiments can be conducted considering the application of derivatives to the acceleration data. It can then explore the jerkiness of movements and therefore the nature of arm movements which typically have minimum jerk (Flash and Hogan, 1985), its relationship with different body parts, for instance, how rapid or slowly we perform arm and legs movements as we grow up (de Vries et al., 1982; Mori and Kuniyoshi, 2012) or the application of higher derivatives of displacement with respect time such as jounce, snap, crackle and pop (Eager et al., 2016).

7.3.2 Nonlinear analyses

While working with different nonlinear analyses we bumped into interesting areas that will be part of our future lines of research.

Embedding parameters

Considering the False Nearest Neighbour method (Cao, 1997) where the values for $E_1(m)$ stop changing to find the minimum embedding dimension, a threshold should be defined in order to obtain the minimum embedding dimension m_0 . Hence, a further investigation is required for the selection of the threshold in the $E_1(m)$, as the selection of the threshold in this thesis is only based on no particular method but visual inspection of the $E_1(m)$ curves.

Similarly, further research is required to be done with regards to the selection of the minimum delay embedding because it is not clear why the choose of the first minimum

Conclusions, contributions and future work

of the AMI is the minimum delay embedding parameter (Kantz and Schreiber, 2003) or why the probability distribution of the AMI function is computed with the use of histograms which depends on a heuristic choice of number of bins for the AMI partitioning (Garcia and Almeida, 2005). Additionally, "the AMI method is proposed for two dimensional reconstructions and then extended to be used in a multidimensional case which is not necessarily hold in higher dimensions" (Gómez-García et al., 2014, p. 156).

Other methodologies for state space reconstruction.

In addition to the Uniform Time-Delay Embedding method to reconstruct state spaces, other methods have been investigated to perform such reconstruction such as: (i) the nonuniform time-delay embedding methodology where the consecutive delayed copies of $\{\mathbf{x}_n\}$ are not equidistant. Such method has been proved to create better representations of the dynamics of the state space to analyse quasiperiodic and multiple time-scale time series (Pecora et al., 2007; Quintana-Duque and Saupe, 2013; Quintana-Duque, 2012, 2016; Uzal et al., 2011), and (ii) uniform 2 time-delay embedding method which takes advantage of finding an embedding window instead of the traditional method of finding the embedding parameters separately (Gómez-García et al., 2014). In general, uniform 2 time-delay embedding method computes m with False Nearest Neighbour (FNN) algorithm and τ is computed as $\tau = d_w/(m - 1)$, where d_w is given by the minimisation of the Minimum Description Length (Small and Tse, 2004).

Both methods (i) the nonuniform time-delay embedding or (ii) the uniform 2 time-delay embedding will create another line of our future research in order to have nonlinear tools that describe better the dynamics of the time series in the reconstructed state spaces.

RQA parameters

Having presented our results with RQA metrics, we believe that further investigation is required to have a better understanding of the RQA metrics and ensure its robustness. For example, Marwan et al. (2007) and Marwan and Webber (2015) reviewed different aspects to compute RPs using different criteria for neighbours, different norms (L_{1-norm} , L_{2-norm} , or $L_{\infty-norm}$) or different methods to select the recurrence threshold ϵ . With regard to the selection of the recurrence threshold, one can determine it by using only certain percentage of the signal ($\sqrt{m_0} \times 10\%$ of the fluctuations of the time series) Letellier (2006), select a determined amount of noise or using a factor based on the standard deviation of the observational noise Marwan et al. (2007).

Advanced RQA quantifications

In addition to the applied RQA metrics (REC, RATIO, DET and ENTR) for recurrence quantification, we believe that other line of future research for this thesis is the investigation of further quantification methodologies of the RP based on complex networks statics, calculation of dynamic invariants, study of the intermittency in the systems, applying different windowing techniques or the study of bivariate recurrence analysis for correlations, couplings, coupling directions or synchronisation between dynamical systems (Marwan et al., 2007; Marwan and Webber, 2015).

7.3.3 Variability in perception of velocity

While conducting the experiments with different arm movements velocities (e.g. normal and faster), we realised that participants perceive velocity in different ways. For instance, some participants considered a normal velocity movement as slow velocity movement and some others considered a slow velocity movement as being performed in normal velocity. With that in mind, we hypothesise that the differences in perception

Conclusions, contributions and future work

of velocities are related to the background of each person, for example, persons who have receive musical training in their infancy are more aware of their body movement. It would also be interesting to ask participants to move in three different velocities without any constrain in order to capture the natural movements of slow, normal and faster velocity arm movements. That sheds light of the need of another lines of research in our future work in order to have better understanding on why each participant perceive body movement velocity differently and how to quantify such variability of perception of movement.

7.3.4 A more rich dataset of time series

It should also be highlighted that the experiments for this thesis are limited to twenty three healthy right-handed participants of a range age of mean 19.8 SD=1.39, for which participants of different ages, state of health and anthropomorphic features would create more richness in the dataset of time series.

Appendix A

Examples of Uniform Time-Delay Embedding

For better understanding regarding the methodology of uniform time-delay embedding, two examples are presented in this appendix: (A.1) using a 20 sample length vector, and (A.2) using a time series from an horizontal movement of a triaxial accelerometer.

A.1 20 sample lenght vector.

For this example, we propose to work with a vector $\{\mathbf{x}_n\}_{n=1}^{20}$ with a sample length $N = 20$ in order to implement an uniform time-delay embedding matrix, \mathbf{X}_τ^m , with embedding dimension of $m = 5$ and delay dimension of $\tau = 3$ (Eq. (3.4)). The representation of

Examples of Uniform Time-Delay Embedding

the uniform time-delay embedding matrix \mathbf{X}_3^5 is as follows

$$\mathbf{X}_3^5 = \begin{pmatrix} \tilde{\mathbf{x}}_n \\ \tilde{\mathbf{x}}_{n-3} \\ \tilde{\mathbf{x}}_{n-6} \\ \tilde{\mathbf{x}}_{n-9} \\ \tilde{\mathbf{x}}_{n-12} \end{pmatrix}^\top \quad (\text{A.1})$$

The dimension of the uniform time-delay embedding matrix is defined by $N - (m - 1)\tau$ rows and m columns. $N - (m - 1)\tau$ is also the sample length of the delayed copies of \mathbf{x}_n which is equal to eight ($20 - ((5 - 1) * 3) = 8$). Therefore, \mathbf{X}_3^5 can be explicitly represented as

$$\mathbf{X}_3^5 = \begin{pmatrix} x_1 & x_2 & x_3 & x_4 & x_5 & x_6 & x_7 & x_8 \\ x_4 & x_5 & x_6 & x_7 & x_8 & x_9 & x_{10} & x_{11} \\ x_7 & x_8 & x_9 & x_{10} & x_{11} & x_{12} & x_{13} & x_{14} \\ x_{10} & x_{11} & x_{12} & x_{13} & x_{14} & x_{15} & x_{16} & x_{17} \\ x_{13} & x_{14} & x_{15} & x_{16} & x_{17} & x_{18} & x_{19} & x_{20} \end{pmatrix}^\top \quad (\text{A.2})$$

After transposing \mathbf{X}_3^5 , one can see that the ranges of values of the uniform time-delay embedded matrix are between $((m - 1)\tau) + 1$ to N (for this example from 13 to 20):

A.2 Time series from an horizontal movement of a triaxial accelerometer.

$$\mathbf{X}_3^5 = \begin{pmatrix} x_1 & x_4 & x_7 & x_{10} & x_{13} \\ x_2 & x_5 & x_8 & x_{11} & x_{14} \\ x_3 & x_6 & x_9 & x_{12} & x_{15} \\ x_4 & x_7 & x_{10} & x_{13} & x_{16} \\ x_5 & x_8 & x_{11} & x_{14} & x_{17} \\ x_6 & x_9 & x_{12} & x_{15} & x_{18} \\ x_7 & x_{10} & x_{13} & x_{16} & x_{19} \\ x_8 & x_{11} & x_{14} & x_{17} & x_{20} \end{pmatrix} = \begin{pmatrix} \mathbf{X}[13] \\ \mathbf{X}[14] \\ \mathbf{X}[15] \\ \mathbf{X}[16] \\ \mathbf{X}[17] \\ \mathbf{X}[18] \\ \mathbf{X}[19] \\ \mathbf{X}[20] \end{pmatrix}. \quad (\text{A.3})$$

A.2 Time series from an horizontal movement of a triaxial accelerometer.

In this example, it is considered a time series of a triaxial accelerometer, (Figure A.1(C)), captured from repetitions of a horizontal trajectory (Figure A.1(A)) performed by user (Figure A.1(B)). From Figure A.1(C)) is evidently that the $A_y(n)$ is the most affected axis of the accelerometer due to the movement's characteristics in the horizontal trajectory. With that in mind, we select $A_y(n)$ as the input time series for the uniform time-delay embedding theorem.

Considering that the sample rate of the data is 50 Hz we have a sample length of $N = 1000$ which corresponds to 20 seconds of data, we have that the minimum embedding parameters are $m = 7$ and $\tau = 11$ for $A_y(n)$. Then, the dimensions of the uniform time-delay embedding matrix, \mathbf{A}_{y11}^7 , are 934 ($N - (m - 1)\tau$) rows and 7 (m)

Examples of Uniform Time-Delay Embedding

columns. $\mathbf{A}_{y_{11}}^7$ is therefore represented as follows:

$$\mathbf{A}_{y_{11}}^7 = \begin{pmatrix} A_y(n) \\ A_y(n-11) \\ A_y(n-22) \\ A_y(n-33) \\ A_y(n-44) \\ A_y(n-55) \\ A_y(n-66) \end{pmatrix}^\top = \begin{pmatrix} a_y(1) & \dots & a_y(934) \\ a_y(12) & \dots & a_y(945) \\ a_y(23) & \dots & a_y(956) \\ a_y(34) & \dots & a_y(967) \\ a_y(45) & \dots & a_y(978) \\ a_y(56) & \dots & a_y(989) \\ a_y(67) & \dots & a_y(1000) \end{pmatrix}^\top \quad (\text{A.4})$$

$$\mathbf{A}_{y_{11}}^7 = \begin{pmatrix} a_y(1) & a_y(12) & a_y(23) & a_y(34) & a_y(45) & a_y(56) & a_y(67) \\ \vdots & \vdots & \vdots & \vdots & \vdots & \vdots & \vdots \\ a_y(934) & a_y(945) & a_y(956) & a_y(967) & a_y(978) & a_y(989) & a_y(1000) \end{pmatrix} = \begin{pmatrix} \mathbf{A}_{y_{11}}^7[67] \\ \vdots \\ \mathbf{A}_{y_{11}}^7[1000] \end{pmatrix}. \quad (\text{A.5})$$

A.2 Time series from an horizontal movement of a triaxial accelerometer.

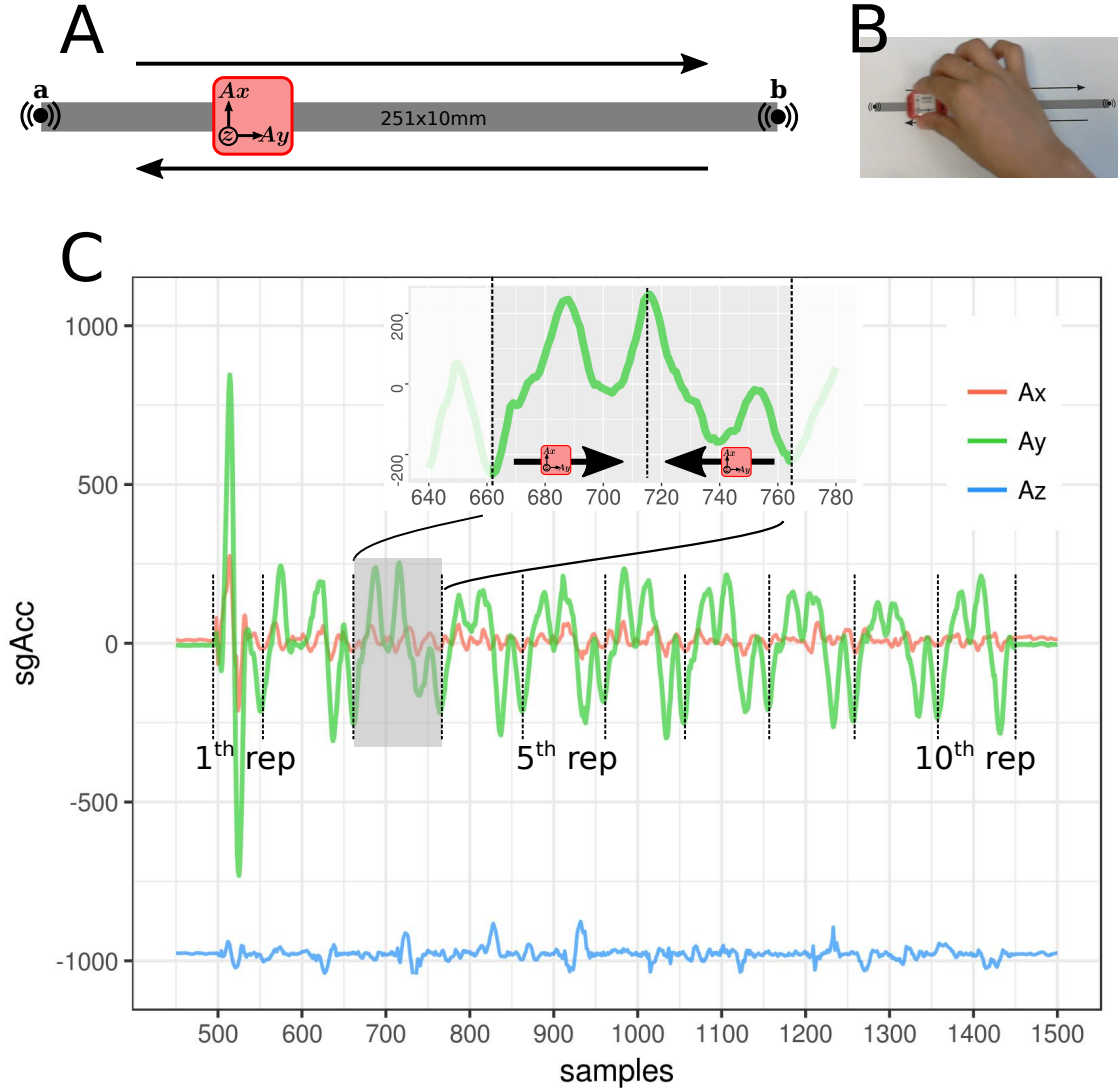


Fig. A.1 (A). Triaxial accelerometer (in red) is moved repetitively across a line of 251 mm from point **a** to **b** and then from **b** to **a**. The points **a** and **b** indicate when a click sound is produced. (B). Person's hand holding and moving the sensor horizontally across the line. (C). Time series for the triaxial accelerometer ($A_x(n)$, $A_y(n)$, $A_z(n)$) for ten repetitive horizontal movements across a line. The top time series only shows A_y axis which corresponds to one cycle of the horizontal movement and the black arrows represent the movement's direction of the accelerometer with respect to the produced time series.

Appendix B

Equipment

B.1 NeMEMsi IMU sensors

For this work, data were collected using NeMEMsi sensors Comotti et al. (2014) that provide 3D accelerometer, 3D magnetometer, 3D gyroscope and quaternions (Figure B.1). It is important to note that NeMEMsi sensors were tested against the state-of-the-art device MTi-30 IMU from xsense. The comparison values between NeMEMsi and MTi-30 in terms of standard deviation of the noise of each component of the Euler angles at a static state are lower than 0.1 degrees. Additionally, the NeMEMsi provide not only to have a lower-power consumption but also the smaller dimensions against other state-of-the-art brands of IMUs.

In the following sections, some features of the IMU are presented, however, we refer the readers to check Comotti et al. (2014) for further details.

Equipment

Sample rate and power consumption

Data streaming can be set up to be streamed at 25 Hz, 50 Hz and 100Hz which affects the power consumption from 29mAh, 32mAh and 35mAh, respectively. For this work, the sample rate were set up to 50 Hz.

Sensors

The outputs of the NeMEMSi sensor include:

Orientation

* Euler angles (Yaw, Pitch and Roll). * Quaternions.

Accelerometer (Linear acceleration)

* Raw and calibrated XYZ measurement from ± 2 / ± 4 / ± 6 / ± 8 / ± 16

Gyroscope (Rate of turn)

* Raw and calibrated XYZ measurement from ± 245 / ± 500 / ± 2000 degrees per second.

Magnetometer (Magnetic field)

* Raw and calibrated XYZ measurement from ± 4 / ± 8 / ± 12 / ± 16 gauss.

Microprocessor

* Arquitecture: ARM 32-bit Cortex M4 CPU with FPU and DSP instructions * Max.frequency: 100MHz * Memory Size: 512 Kbytes * RAM: 128 Kbytes SRAM

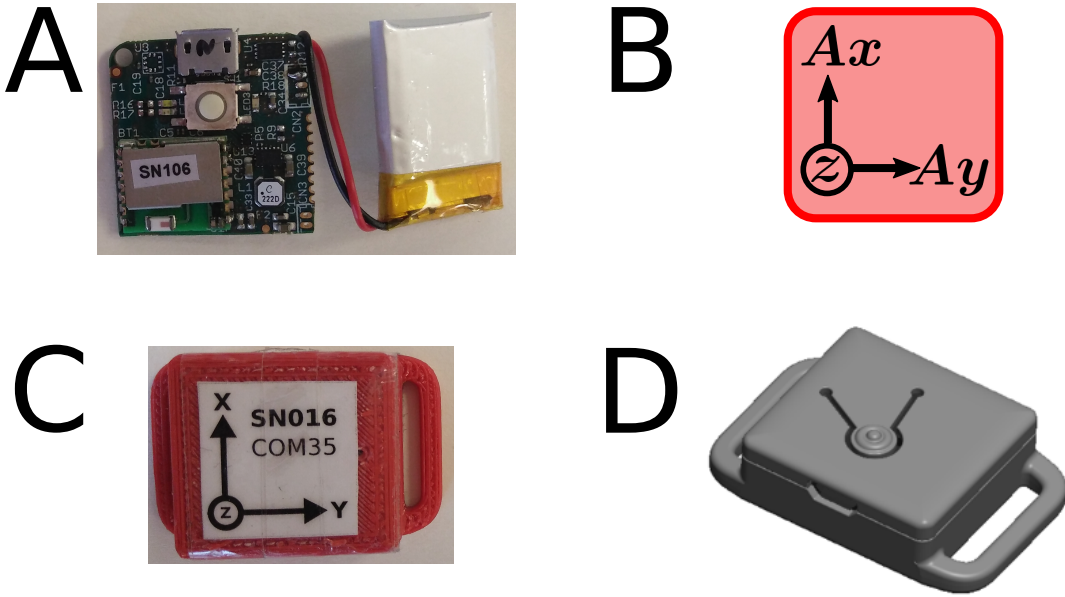


Fig. B.1 Inertial Measurement Sensor: (A) Printed Circuit Board (PCB) with 165mAh battery, (B) axis orientation, (C) real case, and (D) 3D model for the case.

Connectivity

* Bluetooth: Class 2, bluetooth 3.0 * Range: 10 m * Transmission rate: Up to 560 kbps with Service Port to Port * Multipoint: Up to 7 slaves

Form factor

* Electronics physical dimension: 25L x 25W x 4H (mm) * Electronics Weight: 3.3 gr * Dimension with battery and casing: 42L x 28W x 11.5 (mm) * Weight with batter and casing: 15 gr

B.2 Time-series preprocessing

B.2.1 Organising Data in Multidimensional Arrays

Scripts in MATLAB were created to syncronise the data using the clock drift and clock offset values which were provided for each of the NeMEMSi sensors. Then the data from each sensor is aligned in time using using `finddelay()` and `alignsignals()` in MATLAB.

The use of `alignsignals()` is useful when the data is relatively clean that means that when data was noisy the alignment were not even close when two signals were quite similar. Therefore, I decided to program my own `alignsignalsMX()` to use the synchronised data but with different length.

Scripts in R were used for postprocessing the data.

B.2.2 Data Synchronisation

To find the delay between two two sensors that were attached to the same place of the body parts, a function called `finddelayMX()` was created. Such function computes the autocorrelation between two signals using `(xcorr())` then the maximum value of the the autocorrelation function is extracted to create a delay between the values of maximum index in the autocorrelation function and the length of the first signal

The function `alignsignalsMX()` was used to align two signals based on `finddelayMX()`. The function `alignsignalsMX()` use six inputs of which sA and sB are the sensors, then the windowframe of which the information of the signal is extracted from another activities, the MainAxis of which the signal are going to be extracted, the truncate delay that is created to syncrohnise the signals adding an extra delay that is based on the lenght of previous signals and tunning delay that can be useful to tune the delay in the case of the dalay is not appropriate when the signals are too noisy.

Then, it is used the `aligntwosignals()` to align only two signals. The inputs of `aligntwosignals()` are X and Y for the input vectors, truncate delay for the previous delay of two signals and tuning delay in case that signals are two noise and the `xcorr` fail to find an appropriate delay.

B.2.3 Time Alignment

It was taken another approach to align the data in time in which the original synchronised data is manipulated. Given four vectors of time t_1, t_2, t_3, t_4 , it is extracted the minimum and maximum values of the start of the four sequence of time, it was also extacted the minimum and maximum values to the end of the four sequence of time.

However, after aligning the vectors it has then been noticed that there were different values of lenght across vectors i.e.: 1880, 1986, 1987, 1988 Therefore the lenght for the second vector was used as the primary lenght because is the one that is present the minimum value of the three maximum lenghts. Then `interp1(x,v,vq,'phchip')` was used to interpolate the length of each of the vectors such as the length of all vectors is: 1986, 1986, 1986, 1986. It has been choosen the `phchip` since the interpolation present values for each of the points which were different for the NA values from what it has been got when using `linear`.

B.3 Humanoid robot

B.3.1 Hardware

B.3.2 Software

Appendix C

Experiment Design

L^AT_EX.cls files can be accessed system-wide when they are placed in the <texmf>/ tex/ latex directory, where <texmf> is the root directory of the user's T_EX installation. On systems that have a local texmf tree (<texmflocal>), which may be named "texmf-local" or "localtexmf", it may be advisable to install packages in <texmflocal>, rather than <texmf> as the contents of the former, unlike that of the latter, are preserved after the L^AT_EXsystem is reinstalled and/or upgraded.

C.1 Experiment Check List

C.2 Ethics

C.3 Information Sheet

Appendix D

Results for all data

$\text{\LaTeX}.\text{cls}$ files can be accessed system-wide when they are placed in the $\langle\text{texmf}\rangle/\text{tex}/\text{latex}$ directory, where $\langle\text{texmf}\rangle$ is the root directory of the user's \TeX installation. On systems that have a local texmf tree ($\langle\text{texmflocal}\rangle$), which may be named "texmf-local" or "localtexmf", it may be advisable to install packages in $\langle\text{texmflocal}\rangle$, rather than $\langle\text{texmf}\rangle$ as the contents of the former, unlike that of the latter, are preserved after the \LaTeX system is reinstalled and/or upgraded.

D.1 Time Series

D.2 Embedding parameters

D.3 RSSs

D.4 RPs

D.5 RQAs

References

- Aguirre, L. A. and Letellier, C. (2009). Modeling nonlinear dynamics and chaos: A review. *Mathematical Problems in Engineering*, 11(12):1–22.
- Amato, I. (1992). Chaos breaks out at nih, but order may come of it. *Science*, 256(5065):1763–1764.
- Anguita, D., Ghio, A., Oneto, L., Parra, X., and Reyes-Ortiz, J. L. (2013). A public domain dataset for human activity recognition using smartphones. In *21th European Symposium on Artificial Neural Networks, Computational Intelligence and Machine Learning, ESANN 2013*.
- Azami, H. and Escudero, J. (2016). Amplitude-aware permutation entropy: Illustration in spike detection and signal segmentation. *Computer Methods and Programs in Biomedicine*, 128:40 – 51.
- Bandt, C. and Pompe, B. (2002). Permutation entropy: A natural complexity measure for time series. *Phys. Rev. Lett.*, 88:174102.
- Bartlett, R., Wheat, J., and Robins, M. (2007). Is movement variability important for sports biomechanists? *Sports Biomechanics*, 6(2):224–243. PMID: 17892098.
- Benzeghiba, M., Mori, R. D., Deroo, O., Dupont, S., Erbes, T., Jouvet, D., Fissore, L., Laface, P., Mertins, A., Ris, C., Rose, R., Tyagi, V., and Wellekens, C. (2007). Automatic speech recognition and speech variability: A review. *Speech Communication*, 49(10):763 – 786. Intrinsic Speech Variations.
- Bernstein, N. (1967). *The co-ordination and regulation of movements*. Pergamon-Press.
- Bonnet, V., Ramdani, S., Azevedo-Coste, C., Fraisse, P., Mazzà, C., and Cappozzo, A. (2014). Integration of human walking gyroscopic data using empirical mode decomposition. *Sensors*, 14(1):370–381.
- Bradley, E. and Kantz, H. (2015). Nonlinear time-series analysis revisited. *Chaos: An Interdisciplinary Journal of Nonlinear Science*, 25(9):097610.
- Bruijn, S. M., van Dieën, J. H., Meijer, O. G., and Beek, P. J. (2009). Is slow walking more stable? *Journal of Biomechanics*, 42(10):1506 – 1512.
- Bryce, R. and Sprague, K. (2012). Revisiting detrended fluctuation analysis. *Scientific reports*, 2:315.

References

- Caballero, C., Barbado, D., and Moreno, F. (2013). El procesado del desplazamiento del centro de presiones para el estudio de la relación complejidad/rendimiento observada en el control postural en bipedestación. *Revista Andaluza de Medicina del Deporte*, 6(3):101 – 107.
- Caballero, C., Barbado, D., and Moreno, F. J. (2014). Non-linear tools and methodological concerns measuring human movement variability: An overview. *European Journal of Human Movement*, 32:31–81.
- Cao, L. (1997). Practical method for determining the minimum embedding dimension of a scalar time series. *Physica D: Nonlinear Phenomena*, 110:43–50.
- Carroll, J. P. and Freedman, W. (1993). Nonstationary properties of postural sway. *Journal of biomechanics*, 26(4):409–416.
- Casdagli, M., Eubank, S., Farmer, J., and Gibson, J. (1991). State space reconstruction in the presence of noise. *Physica D: Nonlinear Phenomena*, 51(1):52 – 98.
- Cavanaugh, J. T., Kochi, N., and Stergiou, N. (2010). Nonlinear analysis of ambulatory activity patterns in community-dwelling older adults. *The Journals of Gerontology: Series A*, 65A(2):197–203.
- Chen, W., Wang, Z., Xie, H., and Yu, W. (2007). Characterization of surface emg signal based on fuzzy entropy. *IEEE Transactions on Neural Systems and Rehabilitation Engineering*, 15(2):266–272.
- Chen, W., Zhuang, J., Yu, W., and Wang, Z. (2009). Measuring complexity using fuzzyen, apen, and sampen. *Medical Engineering and Physics*, 31(1):61 – 68.
- Chiari, L., Rocchi, L., and Cappello, A. (2002). Stabilometric parameters are affected by anthropometry and foot placement. *Clinical Biomechanics*, 17(9):666 – 677.
- Coffey, N., Harrison, A., Donoghue, O., and Hayes, K. (2011). Common functional principal components analysis: A new approach to analyzing human movement data. *Human Movement Science*, 30(6):1144 – 1166.
- Comotti, D., Galizzi, M., and Vitali, A. (2014). nememsi: One step forward in wireless attitude and heading reference systems. In *2014 International Symposium on Inertial Sensors and Systems (ISISS)*, pages 1–4.
- Costa, M., Goldberger, A. L., and Peng, C.-K. (2002). Multiscale entropy analysis of complex physiologic time series. *Phys. Rev. Lett.*, 89:068102.
- Costa, M., Priplata, A. A., Lipsitz, L. A., Wu, Z., Huang, N. E., Goldberger, A. L., and Peng, C.-K. (2007). Noise and poise: Enhancement of postural complexity in the elderly with a stochastic-resonance-based therapy. *EPL (Europhysics Letters)*, 77(6):68008.
- Daubechies, I., Lu, J., and Wu, H.-T. (2011). Synchrosqueezed wavelet transforms: An empirical mode decomposition-like tool. *Applied and Computational Harmonic Analysis*, 30(2):243 – 261.

References

- de Vries, J., Visser, G., and Prechtel, H. (1982). The emergence of fetal behaviour. i. qualitative aspects. *Early Human Development*, 7(4):301 – 322.
- Delignères, D., Deschamps, T., Legros, A., and Caillou, N. (2003). A methodological note on nonlinear time series analysis: Is the open-and closed-loop model of collins and de luca (1993) a statistical artifact? *Journal of Motor Behavior*, 35(1):86–96. PMID: 12724102.
- Dhingra, R. R., Jacono, F. J., Fishman, M., Loparo, K. A., Rybak, I. A., and Dick, T. E. (2011). Vagal-dependent nonlinear variability in the respiratory pattern of anesthetized, spontaneously breathing rats. *Journal of Applied Physiology*, 111(1):272–284. PMID: 21527661.
- Dingwell, J. B. and Cusumano, J. P. (2000). Nonlinear time series analysis of normal and pathological human walking. *Chaos: An Interdisciplinary Journal of Nonlinear Science*, 10(4):848–863.
- Dingwell, J. B. and Kang, H. G. (2007). Differences between local and orbital dynamic stability during human walking. *Journal of biomechanical engineering*, 129(4):586—593.
- Donker, S. F., Roerdink, M., Greven, A. J., and Beek, P. J. (2007). Regularity of center-of-pressure trajectories depends on the amount of attention invested in postural control. *Experimental Brain Research*, 181(1):1–11.
- Duarte, M. and Sternad, D. (2008). Complexity of human postural control in young and older adults during prolonged standing. *Experimental Brain Research*, 191(3):265–276.
- Eager, D., Pendrill, A.-M., and Reistad, N. (2016). Beyond velocity and acceleration: jerk, snap and higher derivatives. *European Journal of Physics*, 37(6):065008.
- Eckmann, J.-P., Kamphorst, S. O., and Ruelle, D. (1987). Recurrence plots of dynamical systems. *EPL (Europhysics Letters)*, 4(9):973.
- Emrani, S., Gentimis, T., and Krim, H. (2014). Persistent homology of delay embeddings and its application to wheeze detection. *IEEE Signal Processing Letters*, 21(4):459–463.
- Ferdenzi, C., Roberts, S. C., Schirmer, A., Delplanque, S., Cekic, S., Porcherot, C., Cayeux, I., Sander, D., and Grandjean, D. (2013). Variability of affective responses to odors: Culture, gender, and olfactory knowledge. *Chemical Senses*, 38(2):175–186.
- Flandrin, P., Gonçalvès, P., and Rilling, G. (2004). Detrending and denoising with empirical mode decompositions. In *2004 12th European Signal Processing Conference*, pages 1581–1584.
- Flash, T. and Hogan, N. (1985). The coordination of arm movements: an experimentally confirmed mathematical model. *Journal of Neuroscience*, 5(7):1688–1703.
- Frank, J., Mannor, S., and Precup, D. (2010). Activity and gait recognition with time-delay embeddings. *AAAI Conference on Artificial Intelligence*, pages 407–408.

References

- Fraser, A. M. and Swinney, H. L. (1986). Independent coordinates for strange attractors from mutual information. *Phys. Rev. A*, 33:1134–1140.
- Garcia, C. A. and Sawitzki, G. (2016). *nonlinearTseries: Nonlinear Time Series Analysis*. R package version 0.2.4 — For new features, see the 'Changelog' file (in the package source).
- Garcia, S. P. and Almeida, J. S. (2005). Nearest neighbor embedding with different time delays. *Phys. Rev. E*, 71:037204.
- Garland, J., Bradley, E., and Meiss, J. D. (2016). Exploring the topology of dynamical reconstructions. *Physica D: Nonlinear Phenomena*, 334:49 – 59. Topology in Dynamics, Differential Equations, and Data.
- Gates, D. H. and Dingwell, J. B. (2007). Peripheral neuropathy does not alter the fractal dynamics of stride intervals of gait. *Journal of Applied Physiology*, 102(3):965–971. PMID: 17110519.
- Gates, D. H. and Dingwell, J. B. (2008). The effects of neuromuscular fatigue on task performance during repetitive goal-directed movements. *Experimental Brain Research*, 187(4):573–585.
- Gibson, J. F., Farmer, J. D., Casdagli, M., and Eubank, S. (1992). An analytic approach to practical state space reconstruction. *Physica D: Nonlinear Phenomena*, 57(1):1 – 30.
- Goldberger, A. (1996). Non-linear dynamics for clinicians: chaos theory, fractals, and complexity at the bedside. *The Lancet*, 347(9011):1312 – 1314.
- Goldberger, A. L., Peng, C.-K., and Lipsitz, L. A. (2002). What is physiologic complexity and how does it change with aging and disease? *Neurobiology of Aging*, 23(1):23 – 26.
- Goldberger, A. L., Rigney, D. R., and West, B. J. (1990). Chaos and fractals in human physiology. *Scientific American*, 262(2):42–49.
- Görer, B., Salah, A. A., and Akin, H. L. (2013). A robotic fitness coach for the elderly. In Augusto, J. C., Wichert, R., Collier, R., Keyson, D., Salah, A. A., and Tan, A.-H., editors, *Ambient Intelligence*, pages 124–139, Cham. Springer International Publishing.
- Gouaillier, D., Hugel, V., Blazevic, P., Kilner, C., Monceaux, J., Lafourcade, P., Marnier, B., Serre, J., and Maisonnier, B. (2009). Mechatronic design of nao humanoid. In *Proceedings of the 2009 IEEE International Conference on Robotics and Automation, ICRA'09*, pages 2124–2129, Piscataway, NJ, USA. IEEE Press.
- Guastello, S. J. and Gregson, R. A. M. (2011). *Nonlinear Dynamical Systems Analysis for the Behavioral Science Using Real Data*. CRC Press.

References

- Guneyşu, A., Arnrich, B., and Ersoy, C. (2015). Children's rehabilitation with humanoid robots and wearable inertial measurement units. In *Proceedings of the 9th International Conference on Pervasive Computing Technologies for Healthcare, PervasiveHealth '15*, pages 249–252, ICST, Brussels, Belgium, Belgium. ICST (Institute for Computer Sciences, Social-Informatics and Telecommunications Engineering).
- Guneyşu, A., Siyli, R. D., and Salah, A. A. (2014). Auto-evaluation of motion imitation in a child-robot imitation game for upper arm rehabilitation. In *The 23rd IEEE International Symposium on Robot and Human Interactive Communication*, pages 199–204.
- Gómez-García, J. A., Godino-Llorente, J. I., and Castellanos-Dominguez, G. (2014). Non uniform embedding based on relevance analysis with reduced computational complexity: Application to the detection of pathologies from biosignal recordings. *Neurocomputing*, 132(Supplement C):148 – 158. Innovations in Nature Inspired Optimization and Learning Methods Machines learning for Non-Linear Processing.
- Harbourne, R. T. and Stergiou, N. (2009). Movement variability and the use of nonlinear tools: Principles to guide physical therapist practice. *Physical Therapy*, 89(3):267–282.
- Hatze, H. (1986). Motion variability—its definition, quantification, and origin. *Journal of Motor Behavior*, 18(1):5–16. PMID: 15136282.
- Hausdorff, J. M. (2009). Gait dynamics in parkinson's disease: Common and distinct behavior among stride length, gait variability, and fractal-like scaling. *Chaos: An Interdisciplinary Journal of Nonlinear Science*, 19(2):026113.
- Hausdorff, J. M., Peng, C. K., Ladin, Z., Wei, J. Y., and Goldberger, A. L. (1995). Is walking a random walk? evidence for long-range correlations in stride interval of human gait. *Journal of Applied Physiology*, 78(1):349–358. PMID: 7713836.
- Herzfeld, D. J. and Shadmehr, R. (2014). Motor variability is not noise, but grist for the learning mill. *nature neuroscience*, 17(2):149.
- Huang, N. E., Shen, Z., Long, S. R., Wu, M. C., Shih, H. H., Zheng, Q., Yen, N.-C., Tung, C. C., and Liu, H. H. (1998). The empirical mode decomposition and the hilbert spectrum for nonlinear and non-stationary time series analysis. *Proceedings of the Royal Society of London A: Mathematical, Physical and Engineering Sciences*, 454(1971):903–995.
- Huffaker, R., Bittelli, M., and Rosa, R. (2017). *Nonlinear Time Series Analysis with R*. Oxford University Press.
- Ioffe, S. and Szegedy, C. (2015). Batch normalization: Accelerating deep network training by reducing internal covariate shift. *CoRR*, abs/1502.03167.
- Iwanski, J. S. and Bradley, E. (1998). Recurrence plots of experimental data: To embed or not to embed? *Chaos: An Interdisciplinary Journal of Nonlinear Science*, 8(4):861–871.

References

- Kabiraj, L., Saurabh, A., Wahi, P., and Sujith, R. I. (2012). Route to chaos for combustion instability in ducted laminar premixed flames. *Chaos: An Interdisciplinary Journal of Nonlinear Science*, 22(2):023129.
- Kanai, R. and Rees, G. (2011). The structural basis of inter-individual differences in human behaviour and cognition. *Nature Reviews Neuroscience*, 12(4):231.
- Kantz, H. and Schreiber, T. (2003). *Nonlinear Time Series Analysis*. Cambridge University Press, New York, NY, USA.
- Kennel, M. B., Brown, R., and Abarbanel, H. D. I. (1992). Determining embedding dimension for phase-space reconstruction using a geometrical construction. *Phys. Rev. A*, 45:3403–3411.
- Kitagawa, G. and Gersch, W. (1984). A smoothness priors-state space modeling of time series with trend and seasonality. *Journal of the American Statistical Association*, 79(386):378–389.
- Klonowski, W. (2002). Chaotic dynamics applied to signal complexity in phase space and in time domain. *Chaos, Solitons and Fractals*, 14(9):1379 – 1387.
- Klonowski, W. (2007). From conformons to human brains: an informal overview of nonlinear dynamics and its applications in biomedicine. *Nonlinear Biomedical Physics*, 1(1):5.
- Klonowski, W. (2009). Everything you wanted to ask about eeg but were afraid to get the right answer. *Nonlinear Biomedical Physics*, 3(1):2.
- Krakovská, A., Mezeiová, K., and I, H. B. (2015). Use of False Nearest Neighbours for Selecting Variables and Embedding Parameters for State Space Reconstruction. *Journal of Complex Systems*, 2015.
- Krüger, M., Eggert, T., and Straube, A. (2013). Age-related differences in the stabilization of important task variables in reaching movements. *Motor Control*, 17(3):313–320.
- Kurz, M. J. and Hou, J. G. (2010). Levodopa influences the regularity of the ankle joint kinematics in individuals with parkinson’s disease. *Journal of Computational Neuroscience*, 28(1):131–136.
- Kurz, M. J., Markopoulou, K., and Stergiou, N. (2010). Attractor divergence as a metric for assessing walking balance. *Nonlinear dynamics, psychology, and life sciences*, 14(2):151—164.
- Lake, D. E. and Moorman, J. R. (2011). Accurate estimation of entropy in very short physiological time series: the problem of atrial fibrillation detection in implanted ventricular devices. *American Journal of Physiology-Heart and Circulatory Physiology*, 300(1):H319–H325. PMID: 21037227.
- Letellier, C. (2006). Estimating the shannon entropy: Recurrence plots versus symbolic dynamics. *Phys. Rev. Lett.*, 96:254102.

References

- Liao, F., Wang, J., and He, P. (2008). Multi-resolution entropy analysis of gait symmetry in neurological degenerative diseases and amyotrophic lateral sclerosis. *Medical Engineering and Physics*, 30(3):299 – 310.
- MacDonald, S. W., Nyberg, L., and Bäckman, L. (2006). Intra-individual variability in behavior: links to brain structure, neurotransmission and neuronal activity. *Trends in Neurosciences*, 29(8):474 – 480.
- Madeleine, P. and Madsen, T. (2009). Changes in the amount and structure of motor variability during a deboning process are associated with work experience and neck–shoulder discomfort. *Applied Ergonomics*, 40(5):887 – 894.
- Madeleine, P., Mathiassen, S. E., and Arendt-Nielsen, L. (2008). Changes in the degree of motor variability associated with experimental and chronic neck–shoulder pain during a standardised repetitive arm movement. *Experimental Brain Research*, 185(4):689–698.
- Mandic, D. P., u. Rehman, N., Wu, Z., and Huang, N. E. (2013). Empirical mode decomposition-based time-frequency analysis of multivariate signals: The power of adaptive data analysis. *IEEE Signal Processing Magazine*, 30(6):74–86.
- Marwan, N. (2008). A historical review of recurrence plots. *The European Physical Journal Special Topics*, 164(1):3–12.
- Marwan, N. (2011). How to Avoid Potential Pitfalls in Recurrence Plot Based Data Analysis. *International Journal of Bifurcation and Chaos*, 21:1003.
- Marwan, N., Romano, M. C., Thiel, M., and Kurths, J. (2007). Recurrence plots for the analysis of complex systems. *Physics Reports*, 438(5):237 – 329.
- Marwan, N. and Webber, C. L. (2015). Mathematical and computational foundations of recurrence quantifications. In Webber, C. L. and Marwan, N., editors, *Recurrence Quantification Analysis: Theory and Best Practices*, chapter 1, pages 3–43. Springer, Cham, 1 edition.
- Mathiassen, S. E. (2006). Diversity and variation in biomechanical exposure: What is it, and why would we like to know? *Applied Ergonomics*, 37(4):419 – 427. Special Issue: Meeting Diversity in Ergonomics.
- Mert, A. and Akan, A. (2018). Emotion recognition from eeg signals by using multivariate empirical mode decomposition. *Pattern Analysis and Applications*, 21(1):81–89.
- Miller, D. J., Stergiou, N., and Kurz, M. J. (2006). An improved surrogate method for detecting the presence of chaos in gait. *Journal of Biomechanics*, 39(15):2873 – 2876.
- Mori, H. and Kuniyoshi, Y. (2012). Is the developmental order of fetal behaviors self-organized in an uterine environment? In *2012 IEEE International Conference on Development and Learning and Epigenetic Robotics (ICDL)*, pages 1–2.
- Müller, H. and Sternad, D. (2004). Decomposition of variability in the execution of goal-oriented tasks: three components of skill improvement. *Journal of Experimental Psychology: Human Perception and Performance*, 30(1):212.

References

- Newell, K. and Corcos, D. (1993). *Variability and Motor Control*. Human Kinetics Publishers.
- Newell, K. M. and Slifkin, A. B. (1998). The nature of movement variability. In Piek, J. P., editor, *Motor behavior and human skill : a multidisciplinary approach*, chapter 7, pages 143–160. Champaign, IL : Human Kinetics.
- Packard, N. H., Crutchfield, J. P., Farmer, J. D., and Shaw, R. S. (1980). Geometry from a time series. *Phys. Rev. Lett.*, 45:712–716.
- Pecora, L. M., Moniz, L., Nichols, J., and Carroll, T. L. (2007). A unified approach to attractor reconstruction. *Chaos: An Interdisciplinary Journal of Nonlinear Science*, 17(1):013110.
- Pellecchia, G. L. and Shockley, K. (2015). Application of recurrence quantification analysis: Influence of cognitive activity on postural fluctuations. In Riley, M., Van Orden, G., and (U.S.), N. S. F., editors, *Tutorials in Contemporary Nonlinear Methods for the Behavioral Sciences*, chapter 3, pages 95–141. National Science Foundation.
- Peng, C., Havlin, S., Stanley, H. E., and Goldberger, A. L. (1995). Quantification of scaling exponents and crossover phenomena in nonstationary heartbeat time series. *Chaos: An Interdisciplinary Journal of Nonlinear Science*, 5(1):82–87.
- Peng, H., Zhou, C., Hu, H., Chao, F., and Li, J. (2015). Robotic dance in social robotics – a taxonomy. *IEEE Transactions on Human-Machine Systems*, 45(3):281–293.
- Pincus, S. (1995). Approximate entropy (apen) as a complexity measure. *Chaos: An Interdisciplinary Journal of Nonlinear Science*, 5(1):110–117.
- Pincus, S. M. (1991). Approximate entropy as a measure of system complexity. *Proceedings of the National Academy of Sciences of the United States of America*, 88(6):2297–2301.
- Preatoni, E. (2007). *Innovative methods for the analysis of sports movements and for the longitudinal monitoring of individual motor skills*. PhD thesis, Politecnico di Milano.
- Preatoni, E., Ferrario, M., Donà, G., Hamill, J., and Rodano, R. (2010). Motor variability in sports: A non-linear analysis of race walking. *Journal of Sports Sciences*, 28(12):1327–1336. PMID: 20853204.
- Preatoni, E., Hamill, J., Harrison, A. J., Hayes, K., Emmerik, R. E. V., Wilson, C., and Rodano, R. (2013). Movement variability and skills monitoring in sports. *Sports Biomechanics*, 12(2):69–92. PMID: 23898682.
- Press, W. H., Teukolsky, S. A., Vetterling, W. T., and Flannery, B. P. (1992). *Numerical Recipes in C (2Nd Ed.): The Art of Scientific Computing*. Cambridge University Press, New York, NY, USA.

References

- Quintana-Duque, J. and Saupe, D. (2013). *Evidence of Chaos in Indoor Pedaling Motion using Non-linear Methods*. Number July in Performance Analysis of Sport. Routledge.
- Quintana-Duque, J. C. (2012). Non-linear dynamic invariants based on embedding reconstruction of systems for pedaling motion. In Byshko, R., editor, *Sportinformatik 2012 : 9. vom 12.- 14. Sept. 2012 in Konstanz : Beiträge*, pages 28–38. Universität.
- Quintana-Duque, J. C. (2016). *Non-linear methods for the quantification of cyclic motion*. PhD dissertation, University of Konstanz, Konstanz, Germany.
- Rajendra Acharya, U., Paul Joseph, K., Kannathal, N., Lim, C. M., and Suri, J. S. (2006). Heart rate variability: a review. *Medical and Biological Engineering and Computing*, 44(12):1031–1051.
- Rangarajan, G. and Ding, M. (2000). Integrated approach to the assessment of long range correlation in time series data. *Phys. Rev. E*, 61:4991–5001.
- Rehman, N. and Mandic, D. P. (2010). Multivariate empirical mode decomposition. *Proceedings of the Royal Society of London A: Mathematical, Physical and Engineering Sciences*, 466(2117):1291–1302.
- Rhea, C. K., Silver, T. A., Hong, S. L., Ryu, J. H., Studenka, B. E., Hughes, C. M. L., and Haddad, J. M. (2011). Noise and complexity in human postural control: Interpreting the different estimations of entropy. *PLOS ONE*, 6(3):1–9.
- Richman, J. S. and Moorman, J. R. (2000). Physiological time-series analysis using approximate entropy and sample entropy. *American Journal of Physiology-Heart and Circulatory Physiology*, 278(6):H2039–H2049. PMID: 10843903.
- Riley, M., Balasubramaniam, R., and Turvey, M. (1999). Recurrence quantification analysis of postural fluctuations. *Gait and Posture*, 9(1):65 – 78.
- Rosenstein, M. T., Collins, J. J., and Luca, C. J. D. (1993). A practical method for calculating largest lyapunov exponents from small data sets. *Physica D: Nonlinear Phenomena*, 65(1):117 – 134.
- Rosenstein, M. T., Collins, J. J., and Luca, C. J. D. (1994). Reconstruction expansion as a geometry-based framework for choosing proper delay times. *Physica D: Nonlinear Phenomena*, 73(1):82 – 98.
- Samà, A., Ruiz, F. J., Agell, N., Pérez-López, C., Català, A., and Cabestany, J. (2013). Gait identification by means of box approximation geometry of reconstructed attractors in latent space. *Neurocomputing*, 121:79–88.
- Sandlund, J., Röijezon, U., Björklund, M., and Djupsjöbacka, M. (2008). Acuity of goal-directed arm movements to visible targets in chronic neck pain. *Journal of Rehabilitation Medicine*, 40(5):366–374.
- Sandlund, J., Srinivasan, D., Heiden, M., and Mathiassen, S. E. (2017). Differences in motor variability among individuals performing a standardized short-cycle manual task. *Human Movement Science*, 51:17 – 26.

References

- Savitzky, A. and Golay, M. J. E. (1964). Smoothing and differentiation of data by simplified least squares procedures. *Analytical Chemistry*, 36:1627–1639.
- Schafer, R. W. (2011). On the frequency-domain properties of savitzky-golay filters. In *2011 Digital Signal Processing and Signal Processing Education Meeting (DSP/SPE)*, pages 54–59.
- Schumacher, A. (2004). Linear and nonlinear approaches to the analysis of r-r interval variability. *Biological Research For Nursing*, 5(3):211–221. PMID: 14737922.
- Seifert, L., Leblanc, H., Herault, R., Komar, J., Button, C., and Chollet, D. (2011). Inter-individual variability in the upper-lower limb breaststroke coordination. *Human Movement Science*, 30(3):550 – 565.
- Shoaib, M., Bosch, S., Incel, O. D., Scholten, H., and Havinga, P. J. M. (2016). Complex human activity recognition using smartphone and wrist-worn motion sensors. *Sensors*, 16(4).
- signal R developers (2014). *signal: Signal processing*.
- Small, M. and Tse, C. (2004). Optimal embedding parameters: a modelling paradigm. *Physica D: Nonlinear Phenomena*, 194(3):283 – 296.
- Sosnoff, J. J., Valantine, A. D., and Newell, K. M. (2006). Independence between the amount and structure of variability at low force levels. *Neuroscience Letters*, 392(3):165 – 169.
- Sosnoff, J. J. and Voudrie, S. J. (2009). Practice and age-related loss of adaptability in sensorimotor performance. *Journal of Motor Behavior*, 41(2):137–146. PMID: 19201684.
- Srinivasan, D. and Mathiassen, S. E. (2012). Motor variability in occupational health and performance. *Clinical Biomechanics*, 27(10):979 – 993.
- Stergiou, N. (2004). *Innovative analyses of human movement*. Champaign, IL : Human Kinetics.
- Stergiou, N. and Decker, L. M. (2011). Human movement variability, nonlinear dynamics, and pathology: Is there a connection? *Human Movement Science*, 30(5):869 – 888. EWOMS 2009: The European Workshop on Movement Science.
- Stergiou, N., Harbourne, R., and Cavanaugh, J. (2006). Optimal movement variability: a new theoretical perspective for neurologic physical therapy. *Journal of neurologic physical therapy : JNPT*, 30(3):120—129.
- Stergiou, N., Kent, J. A., and McGrath, D. (2016). Human movement variability and aging. *Kinesiology Review*, 5(1):15–22.
- Stins, J., Michielsen, M., Roerdink, M., and Beek, P. (2009). Sway regularity reflects attentional involvement in postural control: Effects of expertise, vision and cognition. *Gait and Posture*, 30(1):106 – 109.

References

- Svendsen, J. H. and Madeleine, P. (2010). Amount and structure of force variability during short, ramp and sustained contractions in males and females. *Human Movement Science*, 29(1):35 – 47.
- Takens, F. (1981). Detecting strange attractors in turbulence. *Dynamical Systems and Turbulence, Warwick 1980: Proceedings of a Symposium Held at the University of Warwick 1979/80*, pages 366–381.
- Tononi, G., Edelman, G. M., and Sporns, O. (1998). Complexity and coherency: integrating information in the brain. *Trends in Cognitive Sciences*, 2(12):474 – 484.
- Trulla, L., Giuliani, A., Zbilut, J., and Webber, C. (1996). Recurrence quantification analysis of the logistic equation with transients. *Physics Letters A*, 223(4):255 – 260.
- Tsuchida, S., Terada, T., and Tsukamoto, M. (2013). A system for practicing formations in dance performance supported by self-propelled screen. In *Proceedings of the 4th Augmented Human International Conference*, AH '13, pages 178–185, New York, NY, USA. ACM.
- Uzal, L. C., Grinblat, G. L., and Verdes, P. F. (2011). Optimal reconstruction of dynamical systems: A noise amplification approach. *Phys. Rev. E*, 84:016223.
- Uzal, L. C. and Verdes, P. F. (2010). Optimal Irregular Delay Embeddings. In *Dynamics Days South America 2010*. National Institute for Space Research.
- Vaillancourt, D. E. and Newell, K. M. (2002). Changing complexity in human behavior and physiology through aging and disease. *Neurobiology of Aging*, 23(1):1 – 11.
- Vaillancourt, D. E. and Newell, K. M. (2003). Aging and the time and frequency structure of force output variability. *Journal of Applied Physiology*, 94(3):903–912. PMID: 12571125.
- Vaillancourt, D. E., Slifkin, A. B., and Newell, K. M. (2001). Regularity of force tremor in parkinson's disease. *Clinical Neurophysiology*, 112(9):1594 – 1603.
- Vaillancourt, D. E., Sosnoff, J. J., and Newell, K. M. (2004). Age-related changes in complexity depend on task dynamics. *Journal of Applied Physiology*, 97(1):454–455. PMID: 15220326.
- Vakharia, V., Gupta, V., and Kankar, P. (2015). A multiscale permutation entropy based approach to select wavelet for fault diagnosis of ball bearings. *Journal of Vibration and Control*, 21(16):3123–3131.
- van Dieën, J. H., Koppes, L. L., and Twisk, J. W. (2010). Postural sway parameters in seated balancing; their reliability and relationship with balancing performance. *Gait and Posture*, 31(1):42 – 46.
- Wagner, H., Pfusterschmied, J., Klous, M., von Duvillard, S. P., and Müller, E. (2012). Movement variability and skill level of various throwing techniques. *Human Movement Science*, 31(1):78 – 90.

References

- Webber, C. L. and Zbilut, J. P. (1994). Dynamical assessment of physiological systems and states using recurrence plot strategies. *Journal of Applied Physiology*, 76(2):965–973. PMID: 8175612.
- Webber, C. L. and Zbilut, J. P. (2005). Recurrence quantification analysis of nonlinear dynamical systems. In Riley, M. A. and Orden, G. C. V., editors, *Tutorials in contemporary nonlinear methods for behavioral science*, chapter 2, pages 26–94. National Science Foundation.
- Wijnants, M. L., Bosman, A. M., Hasselman, F., Cox, R. F., and Van Orden, G. C. (2009). 1/f scaling in movement time changes with practice in precision aiming. *Nonlinear Dynamics, Psychology, and Life Sciences*, 13(1):79–98. cited By 88.
- Wolf, A., Swift, J. B., Swinney, H. L., and Vastano, J. A. (1985). Determining lyapunov exponents from a time series. *Physica D: Nonlinear Phenomena*, 16(3):285 – 317.
- Wu, H. G., Miyamoto, Y. R., Castro, L. N. G., Ölveczky, B. P., and Smith, M. A. (2014). Temporal structure of motor variability is dynamically regulated and predicts motor learning ability. *Nature neuroscience*, 17(2):312.
- Wu, M.-C. and Hu, C.-K. (2006). Empirical mode decomposition and synchrogram approach to cardiorespiratory synchronization. *Phys. Rev. E*, 73:051917.
- Wu, Z. and Huang, N. E. (2004). A study of the characteristics of white noise using the empirical mode decomposition method. *Proceedings of the Royal Society of London A: Mathematical, Physical and Engineering Sciences*, 460(2046):1597–1611.
- Wu, Z. and Huang, N. E. (2009). Ensemble empirical mode decomposition: A noise-assisted data analysis method. *Advances in Adaptive Data Analysis*, 01(01):1–41.
- Xochicale, M. P. (2018). *How Well You Move Dataset*.
- Yang, C. and Wu, C. Q. (2011). A robust method on estimation of lyapunov exponents from a noisy time series. *Nonlinear Dynamics*, 64(3):279–292.
- Yao, C.-Z. and Lin, Q.-W. (2017). Recurrence plots analysis of the cny exchange markets based on phase space reconstruction. *The North American Journal of Economics and Finance*, 42:584 – 596.
- Zbilut, J. P. and Webber, C. L. (1992). Embeddings and delays as derived from quantification of recurrence plots. *Physics Letters A*, 171(3):199 – 203.
- Zunino, L., Zanin, M., Tabak, B. M., Pérez, D. G., and Rosso, O. A. (2009). Forbidden patterns, permutation entropy and stock market inefficiency. *Physica A: Statistical Mechanics and its Applications*, 388(14):2854 – 2864.